**Fakultät für Medizin**

**Klinik und Poliklinik für Innere Medizin II**

# Oncolytic Virotherapy with the Fusogenic VSV-NDV Platform Complementing Adoptive T Cell Therapy

**Teresa Aurelia Krabbe**

Vollständiger Abdruck der von der Fakultät für Medizin der Technischen Universität München zur Erlangung des akademischen Grades eines

**Doctor of Philosophy (Ph.D.)**

genehmigten Dissertation.

**Vorsitzender:** Prof. Dr. Claus Zimmer

**Betreuerin:** Priv.-Doz. Dr. Jennifer Altomonte

**Prüfer der Dissertation:**

1. Prof. Dr. Angela Krackhardt

2. Prof. Dr. Florian Kreppel

Die Dissertation wurde am 30.04.2020 bei der Fakultät für Medizin der Technischen Universität München eingereicht und durch die Fakultät für Medizin am 07.07.2020 angenommen.

# Contents

# 1 Introduction

## 1.1 The Immune System in Cancer

Over the last decades the importance to investigate and understand the immune system and its role in tumor development and tumor progression has become increasingly clear. In 2011, evasion of immune destruction emerged in the revised list of hallmarks of cancer proposed by Hanahan and Weinberg [1, 2]. In the same year, the immune hallmarks of cancer were introduced, suggesting the addition of three directly immune-related hallmarks to the list of alterations essential for malignant growth [3].

***Emerging* Hallmarks of Cancer [1, 2]**

- Self-sufficiency in growth signals
- Insensitivity to antigrowth signals
- Limitless replicative potential
- Ability to evade apoptosis
- Sustained angiogenesis
- Ability to invade the tissues and metastasize
- *Reprogramming of the energy metabolism*
- *Evasion of immune destruction*

**Immune Hallmarks of Cancer [3]**

- Ability to thrive in a chronically inflamed microenvironment
- Ability to evade immune recognition
- Ability to suppress immune reactivity

With this knowledge came the possibility to harness the immune system for efficient tumor treatment as the basis for cancer immunotherapy, which by now is a potent wild card to pull from the deck of treatment options. Before diving into the complexity of cancer immunotherapy, a closer look at the immune system itself and its recognition and elimination of transformed cells will enable a clear assessment of the elements that have been addressed by therapeutic interventions. All ideas and hypotheses raised throughout this doctoral thesis are based on selected elements thereof.

### 1.1.1 Innate and Adaptive Anti-Tumor Immune Response

The immune system responds to invading pathogens in a well-established manner. Immune cells surveilling the periphery respond to foreign structures and mount a humoral and cellular response to clear the invader. In a similar process, transformed cells can be recognized and eliminated spontaneously by the immune system. Transformed cells that escape immune surveillance have acquired a first immune hallmark ("Evasion of immune recognition") and can give rise to tumor lesions growing under the radar of the immune system. However, growing tumors can also give rise to an anti-tumor immune response, for example, by releasing new immunogenic tumor antigens [3].

**Inducing an anti-tumor immune response - Cancer-Immunity Cycle**

In oncology, the steps of the tumor immune response are summarized in the idealistic cancer-immunity cycle (Fig. 1) [4]. Both the innate and adaptive immunity have their part to play in the response. Innate pattern-recognition receptors (PRRs) respond to pathogen-associated molecular patterns (PAMPs) and/or damage-associated molecular patterns (DAMPs) released as tissue mediators in response to different stressors accompanying tumor growth and spontaneous or therapeutically-induced tumor cell death. This contact activates inflammatory signaling cascades, including transcription factor nuclear factor-kappa B (NF-$\kappa$B) and interferon regulatory transcription factor (IRF). The subsequent release of various cytokines and chemokines attracts innate effector cells. In parallel, tumor antigens are released from dying tumor cells (Step 1). At the center of the innate immune response are natural killer (NK) cells, NKT cells, $\gamma\delta$-T cells, macrophages, granulocytes and dendritic cells [5]. The former can eliminate transformed cells through the activation of perforin or death receptor-mediated pathways. As antigen-presenting cells (APCs), especially dendritic cells, set the stage for the adaptive immunity, i.e. the activation of T and B cells. Dendritic cells (DCs) mature upon uptake of (tumor) antigens and start antigen-presentation (Step 2). In the lymph nodes these APCs encounter naïve T cells, which are activated in response to specific peptide-MHC (major histocompatibility complex) combinations that fit a specific T cell receptor (TCR) in a process called priming (Step 3). Activated T cells can access the circulation and infiltrate the tumor (Step 4+5). Both $CD4^+$ helper T cells and cytotoxic $CD8^+$ T lymphocytes (CTL) recognize specific tumor antigens (Step 6). $CD4^+$ T cells induce a Th1 or Th2 helper response depending on co-stimulatory factors present at the tumor site that drive the adaptive immune response in different directions [6]. CTLs destroy antigen-presenting tumor cells through release of cytotoxins or activation of death receptor-mediated pathways (Step 7) and induce inflammatory signaling by releasing cytokines, e.g. interferon gamma (IFN$\gamma$) and tumor necrosis factor-alpha (TNF-$\alpha$).

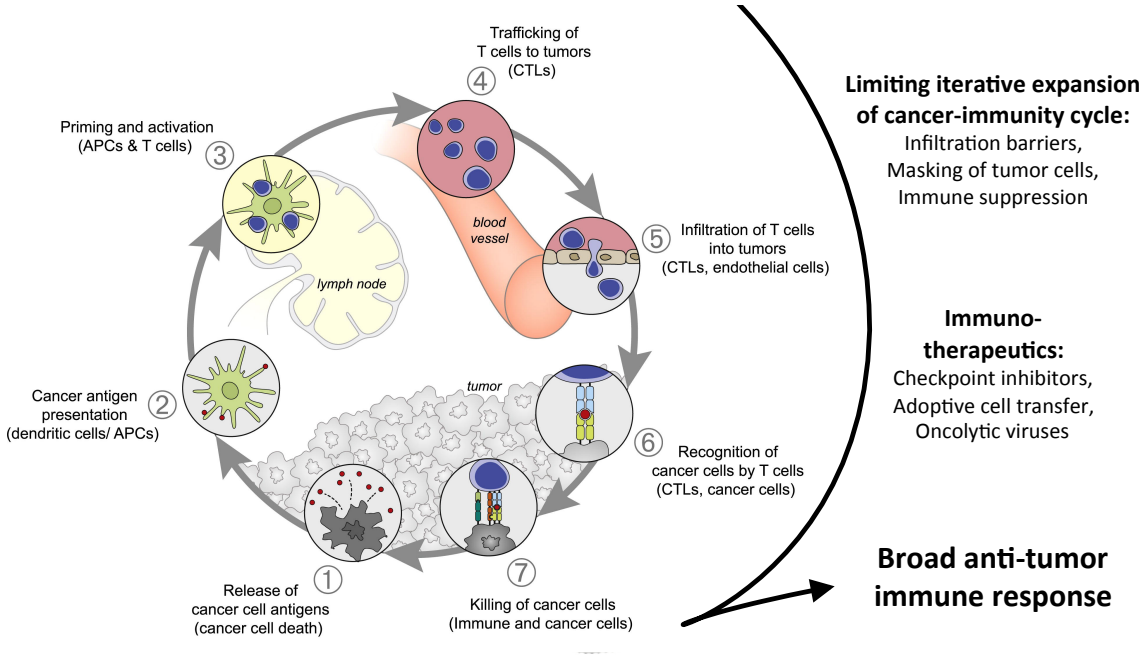


Figure 1: The cancer immunity cycle. Activation and priming of the immune system by dying cancer cells can induce an anti-tumor immune response that is able to eliminate tumor cells and leaves behind memory immune cells to avoid relapse. Tumor cells have developed various mechanisms to avoid immune cell activation. Modified from [4].

This concludes the first iteration of the cancer-immunity cycle. Unhindered progression and iterative expansion can result in the complete clearance of the tumor. Eventually, numbers of immune cells decline and memory cells are left behind to patrol the periphery and mount a fast response upon a secondary recognition. The eventual slowing of the immune response occurs if the immune cells are able to infiltrate and completely eliminate the tumor, but also if tumor cells remain, resulting in an immune equilibrium. The reasons for tumor persistence and relapse can be traced to problems at the individual steps of the cancer-immunity cycle, especially recognition, infiltration and immune suppression.

**Limited recognition and infiltration inhibit the anti-tumor immune response**

Cancer development is characterized by cellular alterations in tissue-derived cells that accumulate over time and cause unlimited replication and eventually their malignant transformation. The immune system, that is trained to differentiate between self and foreign structures, underlies a heavy regulation in order to avoid autoimmune reactions against the body's own tissues. For this reason, the similarity of tumor cells to non-transformed cells provides them with an advantage in that the immune system might not recognize transforming cells, especially in early stages of tumor development.

In later stages, the continued accumulation of genetic and epigenetic changes leads to a more distinctly modified gene expression in tumor cells. Reactivation of silenced genes, typically active during the embryonic phase to support cell proliferation, lead to tumor-associated antigens (TAAs), which are not unique to the tumor, but can be found (possibly at lower expression levels) in other tissues. These antigens tend to be tolerated by the immune system. Mutated proteins that are unique to the tumor tissue give rise to tumor-specific antigens (TSAs) or neoantigens [5]. TSAs appear to provide the most potent antigens for an immune response, however, only a small number of neoantigens can give rise to a robust T cell response [7]. Additionally, only tumor cell subpopulations are affected by immune cells specific for an individual neoantigen. In this way, the immune system imposes selective pressure on tumor cells to eliminate tumor-specific antigens, diminishing antigenic peptide processing or MHC presentation leading to immune tolerance in a process called immunoediting.

Immune infiltration of the tumor tissue itself is also a crucial step towards successful clearance. In general, tumors can be categorized along a gradient of three immunophenotypes based on spatial distribution of $CD8^+$ T cells in the tumor microenvironment, i.e. inflamed, immune excluded and immune desert tumors [8]. Infiltration depends on multiple factors, such as, for example, the vascularization of the tumor and the presence of inflammatory cytokines/chemokines inducing extravasation of lymphocytes into the tumor tissue. Based on the quantification of $CD3^+$ and $CD8^+$ cells within the tumor and at the invasive margin, the immunoscore has been developed and implemented as a robust, standardized scoring system for the categorization of colorectal carcinoma [9]. Tumors can thus be differentiated into well infiltrated (inflamed, hot) tumors with high immunoscore, non-infiltrated (cold) tumors with low immunoscore and tumors with intermediate immunoscore. In these tumors, immune cells are either excluded and accumulate at the tumor margin or immune cells infiltrated but their response is suppressed.

Although tumor cells continue to transform over time and accumulate an ever-increasing mutational burden, that is correlated with higher immune cell infiltration, an unsuccessful clearance is still likely, leading to tissue homeostasis and persistence of the tumor. Unsuccessful clearance is then due to miscellaneous mechanisms of immunosuppression.

### 1.1.2 Immunosuppression

Our immune system is programmed to rapidly respond to invading pathogens, but at the same time, the immune response has to be halted just as quickly to avoid acute cytokine toxicity and autoimmunity. These mechanisms are balanced by a complex signaling network including immune checkpoints, pro- and anti-inflammatory cytokines and chemokines. Tumor-induced immunosuppression is mediated by tumor cells and surrounding cells making up the tumor microenvironment (TME), depending on a multitude of factors, such as the tissue of origin, but also the individual steps of tumor development. Inhibitory signaling and molecular processes in the tumor microenvironment corrupt the critical regulatory immune pathways and provide malignant cells with an immunosuppressive cloak [5, 10]. Characteristics of immune suppression are the expression of inhibitory cytokines (e.g. TGF-β, Interleukin(IL)-10), recruitment of inhibitory immune cells (e.g. regulatory T cells ($T_{reg}$) and myeloid-derived suppressor cells (MDSCs)) and activation of immune checkpoints [11].

Immature myeloid cells are a heterogeneous class of cells that include myeloid-derived suppressor cells (MDSCs) as well as tumor-associated macrophages (TAMs). MDSCs produce nitric oxide (NO) that inhibits T cells. Macrophages play a dual role in modulating tumorigenesis and antitumor host responses. Macrophages have been divided into the M1 and M2 type. M1 macrophage activation is thought to be one of the mediators of Th1-orchestrated antitumor immunity, whereas M2 macrophages have been implicated in tumor promotion. Moreover, tumor-infiltrating DCs are essential in giving rise to a potent anti-tumor immune response, but this is the case only in combination with co-stimulatory signals. In their absence, DCs tolerize the immune system against tumor antigens and thereby contribute to tumor growth and metastasis. Furthermore, regulatory T cells accumulate in the tumor microenvironment, further blunting antitumor T cell responses via production of inhibitory cytokines [5].

Many other molecular interactions within the tumor microenvironment create an inhibitory surrounding for infiltrating immune cells. Tumors produce adenosine as a byproduct of cell death, which inhibits immune responses and enhances local $T_{reg}$ generation and suppressive function via interaction with the adenosine A2a receptor [5]. Both tumor cells and myeloid cells produce tryptophan dioxygenase (TDO) and indoleamine 2,3-dioxygenase (IDO), which deplete tryptophan. Due to different signaling cascades, activated T cells are highly dependent on tryptophan and are therefore sensitive to tryptophan depletion [12].

T cells also require a massive amount of energy to maintain rapid proliferation and effector functions. $CD8^+$ T cells make a metabolic switch and primarily rely on the less efficient metabolic program of glycolysis [13]. Therefore, T cells depend on similar glycolytic pathways as tumor cells for survival. Increased hypoxia and lactic acid production lead to a hostile and acidic TME. This affects the immunometabolism of T cells, including TCR engagement, T-effector activation, differentiation, and proliferation, ultimately resulting in reduced TILs [14].

Tumor cells also use a variety of checkpoints to their advantage, for example, by overexpressing programmed cell death receptor ligand-1 (PD-L1), which in turn leads to exhaustion of programmed cell death receptor-1 (PD-1)-expressing activated T cells. Over the years, numerous checkpoints have been identified laying open a complex network of immune activation and downregulation, among them are cytotoxic T lymphocyte-associated molecule-4 (CTLA-4), T cell immunoglobulin (TIM-3), lymphocyte activation gene (LAG-3), V-domain Ig suppressor of T cell activation (VISTA) and emerging stimulatory pathways (e.g. inducible co-stimulator (ICOS), OX40, 4-1BB) [15].

The variety of cells and pathways involved make the prediction of immunosuppressive mechanisms and the choice of treatment an enormous challenge. Finding the right immunotherapeutic approach will depend on a profound understanding of the immune system, sophisticated bioinformatic analyses and prediction systems as well as a multitude of well characterized treatment options.

## 1.2 Cancer Immunotherapy

In our long struggle against cancer, we have moved from harsh chemotherapeutics to targeting small molecules. Decades of intense research have provided a better understanding of the development of transformed cells, the microenvironment around them and the effects of various treatment regimes. Only the immune system has long been written off as a lost cause, unable to recognize or eliminate the tumor. Recently, however, the immune system has proven us wrong. With immunotherapy on the rise, it looks like the key to cancer therapy might lie in harnessing the immune system, guiding its attack and unleashing its anti-tumor effect. Immunotherapy includes a variety of approaches that reinforce the immune system in its attempt to eradicate the tumor and circumvent the immunosuppressive mechanisms described above [9].

Over the years, more than 25 immunotherapies have been approved, providing over 15 types of cancer with at least one immunotherapeutic treatment option, but many tumors remain difficult to treat. Cancer immunotherapy started with the approval of interferon-$\alpha$ in 1986 for hairy cell leukemia [16], but in recent years, more successful treatments have been approved targeting immune checkpoints CTLA-4, PD-1 and PDL1. While most investigative work evaluates checkpoint inhibitors in combination or new members of the checkpoint network, e.g. TIM3, MAG3, etc., for a possible clinical benefit, other therapeutic approaches are beginning to enter the clinic and the market, such as adoptive T cell transfer, oncolytic viruses and different cancer vaccine strategies.

The immunoscore of the tumor, that is based on the immunophenotype of the innate and adaptive anti-tumor immune responses, can be used to predict the potential success of different immunotherapeutic approaches. Well infiltrated (hot) tumors are assumed to respond well to immunotherapies alleviating the immune suppression. Non-infiltrated (cold) tumors have low chances to respond to immunotherapy, because they lack an already existing immune response. Tumors with intermediate immunoscore, where immune cells are excluded and accumulate at the tumor margin, could respond if the infiltration barrier is broken by the immunotherapeutic agent. These immunophenotypes are also characterized by a variety of other factors, such as the presence of MHC class I (MHC-I) and PD-L1 on the tumor cell surface and amount of the suppressive cytokine TGF$\beta$ in the tumor microenvironment [8].

Clinical experience has shown that over 50% of patients well suited to respond to checkpoint inhibition (e.g. high PD-L1 expression) will not respond to these agents after all [17]. This phenomenon is termed "primary immune escape" and hints at the complexity of immunotherapeutic approaches. "Secondary immune escape", on the other hand, involves responding patients with tumor regression lasting years ultimately experiencing disease progression [18]. Research on all aspects of cancer immunotherapy is in full swing, including the characterization of predictive markers, new agents and especially combination approaches, that will be discussed in more detail later.

### 1.2.1 Checkpoint Inhibition

As already mentioned, tumor cells corrupt immune checkpoints to avoid T cell activation and destruction by the immune system. CTLA-4 was the first checkpoint inhibitor targeted with antibodies in the clinic. It is an intracellular protein in resting T cells, that is translocated to the cell surface after TCR engagement and co-stimulatory signaling through CD28. Here, CTLA-4 outcompetes CD28 for binding to critical co-stimulatory molecules (CD80, CD86) and mediates inhibitory signaling into the T cell, resulting in arrest of both proliferation and activation [19–21]. The major role of CTLA-4 appears to affect downmodulation of $CD4^+$ helper T cell activity and enhancement of $T_{reg}$ suppressive activity.

Besides CTLA-4, the PD-1 pathway has been most extensively studied and tested in preclinical, as well as clinical studies. Monoclonal antibodies targeting PD-1 and its ligand PD-L1 have shown great success in treating solid tumors with an inflamed immune phenotype. The pathway selectively regulates immune responses in tissues, rather than globally regulating the activation of T cells, as does CTLA-4 [10]. The difference is illustrated in Figure 2.

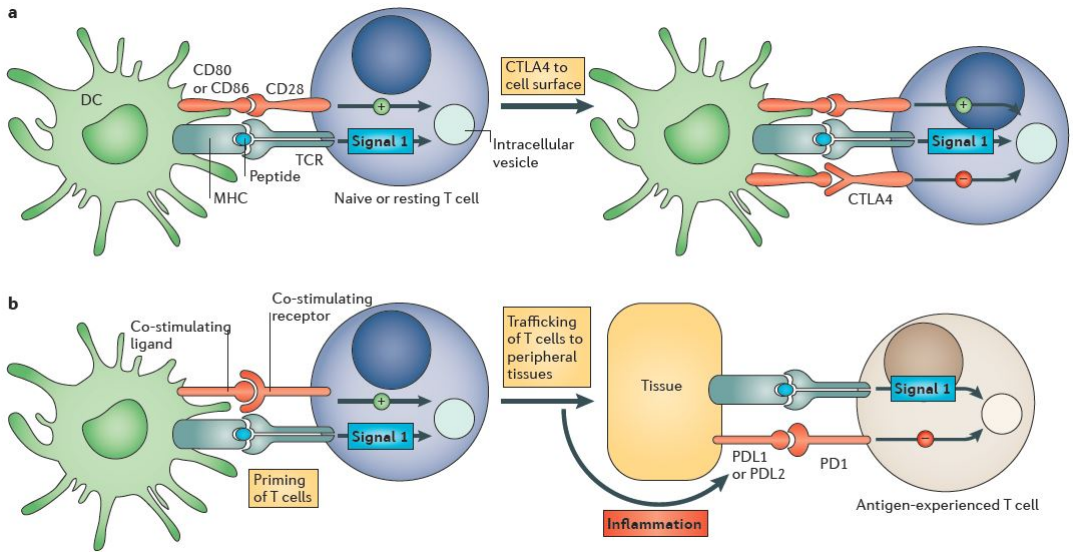


Figure 2: Schematic illustration of cellular interactions with checkpoint inhibitors CTLA-4 and PD-1 [10]. (A) CTLA-4 is translocated to the cell membrane upon dendritic cell (DC) interaction and induces inhibitory signaling in the T cell by outcompeting CD28 binding to CD80/CD86. (B) PD-L1 is upregulated on tumor cells upon inflammation and interacts with PD-1 expressed by activated T cells inducing an exhausted phenotype.

In 1992, Ishida *et al.* published a paper introducing a novel protein induced upon programmed cell death [22]. Only 10 years later, the connection between the PD-1 pathway and cancer immunotherapy was established. In 2002, research showed that mouse tumors with forced expression of PD-L1 become resistant to elimination by the immune system and, furthermore, that expression of the gene encoding PD-L1 is selectively upregulated in many human cancers [23]. Both PD-1 and PD-L1 have been successfully targeted by monoclonal antibodies that were approved for clinical use and designed to block the interaction between PD-L1, expressed by tumor cells, and PD-1, expressed by tumor-infiltrating T cells, leading to enhanced antitumor $CD8^+$ T cell responses and tumor regression. The impact of PD-L1 expressed by immune cells has not been well defined, but PD-1 signaling is widely accepted to be the most important receptor involved in maintaining the exhausted phenotype of activated T cells [13]. Tumors with deficiency in the mismatch-repair pathway for DNA repair or with high microsatellite instability are highly immunogenic. These types of tumors, regardless of tumor origin, generate multitudes of novel antigens due to their high mutational burden, making them ideal targets for $CD8^+$ T cell responses reinvigorated by PD-L1/PD-1 checkpoint blockade therapy [24].

Inhibitory immune checkpoints have been a vital piece in the puzzle that is tumor immunity. The impact of CTLA-4 and PD-1 therapies on cancer research and treatment is reflected in the Nobel Prize in Physiology or Medicine of 2018 being awarded to Professor James Allison and Professor Tasuku Honjo for their research on CTLA-4 and PD-1, respectively. Despite these successes, only 10-30% of the overall patient population respond to checkpoint inhibition [25]. Combination of CTLA-4 and PD-1 monoclonal antibodies led to an increase of the response rates and median survival time in a variety of cancer patients [26]. One of the reasons is that checkpoint inhibitors work together with an already existing immune response against the tumor, increasing its value in highly immunogenic tumors. Other therapies have to be used to target tumors with an excluded or desert immunophenotype.

### 1.2.2 Adoptive Cell Therapy (ACT)

Adoptive cell transfer is based on the therapeutic principle that potent tumor-specific immune cells, e.g. antigen-specific T cells, can induce tumor clearance. Due to various reasons discussed earlier, the patient's own T cells were not able to mount an efficient anti-tumor response. The therapeutic potency of adoptively transferred cells, including T cells, cytokine induced killer cells (CIKs) and dendritic cells, has been investigated in clinical trials with T cell transfer being the most successful approach so far.

ACT-based immunotherapy was first described in 1988 in combination with IL-2 to treat patients with metastatic melanoma [27]. A real improvement of efficacy, however, came in 2002 with the introduction of an immunodepleting preparative regimen given before the adoptive transfer. This results in the clonal repopulation of patients with anti-tumor T cells [28]. Adoptive T cell transfer has recently shown great success in the clinic targeting leukemic cells. Due to difficulties with tumor infiltration, tumor recognition and suppressive features of the tumor microenvironment mentioned earlier, adoptive cell therapy is still of limited use in solid tumors.

In principle, antigen-specific cytotoxic T cells, usually the patient's own (tumor-infiltrating) lymphocytes are collected, expanded *in vitro* and are then injected back into the patient to induce an anti-tumor immune response. To improve tumor recognition and elimination, lymphocytes have been engineered to express receptors against tumor antigens or surface structures. Since only tumor cells presenting the correct antigen are eliminated, this method relies, at least in part, on the patient's immune system to destroy the remaining tumor cells. The choice of tumor target is essential to the therapeutic outcome and defines the T cell engineering approach to be used, i.e. TCR or CAR transduced T cells (Fig. 3).

**TCR-transduced T cells**

One way to engineer T cells is the transduction of T cells with a tumor-specific T cell receptor. Analogous to an endogenous TCR, the transduced version consists of two different polypeptide chains, the T cell receptor $\alpha$ (TCR$\alpha$) and $\beta$ ($\beta$) chains (Fig. 3 A). The chains are linked by a disulfide bond and structurally resemble the Fab fragment of an immunoglobulin molecule. The chains are made up of an amino-terminal variable (V) region, a constant (C) region, and a short hinge region containing the cysteine residue forming the disulfide bond between the chains. Each chain ends in a short cytoplasmic tail after spanning the lipid bilayer by a hydrophobic transmembrane domain [6].

Identifying the TCRs to be used in therapy is a challenge, since all expressed proteins, including intracellular proteins, could potentially be targeted. Treatment outcome is limited by antigen and/or MHC downregulation. Mutagenesis of tumor cells especially effects the intracellular protein repertoire, generating potential targets for a very specific recognition by TCR-transduced T cells inducing tumor cell death. Additionally, TCRs have evolved an extremely efficient signal-amplification system capable of detecting very low levels of tumor-derived peptides [29].

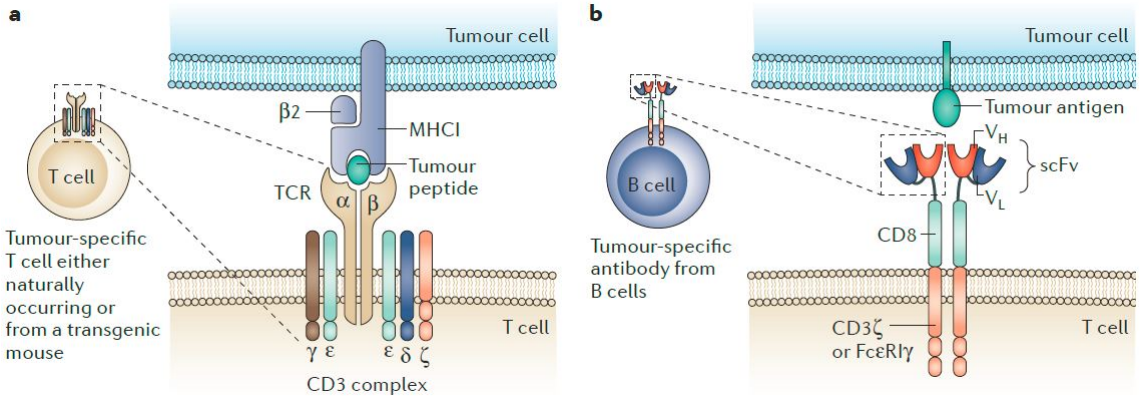


Figure 3: Schematic illustration of the T cell receptor (TCR) and the B cell-derived chimeric antigen receptor (CAR) [30]. (A) The $\alpha$- and $\beta$-chains of the TCR feature a constant and variable domain recognizing the tumor peptide presented by an MHC class I complex (MHCI) consisting of the polymorphic heavy $\alpha$-subunit and small invariant $\beta 2$ microglobulin subunit. (B) The CAR is composed of a B cell-derived extracellular TAA-specific single-chain antibody variable fragment (scFv) that is linked, via hinge and transmembrane domains, to an intracellular signaling domain.

### CAR T cells

Another way to engineer tumor-specific T cells is the transduction of T cells with a chimeric antigen receptor (CAR). The CAR is composed of an extracellular TAA-specific single-chain antibody variable fragment (scFv) that is linked, via hinge and transmembrane domains, to an intracellular signaling domain [30] (Fig. 3 B). This enables recognition of three-dimensional protein structures present on the tumor cell surface as opposed to peptides presented by MHC, which limits the target pool in comparison. In 2017, the first CAR-T cell treatment directed against the CD19 peptide was approved for treatment of B cell lymphoma after proving efficacy in a phase 2 trial showing a complete response in 83% of patients within 3 months of infusion [31]. CARs have an 'off the shelf' advantage over TCRs, since HLA matching is not necessary. This could also improve therapy of tumors that are frequently found to have low or absent expression of HLA class I molecules.

Moreover, synthetic CAR signaling may confer an advantage over conventional TCR signaling in that they are unaffected by some of the immunosuppressive aspects of the tumor microenvironment. The greater sensitivity of TCRs in response to peptides may render them inherently safer than CARs. On the other hand, the preclinical testing to predict off-tumor but on-target toxicity is more straightforward than for TCRs. Given the responsiveness to peptides with low abundance, expression of targeted antigens in non-tumor tissue must be ascertained [29].

In both cases, secondary escape mechanisms have been well documented. Loss of tumor antigen targeted by the CARs has been shown to be associated with loss of clinical benefit in lymphomas treated with CD19 CAR-T cells [29,32]. Loss of functional β2-microglobulin [33] and loss of specific HLA haplotypes [34] in melanoma and CRC treated with TCR T cells also resulted in secondary escape. Since CARs and TCRs recognize very different structures, the availability of surface or internal tumor-specific peptides will be a deciding factor for which T cell engineering approach to use in therapy and will depend on the individual tumor. The experiments in this doctoral thesis are based on tumors expressing model tumor antigens, i.e. OVA and SV40 LTAg. These are intracellular proteins, so TCR-transduced T cells were used in all experiments.

### 1.2.3 Oncolytic Viruses

Oncolytic viruses (OVs) are a group of replication-competent viruses that are either inherently tumor selective or have been engineered to preferentially replicate in tumor cells and destroy them. For a long time, OVs have been perceived as unpredictable tumor cell killers with little chance to ever reach the clinic. With the rise of immunotherapy, this perception has changed [35]. Today, oncolytic viruses are seen as promising multifaceted immunotherapeutic vectors and T-Vec (Imlygic, Amgen), an oncolytic herpes simplex virus 1 (HSV-1) expressing granulocyte-macrophage colony-stimulating factor (GM-CSF), has performed well in clinical trials and was approved by the FDA in 2015 for the treatment of malignant melanoma [36].

A multitude of viruses can be harnessed as oncolytic agents. DNA viruses, e.g. adenoviruses and herpes simplex virus, as well as RNA viruses, e.g. measles, Newcastle Disease Virus (NDV) or vesicular stomatitis virus (VSV), have been investigated for their oncolytic potential. Reasons for tumor specificity vary, but are usually based on the principle that tumor cells deregulate signaling cascades in order to achieve unrestrained proliferation and immune escape.

Commonly, tumor cells downregulate expression of type I IFN receptors, inactivate downstream signaling through the JAK-STAT pathway or deregulate PKR activation [36, 37]. Viruses that are sensitive to interferon effects will preferably replicate in tumor cells, while viral replication is suppressed in healthy cells with intact IFN signaling. As a "living" therapy, oncolytic viruses come with their own risks and side effects, but they provide access to a new set of treatment possibilities, especially considering immune desert tumors lacking immune cell infiltration.

The difficulty with replication-competent OVs is to balance efficacy and safety. In general, a more potent virus would yield more severe off-target effects, while a less potent, safer virus would feature attenuated replication and reduced cytotoxicity. With immunotherapy in mind, oncolytic virus design has recently focused on their ability to activate the immune system instead of increasing their oncolytic potential. Viral infection alone, but also virus-induced tumor cell death, is immunogenic. And although part of the immune response will target viral proteins, neoantigens from infected tumor cells will also be processed within antigen presenting cells as part of the innate immune response and presented to naïve T cells in the lymph nodes. Since the induction of antigen-specific T cell responses depends on APC priming accompanied by inflammatory signals, the process benefits from virus-induced inflammation during the priming against tumor neoantigens. Anti-tumor immunity is promoted, while peripheral tolerance to the tumor antigens is deflected [4].

Together the primary oncolytic effect and secondary induction of a broad anti-tumor immune response can lead to effective tumor cell clearance and complete regression in animal models [38]. Promising data have resulted in much excitement surrounding OV development, with over 1,000 agents in preclinical development. However, only a fraction has been tested in clinical trials, where oncolytic agents, for the most part, have not been able to live up to their therapeutic potential. Although safe, viroimmunotherapy has resulted in limited efficacy especially after systemic administration [39]. To overcome these limitations, new oncolytic virus platforms are being designed for systemic delivery and potent induction of a broad and effective anti-tumor immune response. One of these novel oncolytic viruses has been introduced in 2018 by our group as a hybrid platform engineered from VSV and NDV [40].

### VSV-NDV as a novel hybrid oncolytic virus platform

Throughout this thesis, experiments are based on the VSV-NDV platform or variants thereof with integrated transgenes. VSV-NDV was engineered by replacing the VSV glycoprotein (VSV-G) within the VSV genome with the surface proteins of NDV (Fig. 4).

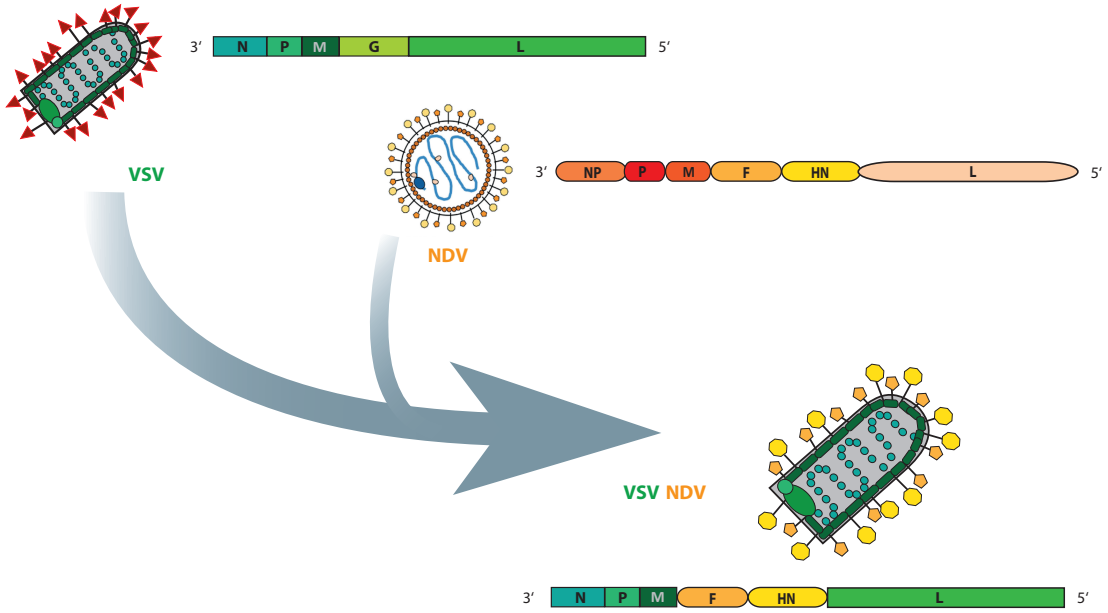


Figure 4: Schematic illustration of the hybrid VSV-NDV particle and its parental virus particles, i.e. vesicular stomatitis virus (VSV) and Newcastle disease virus (NDV), as well as their genomic structure to visualize replacement of VSV-G with NDV-F and NDV-HN.

This design enables VSV-NDV to use the strengths of both its parental viruses and overcome the limitations of each. With its fusion-based mechanism of action, VSV-NDV is a potent hybrid oncolytic virus platform with unique properties, including fusogenic cell death. A short introduction to the parental virus constructs VSV and NDV will serve to demonstrate the rationale behind VSV-NDV design and improve understanding of the unique assets of this hybrid platform.

### Vesicular Stomatitis Virus (VSV)

VSV is a member of the genus *Vesiculovirus* of the family *Rhabdoviridae*. It is an arbovirus (arthropod-borne virus) infecting insects, cattle, horses and pigs. In infected humans it causes flu-like symptoms, although they are not the natural hosts. Virions are enveloped, bullet shaped and approximately 180 nm long [41]. VSV owes its oncolytic effect to tumor cell defects in the interferon pathway [42]. For example, down-regulation of type I interferon receptor sensitizes tumor cells to VSV-induced cell death [43].

VSV features a single stranded, negative-sense RNA genome with roughly 11,000 nucleotides comprising five genes (3' N-P-M-G-L 5'): nucleoprotein (N), phosphoprotein (P), matrix protein (M), glycoprotein (G) and large protein (L).

As is the case for RNA viruses, replication takes place in the cytoplasm. VSV does not appear to undergo genetic recombination, exhibit reassortment activity nor does it seem to have any known transforming potential or integrate any part of its genome into the host [44]. During transcription the respective amounts of the individual mRNAs decrease with distance from the 3' end of the genome due to a single polymerase entry site [45]. The M-protein is a multifunctional protein playing a major role in virus assembly and the cytopathic effects observed in infected cells, i.e. cell rounding, disorganization of the cytoskeleton, inhibition of cellular gene expression and induction of apoptosis [46]. For cell entry, VSV-G binds to the LDL receptor which is ubiquitously expressed and guarantees a very wide host cell range. This characteristic has been used in various fields of research to improve infectivity by pseudotyping viruses with VSV-G [47]. One of the drawbacks of this broad tropism, however, is off-target effects. Severe neuro- and hepatotoxic side effects of VSV treatment have been observed, especially in rodent models [48], but also non-human primates [49].

In order to provide the potency of VSV as an oncolytic agent in therapy, different strategies have been implemented to restrict off-target effects. Modifications of the M protein, i.e. deletion of the critical amino acid methionine at position 51 (M51) or mutation of this amino acid to arginine (M51R) resulted in virus particles unable to restrict host translation with little or no loss of effectiveness, respectively [50]. An attenuated virus expressing IFNβ, i.e. VSV-IFNβ-NIS showed no neurotoxic side effects in animals [51]. The agent is currently being tested for multiple indications in phase I clinical trials. Glycoprotein replacement is another successful strategy. Wollmann *et al.* compared different viral glycoproteins in the VSV backbone and found Lassa-VSV to be effective and safe in the treatment of brain tumors [52], while Muik *et al.* engineered VSV to express the glycoprotein of lymphocytic choriomeningitis virus (LCMV) in order to address the issue of neuroattentuation and G-antibody mediated viral neutralization [53]. In a similar approach, the VSV-NDV vector was designed by replacing VSV-G with the NDV surface proteins (Fig. 4). Most characteristics of VSV mentioned earlier, such as rapid replication in the cytoplasm and lack of integration into the host genome, can be analogously transferred to VSV-NDV. Attachment and internalization, however, are dependent on the new NDV surface proteins.

**Newcastle Disease Virus (NDV)**

NDV is an avian virus and member of the family *Paramyxoviridae* (genus *Avulavirus*). NDV strains can be categorized as velogenic (highly virulent), mesogenic (intermediate virulence), or lentogenic (nonvirulent). Velogenic strains cause severe symptoms and mortality in infected birds. In exposed humans, NDV can cause mild conjunctivitis and influenza-like symptoms. Paramyxoviruses have round virions ranging from 150 to 250 nm in diameter and containing non-segmented single strand negative-sense RNA genomes [54]. The NDV genome with roughly 16,000 nucleotides consists of six genes (3' NP-P-M-F-HN-L 5'): nucleoprotein (NP), phosphoprotein (P), matrix protein (M), fusion protein (F), hemagglutinin neuraminidase (HN) and large protein (L).

The HN protein mediates the attachment of the virus to host target cells, whereas the F protein allows the fusion of the viral envelope with the cellular membrane of the target cell. For fusion to occur, paramyxoviruses require the co-expression of the attachment and fusion protein. Since this fusion event is independent of pH, not only the viral envelope fuses with the cell membrane, but infected cells expressing viral glycoproteins on their surface can also fuse with adjacent cells [55]. For attachment, the expression of $\alpha$2,3 and $\alpha$2,6 N-linked sialic acids on the cell surface allow efficient interaction of NDV-HN with target cells [56]. Sialic acid is ubiquitously expressed and allows infection of a broad range of cells. In contrast to VSV, however, NDV did not show severe cytotoxic side effects in patients with advanced solid cancers even when administered intravenously up to very high doses of $1.2\times10^{11}$ plaque forming units (PFU)/m$^2$ [57].

**Fusogenicity as an immunogenic cell death**

Due to the expression of the enhanced fusion protein during VSV-NDV replication, its cytotoxic effect is characterized by the formation of multinucleated giant cells, i.e. syncytia (Fig. 5). These large areas of fused dying cells result in an immunogenic cell death, characterized by immunogenic markers, such as HMGB1, HSP70 and ATP, being released [40]. The benefits of fusogenicity in oncolytic virotherapy have gained interest and have been reviewed in detail [58, 59] and include, for example, a unique mechanism of virus spread through fusing tumor cells. This optimizes viral spread while reducing the release of virions resulting in fewer circulating virus particles. This is an additional safety aspect considering shedding of the agent. To increase the fusogenicity of rVSV-NDV the fusion protein of NDV was further modified [40]. A polybasic cleavage site was introduced into the F protein to generate rNDV/F3aa [60]. Additionally, a single amino acid was substituted from leucine to alanine at amino acid 289 (L289A) in the F3aa-modified fusion protein [61].

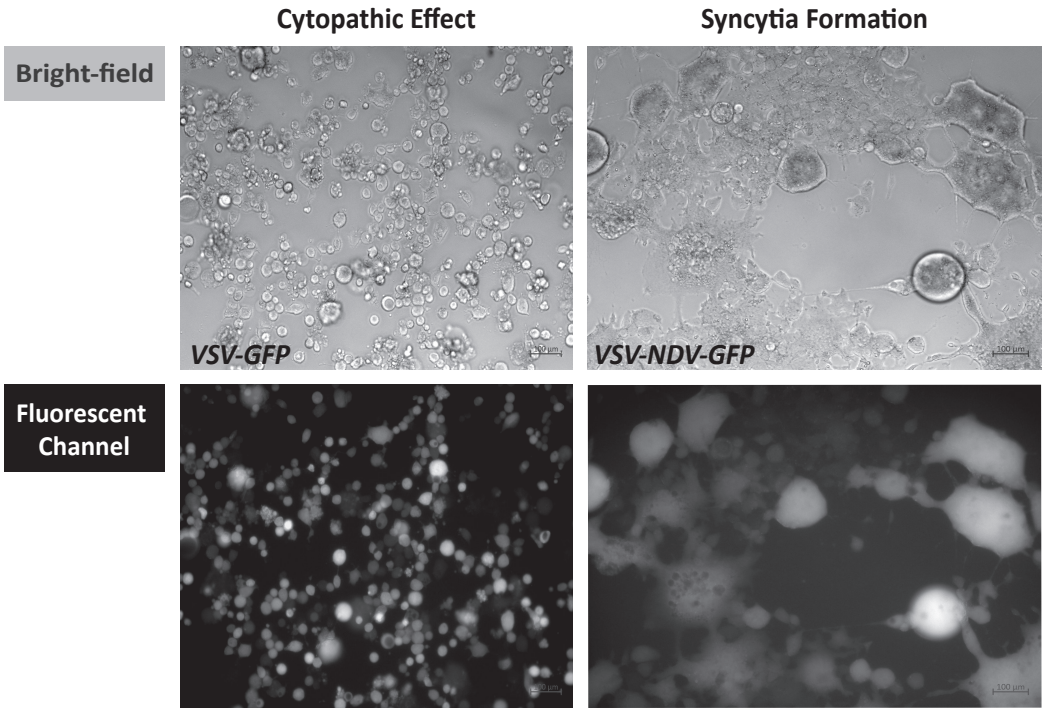


Figure 5: Visualization of the differences between the traditional cytopathic effect induced by VSV infection and the fusogenic effect of VSV-NDV infection. Huh7 cells were infected with VSV-GFP or VSV-NDV-GFP (MOI 0.01) and representative images captured 24 h later.

## 1.3 Combination Therapy

The combination of multiple treatment options seems to be the most promising approach to achieve complete regression and prevent tumor relapse by escape variants. There has been a striking increase in clinical trials evaluating combination therapies indicating the importance of this approach in patient care [62]. While these combination approaches are complicated and pose challenges in development and testing, most therapeutic regimens with curative potential are made up of multiple agents [63].

The optimal combination approach may require multiple therapeutics modulating individual steps in the cancer immunity cycle leading up to the development of a broad and efficient anti-tumor immune response [11]. A complete curative regimen might include agents that eliminate cancer cells to reduce tumor burden, agents that sensitize the cancer to immunotherapy and that modulate the tumor microenvironment, thereby acting on the already existing anti-tumor immune response, and agents that activate an endogenous anti-tumor immune response, driving immune cell infiltration and development of a long-term memory response [8]. The exceptional benefits of combining oncolytic virotherapy with adoptive T cell transfer are summarized in Figure 6 and explained in more detail in the next paragraph.

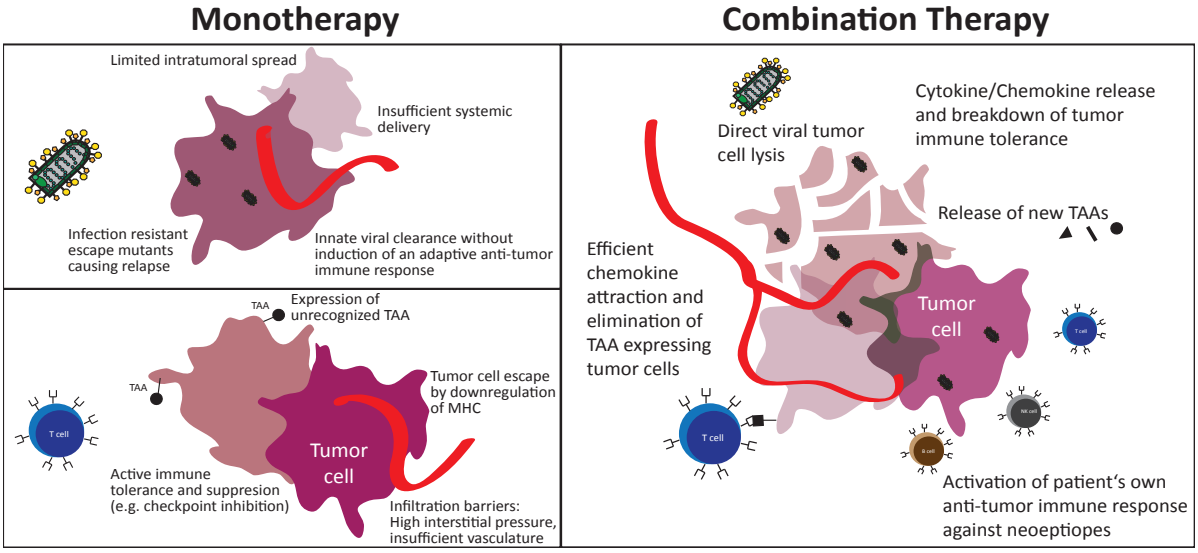


Figure 6: Schematic illustration of the combination benefits in contrast to the monotherapeutic limitations of oncolytic viruses and adoptive T cell transfer. In combination, oncolytic virotherapy debulks the tumor and inflammation counteracts the suppressive mechanisms of the TME, which enables infiltration of transferred T cells and liberates their anti-tumor activity. Combination effects also activate endogenous immune cell responses against neoantigens resulting in a broad anti-tumor immune response.

### Benefits of oncolytic viruses in combination therapy

With their multifaceted mechanism of action, oncolytic viruses are potent immunotherapeutic agents on their own. Their direct oncolytic effect leads to debulking of the tumor and the release of cytokines and tumor associated antigens, while their indirect effect induces an inflammation-dependent change in the tumor microenvironment that enables immune cell infiltration and activation of a patient-derived anti-tumor immune response. Especially in tumor types that are defined as immunologically cold, e.g. pancreatic tumors, inflammation and oncolytic virus-mediated cell death can turn them into "hot" tumors [64]. Viral infection of tumors can also overcome resistance to PD-1-immunotherapy by broadening neoantigen-directed T cell responses [65]. Poor systemic delivery and spread throughout the tumor as well as rapid elimination of the virus by the innate immune system often limit the effect of oncolytic viruses. In order to achieve complete clearance, a combination approach is called for that builds on the direct and indirect oncolytic effects.

Table 1: Combination Approaches in Literature

| **Oncolytic Virus** | **Therapeutic Transgene** | **Adoptive Cell Transfer** | **Combination Effect** | **Reference** |
|---|---|---|---|---|
| Adenovirus | CD44v6-targeting BiTE, IL-12, PD-L1 Ab | HER2.CAR Tcells | Sustained disease control of HER2+ and HER2- tumors | Porter 2020 |
| Adenovirus | Hsp70 | Cytokine-induced killer cells | Improved anti-tumor effect in PDTX models of HCC | Hu 2015 |
| Adenovirus | human GM-CSF | OVA-specific T cells | Reduced tumor growth of subcutaneous B16.OVA tumors | Tahtinen 2015 |
| Adenovirus | RANTES, IL-15 | GD2.CAR T cells | Increased survival in xenograft models | Nishio 2014 |
| Adenovirus | TNF-alpha, IL-2 | OVA-specific T cells | Superior to lymphodepletion in subcutaneous B16.OVA tumors | Santos 2018 |
| Adenovirus | TNF-alpha, IL-2 | Tumor infiltrating lymphocytes | Improved therapy of B16 melanoma and rechallenge with B16-F10 | Havunen 2017 |
| Adenovirus | TNF-alpha, IL-2 | meso-CAR T cells | Tumor regression in mice engrafted with PDA tumors | Watanabe 2018 |
| Adenovirus | | Mesenchymal stem cells | Induced immune response in subcutaneous CMT64-6 tumors | Morales-Molina 2018 |
| Adenovirus | EGFR-targeting BiTe | FR-a.CART cells | Improved anti-tumor effect in HCT116 tumors in NSG mice | Wing 2018 |
| Adenovirus | IL12 | Cytokine-induced killer cells | Improved anti-tumor effect in Huh7 tumors in SCID mice | Yang 2012 |
| Adenovirus | IL-12p70, PDL1 | HER2.CAR Tcells | Improved therapy of HNSCC xenograft and orthotopic model | Rosewell Shaw 2017 |
| Adenovirus | PD-L1 mini-body | HER2.CAR Tcells | Controlled tumor growth in solid tumors | Tanoue 2017 |
| Herpes Simplex Virus-2 | | OVA-specific T cells | Reduced tumor growth in Panc02-H7-OVA tumors in NSG mice | Fu 2015 |
| Measles Virus (MV) | | Cytokine-induced killer cells | Improved therapy of subcutaneous HCC xenograft model | Chen 2017 |
| Moloney MuLVV-Based Retrovirus | IL-12, HSV-tk | OVA-specific T cells | Hitchhiking enhances ACT in B16.OVA tumors and metastasis | Cole 2005 |
| Myxoma virus | | SIY-specific T cells | Enhanced T cell therapy for murine melanoma brain tumors | Thomas 2011 |
| Newcastle Disease Virus (NDV) | | Isolated T cells (murine + human) | Cross infection of tumor cells through viral hitchhiking | Pfirschke 2009 |
| Reovirus | | Cytokine-induced killer cells | Cross infection of tumor cells through viral hitchhiking | Zhao 2017 |
| Vaccinia Virus | CXCL11 | meso-CAR T cells | Improved therapy of TC1-meso tumors | Moon 2018 |
| Vaccinia Virus (vvDD) | | Cytokine-induced killer cells | Prolonged survival through viral hitchhiking | Thorne 2006, 2010 |
| Vaccinia Virus, Myxoma Virus | IL15Ralpha | GARC-1-specific T cells | Improved anti-tumor response in intracranial GL261 NS tumors | Tang 2020 |
| Vesicular Stomatitis Virus | hgp100 | gp100-specific T cells (Pmel) | Improved tumor control in B16 tumors | Shim 2017 |
| Vesicular Stomatitis Virus | hgp100 | Antigen specific T cells (OTI, Pmel) | Sustained disease control of B16 tumors | Rommelfanger 2012 |
| Vesicular Stomatitis Virus | OVA, hgp100 | Antigen specific T cells (OTI, Pmel) | Improved anti-tumor response in B16 tumors and metastasis | Wongthida 2011 |
| Vesicular Stomatitis Virus (deltaM51) | | OVA-specific T cells (OTI) | Improved therapy of B16 tumors and metastasis | Qiao 2008 |
| Vesicular Stomatitis Virus, Vaccinia Virus | gp33, deltaG-gp33, deltaB18R-gp33 | gp33-specific T cells (P14) | Tumor regression in mice with B16 tumors | Walsh 2019 |
| Vesicular Stomatitis Virus, Vaccinia Virus | deltaM51-GFP, vvDD-GFP | HER2.CAR T cells | Cross infection of tumor cells through viral hitchhiking | VanSeggelen 2015 |
| Vesicular Stomatitis Viurs | | MPO-specific T cells | Improved therapy of subcutaneous ML2 tumors in NSG mice | Melzer 2018 |

Adoptive T cell transfer has already proven its worth as a monotherapeutic agent in the treatment of leukemia. Since T cells used in ACT are, in general, as sensitive to the suppressive tumor microenvironment as endogenous immune cells, they are also prime candidates for immunotherapeutic combination approaches in order to improve their therapeutic effect especially in solid tumors. Oncolytic debulking of the tumor, and the inflammatory signals released in response to infection, facilitate immune cell recruitment and infiltration.

Combining adoptive T cell transfer with oncolytic virotherapy seems a daunting task considering the complexities of both treatments. Over the years, however, different groups have tried different approaches to combine oncolytic viruses and adoptive T cell transfer. Examples for different oncolytic viruses and different delivery cells are mentioned here and summarized in Table 1. These studies show the broad applicability of this combination approach.

In 2005, Cole *et al.* demonstrated in a first combination approach that loading of $CD8^+$ antigen-specific T cells with retroviral particles containing cytokine genes improved therapy of metastatic melanoma [66]. Synergistic effects of $CD8^+$ T cell delivery of VSV have also been reported [67–69]. Thorne *et al.* used cytokine-induced killer cells to improve delivery and efficacy of oncolytic vaccinia virus therapy [70, 71]. Recently, Zhao *et al.* showed that the same cells could also be used in combination with reovirus to improve tumor cytotoxicity in vitro [72]. Fu *et al.* used an oncolytic virus derived from HSV-2 to guide migration of adoptively transferred T cells to tumor sites and prolonged persistence at the tumor site [73]. In HCC treatment, 7 injections of oncolytic measles virus enhanced the antitumor response of 6 injections of $CD8^+$ NKGD2D cells over a period of 5 weeks in the work of Chen *et al.* [11]. Pfirschke *et al.* also tested delivery of NDV in various cell carriers *in vitro* [74]. Additionally, CAR-T cells have been shown to carry RNA and DNA virus particles without losing function or expression characteristics [75].

Since immunologically hot tumors also respond better to immune checkpoint inhibitors, the possibility of a triple combination arises. Oncolytic viruses have been shown to overcome systemic tumor resistance to immune checkpoint blockade [76]. In a three-pronged approach, oncolytic viruses would prepare the tumor for T cell therapy, while checkpoint inhibitors prevent early down-regulation of the T cell response.

## 1.4 Aim of this Thesis

The objective of this doctoral work was to evaluate the potential immunotherapeutic benefit of combining the oncolytic VSV-NDV platform with adoptively transferred tumor-specific T cells. Based on literature describing successful combination approaches (Tab. 1) and the immunogenicity of the fusogenic cytotoxic effect of VSV-NDV [40], it was hypothesized that VSV-NDV activity with its primary tumor debulking effect and secondary changes in the tumor microenvironment could complement adoptive cell transfer in an experimental immunotherapy. A two-pronged approach was adopted to establish and characterize both treatment platforms in parallel, followed by the evaluation of the combination *in vitro* and *in vivo* (Fig. 7).

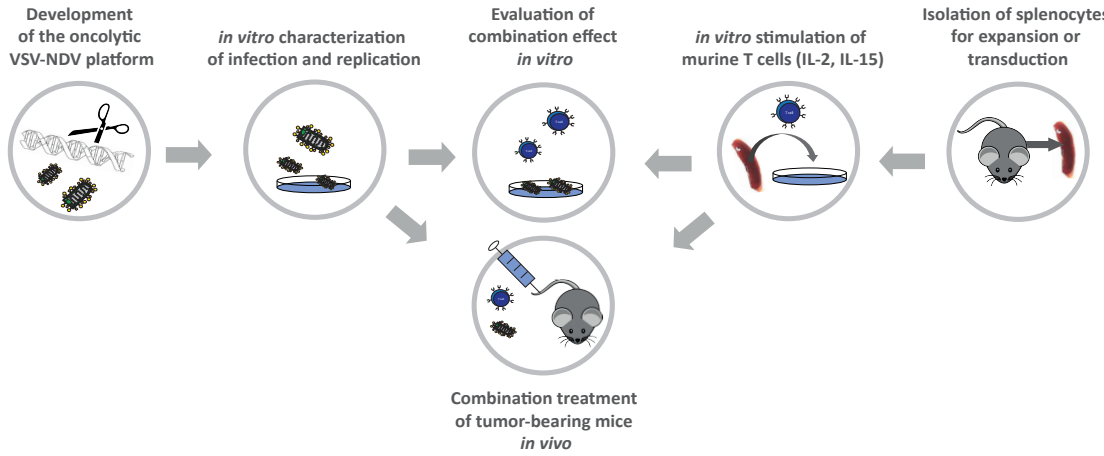


Figure 7: Illustrated summary of the two-pronged experimental approach of this doctoral thesis. Independently, development and characterization of the oncolytic VSV-NDV platform, as well as T cell isolation, culture and transduction with tumor antigen-specific TCRs, are established, followed by an evaluation of combination effects *in vitro* and *in vivo*.

Combination approaches that address multiple factors involved in tumor progression or immunosuppression have shown promise in achieving complete remission. With over 1,000 clinical trials testing various immunotherapeutic combinations, there is a critical need to be able to assess these combinations in adequately predictive preclinical models [16]. Limited understanding of the biological complexity of these approaches limits their development and transfer to the clinic. Experiments conducted and discussed in the scope of this doctoral thesis will elucidate combination effects of oncolytic viruses and adoptive T cell transfer in different tumor models in order to evaluate their future potential in patient treatment.

# 2 Materials and Methods

## 2.1 Materials

### 2.1.1 Chemicals, Reagents and Kits

Table 2: Chemicals & Reagents

| **Reagents** | **Company** |
|---|---|
| Forene 100% (V/V) | AbbVie |
| CD3 (anti-mouse) Clone 145-2C11 | BD Pharmingen |
| CD28 (anti-mouse) Clone 37.51 | BD Pharmingen |
| Red Blood Cell Lysis Buffer (10x) | BioLegend |
| Precision Plus Protein Dual Color Standards | Bio-Rad Laboratories |
| 30% Acrylamide/Bis Solution 37.5:1 | Bio-Rad Laboratories |
| 10x TGS (Running Buffer) | Bio-Rad Laboratories |
| One-step transfer buffer | Bio-Rad Laboratories |
| TEMED | Bio-Rad Laboratories |
| Stacking Gel Buffer | Bio-Rad Laboratories |
| Resolving Gel Buffer | Bio-Rad Laboratories |
| 2x Laemmli Sample Buffer | Bio-Rad Laboratories |
| Tween 20 | Bio-Rad Laboratories |
| Tris (1 M) | Bio-Rad Laboratories |
| Lysis buffer | Cell Signaling |
| Non-essential Amino Acid Solution (100x) | GE Healthcare |
| SIINFEKL peptide (OVA) | IBA Lifesciences |
| 2-Mercaptoethanol | Invitrogen |
| SVYDFFVWL peptide (TRP2) | MBL International |
| Recombinant human IL-15 | Miltenyi Biotec |
| Recombinant human IL-2 (Proleukin 18x106 IE) | Novartis |
| 80% Ethanol | Otto Fischar |
| DPBS with Ca2+, Mg2+ | PAN-Biotech |
| Protease Inhibitor | Roche |
| Triton X 100 | Roth |
| BSA | Sigma-Aldrich |
| Protaminsulfat | Sigma-Aldrich |
| Ampicillin Sodium Salt | Sigma-Aldrich |
| Sodium Pyruvate (100 mM) | Sigma-Aldrich |
| Tryptose Phosphate Broth | Sigma-Aldrich |

| | |
|---|---|
| Penicillin-Streptomycin (10.000U Pen + 10mg/ml Strep) | Sigma-Aldrich |
| Dulbecco's phosphate buffered saline (D-PBS) | Sigma-Aldrich |
| Sucrose (molecular biology grade) | Sigma-Aldrich |
| Skim Milk Powder | Sigma-Aldrich |
| LB Broth | Sigma-Aldrich |
| LB Agar | Sigma-Aldrich |
| Puromycin | Sigma-Aldrich |
| Blasticidine S hydrochloride | Sigma-Aldrich |
| Luminol | Sigma-Aldrich |
| p-coumaric acid | Sigma-Aldrich |
| Hydrogen peroxide | Sigma-Aldrich |
| RetroNectin | TaKaRa |
| Subcloning Efficiency DH5alpha Competent Cells | Thermo Fisher Scientific |
| MAX Efficiency Stbl2 Competent Cells | Thermo Fisher Scientific |
| Gibco Glasgow's MEM (GMEM-BHK) | Thermo Fisher Scientific |
| OptiPro SFM | Thermo Fisher Scientific |
| RPMI 1640 Medium, GlutaMAX-I | Thermo Fisher Scientific |
| DMEM F12, GlutaMAX-I | Thermo Fisher Scientific |
| DMEM, GlutaMAX-I | Thermo Fisher Scientific |
| CellTrace Far Red Cell Proliferation Kit | Thermo Fisher Scientific |
| Dynabeads Murine T-Activator CD3/CD28 | Thermo Fisher Scientific |
| Lipofectamine 2000 | Thermo Fisher Scientific |
| Pierce BCA Protein Assay Kit | Thermo Fisher Scientific |

Table 3: Kits

| Kit | Company |
|---|---|
| innuPREP RNA Mini Kit 2.0 | analytikjena |
| LEGENDplex Mouse Inflammation Panel (13-plex) | BioLegend |
| ALLin HiFi DNA Polymerase | highQu |
| Quick Ligation Kit | New England Biolabs |
| CytoTox 96 Non-Radioactive Cytotoxicity Assay | Promega |
| QIAEX II Gel Extraction Kit | QIAGEN |
| Plasmid Mini Kit | QIAGEN |
| Plasmid Midi Kit | QIAGEN |
| QIAquick PCR Purification Kit | QIAGEN |
| Chemokine Multi-Analyte ELISArray | QIAGEN |
| OneStep RT-PCR Kit | QIAGEN |

### 2.1.2 Appliances and Consumable Material

Table 4: Appliances

| Appliances | Company |
|---|---|
| xCelligence RTCA DP | ACEA Biosciences |
| CytoFLEX S | Beckman Coulter |
| Optimo XL-100K Ultracentrifuge | Beckman Coulter |
| Rotor 70 Ti | Beckman Coulter |
| ChemiDoc XRS+ | Bio-Rad Laboratories |
| Centrifuge 5702 R | Eppendorf |
| Centrifuge 5415 R | Eppendorf |
| Centrifuge 5424 | Eppendorf |
| Biological Microscope | Exacta-Optech |
| Varioklav Dampfsterilisator EP-Z | HP Medizintechnik GmbH |
| Mini Gel Tank | Invitrogen |
| MSS Tec 3 Isoflurane Vaporiser | MSS International |
| Fridge + Freezer | Siemens |
| Sunrise absorbance microplate reader | Tecan |
| Heracell 240 CO2 Incubator | Thermo Fisher Scientific |
| Nanodrop Lite Spectrophotometer | Thermo Fisher Scientific |
| Pierce Fast Semi-Dry Blotter | Thermo Fisher Scientific |
| Herafreeze HFU T Serie -86 | Thermo Fisher Scientific |
| Heraeus Horizontal Laminar Flow Cabinet | Thermo Fisher Scientific |
| Axiovert 40 CFL Fluorescence microscope | Zeiss |

Table 5: Consumable Material

| **Consumables** | **Company** |
|---|---|
| Non-tissue culture-treated 24-well plates | Thermo Fisher Scientific |
| Tissue culture flasks (T25, T75) | TPP |
| Tissue culture plates (96, 24, 6-well) | TPP |
| Serological pipette (50, 20, 10, 5ml) | Greiner Bio-One |
| Aspiration pipette | Thermo Fisher Scientific |
| Pipette filter tips (1000, 200, 20, 10ul) | StarLab |
| Tubes (50, 15ml) | Greiner Bio-One |
| Reagent tubes (2, 1.5ml) | Sarstedt |
| FACS round bottom 96-well plates | Thermo Fisher Scientific |

| | |
|---|---|
| E-Plate VIEW 16 | ACEA Biosciences Inc. |
| Amicon Ultra 2 mL Centrifugal Filters | Merck |
| Cell strainer 40 | Greiner Bio-One |
| Cell strainer 100 | Greiner Bio-One |
| 500 ml Filter system | Corning |
| Filtropur S 0.45 | Sarstedt |
| Combitips advanced 5ml | Eppendorf |
| Low strength adhesive film | NeoLab |
| 1.4 ml non-coded push cap tubes U-bottom | Micronic |
| Parafilm M | Bemis |
| Petri Dish | BD Falcon |
| Injekt 40 Solo Syringes | BRAUN |
| BD Plastipak (1ml 27G) | BD |
| BD Plastipak (1ml-SubQ 26G) | BD |
| Disposable hypodermic needle (30G, 27G, 20G) | BRAUN |
| Microvettes (EDTA coated) | Sarstedt |
| Feather disposable scalpel #21 | pfm medical |
| Disposable bags | Sarstedt |
| PCR tube stripes | Kisker Biotech |
| Omnifix Syringes (2ml, 3ml, 5ml, 10ml) | BRAUN |
| Supra Blood Lancets | megro |
| Comply Steam Indicator Tape | 3M |

### 2.1.3 Software

FlowJo™ v10.6.2 (FlowJo, LLC; Ashland, USA)

Microsoft Office Professional Plus 2013 (Microsoft; Redmond, USA)

Adobe (Dublin, Ireland)

GraphPad PRISM 8 (GraphPad; La Jolla, USA)

MiKTeX 2.9 (MiKTeX; Berlin, Germany)

EndNote X9 (Clarivate Analytics; Philadelphia, USA)

Magellan$^{TM}$ (Tecan; Männedorf, Switzerland)

## 2.2 Methods

### 2.2.1 Cell Culture

All cells were cultured at 37°C, 90% relative humidity and 5% $CO_2$. Adherent cell lines were used for experiments and passaged when they reached a confluency of 80-90%. Non-adherent T cells were maintained at a density of 2-3$\times 10^6$ cells/ml.

**Human HCC and pancreatic cancer cell lines**

The human hepatocellular carcinoma cell lines (Huh7, HepG2) and human pancreatic cancer cell lines (PatuT, PSN-1, MiaPaCa and BxPC3) were cultured in DMEM GlutaMAX$^{TM}$-I (Gibco) supplemented with 10% heat inactivated fetal calf serum (FCS), MEM non-essential amino acids, sodium pyruvate, penicillin (50 U/ml) and streptomycin (50 µg/ml).

**Murine Melanoma**

The B16 murine melanoma cell line expressing the ovalbumin (OVA) protein was cultured in DMEM GlutaMAX$^{TM}$-I supplemented with 10% heat inactivated fetal calf serum (FCS), MEM non-essential amino acids, sodium pyruvate, penicillin (50 U/ml) and streptomycin (50 µg/ml). The B16-F10 clone without OVA was cultured analogously, and both were kindly provided by Simon Heidegger (Klinik und Poliklinik für Innere Medizin III, Klinikum rechts der Isar, Munich).

**HCC (subclone #27-14)**

The murine HCC clone 27-14 was isolated from a tumor from the inducible CreLoxP system in the AST mouse model. It was cultured in DMEM GlutaMAX$^{TM}$-I medium supplemented with 10% heat inactivated fetal calf serum (FCS), MEM non-essential amino acids, sodium pyruvate, penicillin (50 U/ml) and streptomycin (50 µg/ml). Selected isolated clones were characterized in detail within the scope of a master thesis project by Sonja Glauss (data shown for HCCc27-14).

**PlatE**

The Platinum-E (PlatE) cell line was generated based on the 293T cell line and kindly provided by Matthias Leisegang (Max-Delbrück-Center for Molecular Medicine, Berlin). It is cultured in DMEM GlutaMAX$^{TM}$-I medium supplemented with 10% heat inactivated FCS as well as pyromycin (1 µg/ml) and blasticidin (10 µg/ml) to uphold the selective pressure. The packaging constructs utilize the EF1a promoter to express virus structural proteins gag-pol and env [77].

**AGE1.CR.pIX**

The adherent version of the AGE1.CR.pIX cell line was derived from embryonic muscovy duck retina cells and provided by ProBioGen AG [78, 79]. It was used for virus production and titer determination. It is cultured in DMEM F12 GlutaMAX$^{TM}$-I supplemented with 10% heat inactivated FCS.

**OTI T cells**

OTI T cells were isolated from the spleens of OTI mice and cultured in murine T cell medium (mTCM), i.e. RPMI GlutaMAX$^{TM}$-I medium supplemented with 10% heat inactivated FCS, MEM non-essential amino acids, sodium pyruvate, ß-mercaptoethanol (50 mM). The homozygous OTI mice (kindly provided by Melanie Kimm, Institute for Radiology, Klinikum rechts der Isar, Munich) produce T cells expressing transgenic Tcra-V2 and Tcrb-V5 T cell receptor chains in order to recognize the SIINFEKL peptide (ovalbumin residues 257-264) in the context of the H-2K$^d$ MHC class I alloantigen.

**TCR-transduced T cells**

Spleens were harvested from C57BL/6 mice and prepared as a single-cell suspension with prior lysis of red blood cells (RBC Lysis Buffer, BioLegend). Splenocytes were cultured 24 h in mTCM supplemented with 1 µg/ml anti-CD3 (clone 145-2C11), 0.1 µg/ml anti-CD28 (clone 37.51) purified Ab (BD) and 40 U/ml IL-2. The T cells were transduced with a retroviral construct encoding the TCR sequence specific for MHC class I protein, H-2D$^b$, in complex with the SV40-LTAg peptide SAINNYAQKL (Fig. 8), kindly provided by Ana Textor at Max-Delbrück-Center Berlin [80].

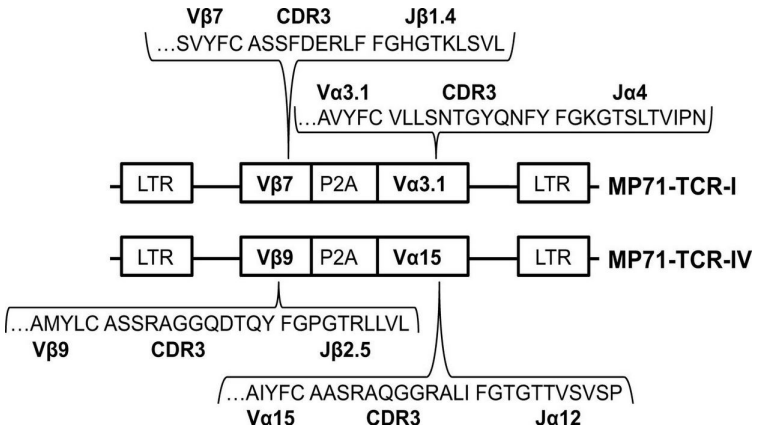


Figure 8: Schematic view of the plasmid MP71-TCR-I encoding the Vβ7 and Vα3.1 chains specific for recognizing the LTAg peptide SAINNYAQKL presented by MHC-I. This plasmid was used in combination with the PlatE cell line to produce retroviral particles able to transduce murine T cells with the specific T cell receptor [80].

Retroviral particles containing the TCR gene were produced by transfecting the PlatE cell line with the pMP71-TCR plasmid. The MP71 vectors were designed for high-level transgene expression in T lymphocytes [81]. Mock transfected cells were used to produce mock-transduced T cells as control. RetroNectin (TaKaRa) coated plates were spin-inoculated with 1 ml/well retroviral supernatant for 1 h at 3000 x g and 4°C. $1\times10^6$ splenocytes/well were then transferred to the coated plates and supplemented with retroviral supernatant, 4 µg/ml protamine sulfate, 40 U/ml IL-2, and CD3/CD28 beads (Dynabeads, ThermoFisherScientific) to 2 ml/well. The cells were spin-inoculated for 1 h at 800 g and 32°C. After another overnight incubation, 1 ml/well of supernatant was removed and replaced with 1 ml fresh virus supernatant, followed by a second spin-inoculation for 1 h at 300 x g and 32°C (Fig. 9).

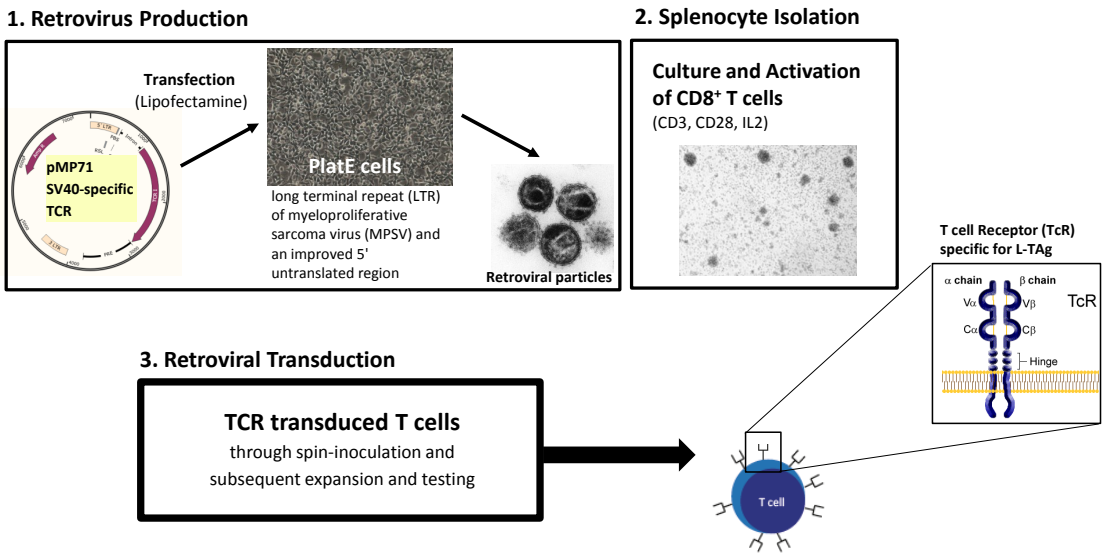


Figure 9: Schematic illustration of the process behind murine TCR transduction. Retroviral particles carrying the antigen-specific TCR gene are produced in PlatE cells via transfection and used in spin-inoculation of isolated splenocytes. After a three-day incubation and expansion period, transduction rate is measured via flow cytometry.

Cells were then transferred into a culture flask in 10 ml mTCM supplemented with 50 ng/ml IL-15 and expanded in culture for 72 h, before determining the level of TCR surface expression via flow cytometry using an anti-CD8 and anti-TCR-β7 chain antibody. Effector-to-target ratios were based on the transduction rate and control cell number was adjusted accordingly.

### 2.2.2 Viruses

**Vesicular Stomatitis Virus (VSV)**

Recombinant VSV vectors expressing the green fluorescent protein (GFP) reporter (referred to herein as VSV) were used. Stocks were produced in BHK-21 cells and purified by sucrose gradient from supernatant, in accordance with a previously established protocol [82].

**Newcastle Disease Virus (NDV)**

Recombinant NDV harboring the F3aa (L289A) mutations and expressing the GFP reporter gene (rNDV/F3aa(L289A)-GFP (referred to herein as NDV) was engineered and rescued as previously described (11). The virus was amplified in embryonated pathogen-free chicken eggs (Charles River Laboratories) and purified by sucrose gradient.

**VSV-NDV**

For the engineered rVSV-NDV, the VSV Indiana strain (NCBI GenBank accession No. J02428.1) was used as a backbone. Only the VSV glycoprotein was replaced with the surface proteins (HN and F) of the NDV Hitchner B1 strain (GenBank accession No. AF375823). To increase oncolytic potency of the highly attenuated lentogenic Hitchner B1 NDV strain, a polybasic cleavage site had been introduced into the F protein to generate rNDV/F3aa [60]. To increase the fusogenicity of rVSV-NDV, a single amino acid had been substituted from leucine to alanine at amino acid 289 (L289A) in the F3aa-modified fusion protein [61].

**Virus Cloning**

To simplify genetic engineering of the pVSV-NDV and pVSV genome, a multi-cloning site (MCS), consisting of three restriction sites for the restriction enzymes AscI, KpnI and AvrII (NewEnglandBiolabs) was introduced between the HN and L gene or G and L gene, respectively. The forward and reverse primer pairs were synthesized at Metabion, Germany (Tab. 6) and digested at 37°C for 2 h with restriction enzymes PmeI and HpaI. Similarly, the plasmid was linearized by restriction digest with PmeI and HpaI (plasmid position 7158 and 7454, respectively). Digestion products were loaded on a 1% agarose gel and separated by size, so that digested products could be cut from the gel and purified (QIAEXII; QIAGEN) for ligation (Quick Ligation; NEB) and subsequent transformation of MAX Efficiency Stbl2 Competent Cells (Thermo Fisher Scientific) for plasmid production. Successful cloning was confirmed by a control digest and subsequent sequencing of the insert region. Cloning of transgenes into the plasmid backbone was performed analogously via two suitable restriction sites within the MCS (Fig. 12).

Table 6: Cloning primers.

| Gene Fragement | Forward Primer (5'-3') | Reverse Primer (5'-3') |
|---|---|---|
| MCS (KpnI, AvrII, AscI) | TGAACTACATTGTT<br>TAAACAGCTAGGCG<br>CGCCAGCAAGGTAC<br>CATACTTCCTAGGG<br>CTAGCGGCCTCAA<br>TTATAT | GGGATGGAGTTCTT<br>GAGATGTTAACA<br>TCGCTAT |
| GFP | ACTTAGAGGTACCT<br>ATGAAAAAAACTAA<br>CAGCAATCATGAG<br>CAAGGGCGAGGAAC | GGACGAGCTGTA<br>CAAGTGACCTAGG<br>ACTTAGA |
| Tyrosinase | ACTTAGAGGTACC<br>TATGAAAAAAACT<br>AACAGCAATCATGT<br>TCTTGGCTGTTTTG | GTATCAGAGCCATC<br>TGTAACCTAGGAC<br>TTAGA |
| Thymidine kinase | ACTTAGAGGCGCGC<br>CTATGAAAAAAACT<br>AACAGCAATCATGG<br>CTTCGTACCCCGGCC | GAGATGGGGGAGG<br>CTAACTGACCTAGG<br>ACTTAGA |
| soluble PD1-Fc | ACTTAGAACCGGT<br>TTGGCGCGCCTATG<br>AAAAAAACTAACA<br>GCAATCATGCAGAT<br>CCCACAGGCGCC | GCCTCTCCCTGTCT<br>CCGGGTAAATGACCT<br>AGG ACTTAGA |

**Virus Rescue**

For the generation of infectious recombinant VSV vectors, a reverse genetics system has been established [83]. Using a variation of this system, recombinant VSV-NDV vectors with modifications to the viral genome, or with foreign transgenes, can be rescued [40]. The first infectious virus particle is generated by infecting BHK-21 cells in a 6-well plate with a recombinant vaccinia virus expressing the phage T7 RNA polymerase (vTF7-3 [84]) for 1 h at room temperature (RT), followed by a lipofectamine transfection with the plasmid containing the full-length anti-genomic VSV-NDV cDNA (2 µg) as well as helper plasmids containing the maraba virus genes N (1 µg), P (0.8 µg), L (0.4 µg) and VSV-G (0.25 µg) driven by the T7 promoter (Fig. 10).

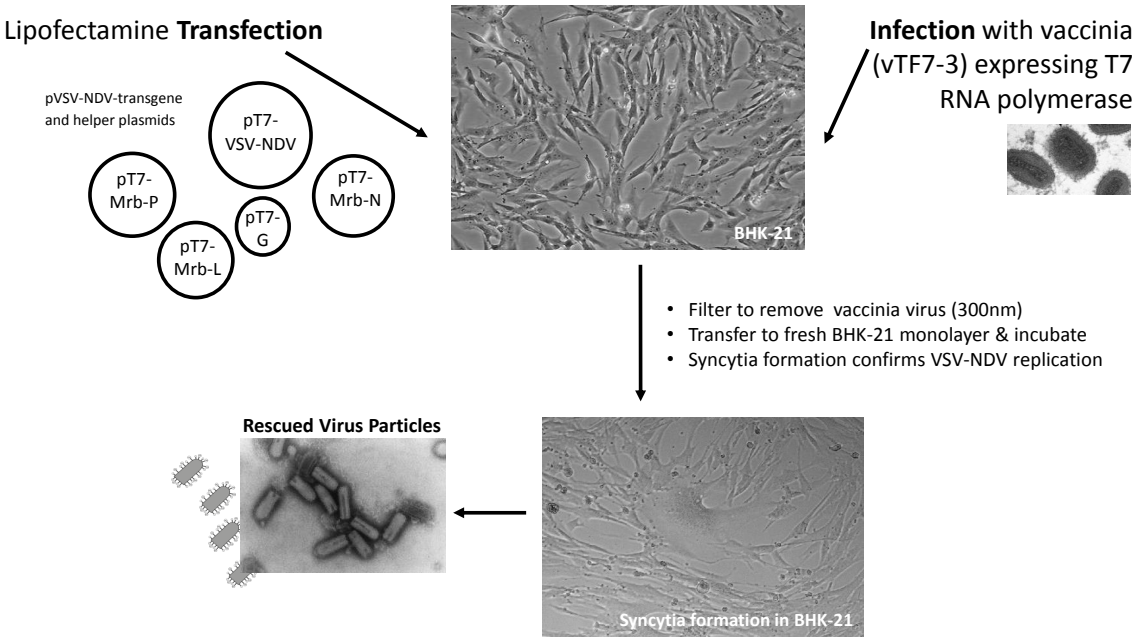


Figure 10: Set-up of the reverse genetics rescue system for VSV-NDV virions. BHK-21 cells are transfected with the cloned viral vector plasmid, as well as the maraba-derived rescue plasmids and co-infected with vaccinia virus expressing the T7 polymerase. After a 24 h incubation period, the supernatant is filtered and transferred to fresh BHK-21 cells to allow infection and syncytia formation by newly formed VSV-NDV virions.

48 h post-transfection cells are lysed via one freeze-and-thaw cycle, centrifuged (5 min, 10,000 x g) and filtered (0.22 µm filter) to remove cell debris and remaining vaccinia virus before transfer onto fresh BHK-21 cells. Wells that showed syncytia were harvested and plaque purified before large-scale virus production on AGE cells.

### Virus Production

For production, AGE cells were seeded into 15 cm dishes and confluent monolayers were infected with a multiplicity of infection (MOI) of 0.001 for 48 h at 37°C. Medium was then centrifuged and the supernatant directly used for ultracentrifugation, while the cell pellet from the medium was pooled with the cell monolayer harvested after a short incubation in 0.001% TritonX in PBS. Harvested cells were sonicated for 3 min and vortexed to lyse cells and free virions and then centrifuged to remove cell debris. These supernatants were then also used for ultracentrifugation. All ultracentrifugation steps were performed at 65,000 rcf for 1 h at 4°C. Pelleted virus was pooled and purified via a second ultracentrifugation over a sucrose gradient comprising 60, 30 and 10% sucrose solutions. The virus band was then isolated and aliquoted for *in vitro* use, or sucrose was removed by another ultracentrifugation step, followed by resuspending the virus pellet in PBS for *in vivo* experiments. Virus aliquots were stored at -80°C until use.

### 2.2.3 In Vitro Studies

**Growth Curves**

Growth curve analysis of virus replication in different cell lines (Huh7, B16-OVA, B16-F10 and HCCc27-14) was performed by measuring virus titers, as well as cytotoxicity at 16, 24, 48 and 72 h after infection. Cells were seeded at 70-80% confluency the day before infection. For infection, cells were incubated with either rVSV, rNDV or rVSV-NDV at the indicated MOI or PBS as negative control for 1 h at 37°C in PBS with $Ca^{2+}$ and $Mg^{2+}$. Cells were then washed 3x to remove remaining free virus particles, and the corresponding cell culture medium was added. For visualization, images of the infection progress were captured at 200x magnification on an Axiovert 40CFL microscope (Zeiss) at 16, 24 and 48 h post-infection, and representative images were captured with an AxioCam ICm1 camera (Zeiss) attached to the microscope.

Infectious virus titer is measured with a 50% Tissue Culture Infective Dose (TCID50) assay. A serial dilution of the sample in quadruplicate is added to a monolayer of AGE cells seeded in a 96-well format the day before. After 72 h incubation, infected wells were counted and calculation of the 50% endpoint titer was performed, according to the Spearman and Karber algorithm, in order to determine the concentration of infectious particles in the sample. As a baseline virus titer, a 0 h sample was taken from fresh medium directly after washing.

**Cytotoxicity**

For cytotoxicity determination, released lactate dehydrogenase (LDH) in cell culture supernatant was measured. The LDH assay was performed according to the manufacturer's protocol (CytoTox 96 Non-Radioactive Cytotoxicity Assay, Promega). In short, supernatant from cell culture experiments was incubated 30min with substrate diluted in assay buffer. After the incubation period a stopping solution was added and absorption at 450nm wavelength detected with a plate reader. All results were normalized to a maximum release control, i.e. one well of untreated cells were incubated for 15 min with lysis buffer.

As an alternative indirect measurement of cytotoxicity, the xCelligence system was used to continuously monitor resistance at the bottom of a specifically designed E-plate. The cell index represents the resistance and is influenced by attachment and morphology of adherent cells. This device, together with 16-well E-plates were kindly provided by ACEA Biosciences as part of a 6-month research grant. Different tumor cells were seeded one day prior to infection into the 16-well E-plate to establish attachment kinetics and baseline cell index. Virus was then added at MOI 0.1 at the indicated time, and the plate was incubated on the xCelligence for resistance monitoring.

**Co-Culture**

For co-culture experiments, tumor cells were seeded, infected the next day and incubated up to 24 h before T cell (OTI or transduced) addition. The number of TCR-transduced T cells for each indicated effector to target ratio was calculated according to the transduction rate in order to keep the ratios of antigen specific cells similar. The number of untransduced control T cells was adjusted accordingly. Cytotoxicity was measured by LDH analysis at indicated times after infection. T cell activation and tumor cell response were analyzed by flow cytometry.

**Flow Cytometry**

Flow cytometric analysis was performed using the CytoFlex platform. If not stated otherwise, all samples used were washed in PBS, incubated for 1 h at RT with one or more of the indicated staining antibodies (Tab. 7), washed again and analyzed.

Table 7: Reagents and Antibodies for Flow Cytometry

| **Reagents** | **Company** |
|---|---|
| CD3 - FITC | Miltenyi Biotec |
| CD4 - APC/Vio770 | Miltenyi Biotec |
| CD8 - APC (clone 53-6.7) | BioLegend |
| CD274 (PD-L1) - PE/Cy7 | BioLegend |
| MHC Class I (H2Db) | invitrogen |
| PD-1 PerCP Vio700 | Miltenyi Biotec |
| CD-25 - PE/Vio770 | Miltenyi Biotec |
| CD-69 - VioBlue | Miltenyi Biotec |
| TCR-beta7 chain - PE (clone H57-597) | eBiosciences |
| IFNgamma - FITC | eBiosciences |
| TNFalpha - PE/Cy7 | eBiosciences |
| Granzyme B - PE | Miltenyi Biotec |
| Viobility (405/520) Fixable Dye | Miltenyi Biotec |
| H-2Db SV40 large Tag (206-215) MHC-Tetramer-SAINNYAQKL-PE | MBL International |
| iTAg H-2Kb OVA MHC-Tetramer-SIINFEKL-PE | MBL International |
| T-Select H-2Kb VSV-NP(52-59) MHC-Tetramer-RGYVYQGL-PE | MBL International |
| FcR Blocking Reagent (mouse) | Miltenyi Biotech |
| UltraComp eBeads | ThermoFisher Scientific |

**Cytokine Array**

Analysis of cytokine release was performed with cell-culture supernatant and plasma samples from *in vivo* kinetics experiments. To allow the screening of multiple analytes, the Mouse Inflammation Panel (LEGENDplex, BioLegend) was chosen as a multiplex assay. This is a bead-based immunoassay, whereby a soluble analyte is captured between two antibodies and quantified by flow cytometry. Cell culture supernatant was prepared by centrifugation of the sample to remove debris. Samples were then stored at -20°C for later analysis.

**Western Blot**

Western blot analysis was used to confirm transgene expression in infected cells by determining synthesis of the corresponding protein. Cells were infected with different virus constructs and cultured in 24-well plates. To generate samples, cell culture supernatant was centrifuged to remove cell debris and then transferred to an Amplicon Ultra filter column with a 15kD cut-off and centrifuged for 30 min at 3000 x g in order to concentrate the medium. The cells, on the other hand, were incubated for 5 min in lysis buffer supplemented with protease inhibitor (Roche) to lyse the cells after a washing step in PBS. The lysates were then transferred into tubes and centrifuged for 10 min at 10,000 g to remove cell debris. Lysates and concentrated supernatants were transferred into new tubes and protein concentrations were determined using a Nanodrop spectrophotometer at a wavelength of 280 nm and adjusted if necessary. Loading dye was prepared by adding 10% of β-mercaptoethanol to loading buffer. Lysates were mixed with loading dye (1:1), and proteins were denatured at 95°C for 5 min. 10% polyacrylamide gels were used for optimal protein separation in the SDS-PAGE.

Before blotting, the polyvinylidene fluoride (PVDF) membrane was activated in methanol (1 min), washed in water (1 min) and then equilibrated in transfer buffer (OneStep, Bio-Rad) for at least 1 min. Finally, the gel was placed on the membrane and packed tightly into a suitable blotting device (semi-dry blotting) between Whatman blotting paper, so that the separated proteins could be transferred from the gel to the membrane in an electrical field. After successful transfer, non-specific binding sites were blocked by incubating the membranes with 5% milk diluted in PBS containing 0.2% Tween20 (PBS-T) for 1 h at room temperature. Specific primary antibodies were incubated with the membrane for 1 h at room temperature or overnight at 4°C. Primary antibodies were diluted in 1% milk in 0.05% PBS-T. After removal of unbound primary antibody, the membranes were washed three times in 0.2% PBS-T and incubated for 30 min with secondary antibodies coupled to horseradish peroxidase (HRP) and according to the production species of the primary antibody (Tab. 8).

Before detection, unbound secondary antibody was removed, membranes were washed three times in 0.2% PBS-T and incubated for 1 min in ECL solution prepared with Luminol, p-cumaric acid and Tris buffer. The chemiluminescent signal of specific protein bands was visualized using the ChemiDoc XRS+ imaging device (Bio-Rad).

Table 8: Western Blot Antibodies

| **Antibodies** | **Company** |
|---|---|
| anti-beta-actin (ms) | Sigma Aldrich |
| anti-beta-tubulin (rb) | Sigma Aldrich |
| anti-PD-1 (gt) | Cell Signaling Technology |
| anti-HSV-1 TK (gt) | Santa Cruz Biotechnology |
| anti-VSV-M [23H12] (ms) | Kerafast |
| anti-VSV-G (rb) | Rockland |
| goat-anti-mouse-HRP | JacksonImmuno Research Laboratories |
| goat-anti-rabbit-HRP | JacksonImmuno Research Laboratories |
| donkey-anti-goat-HRP | JacksonImmuno Research Laboratories |

### 2.2.4 In Vivo Studies

All animal experiments were performed in accordance with protocols approved by the institute's Center for Preclinical Research and the regional government commission for animal protection (Regierung von Oberbayern, Munich).

**Melanoma Survival**

Six-week-old female C57BL/6J mice were shaved and then injected with $2.4\times10^5$ (right flank) and $1.2\times10^5$ (left flank) B16-OVA cells subcutaneously. One week after tumor implantation (approximate tumor size 20 – 50 $mm^3$), the treatment was initiated. Treatment schedules for the experiments are provided with the results. Tumor width and length was measured regularly with a caliper and the volume calculated according to the modified ellipsoid formula: Tumor volume = $1/2(\text{length}\times\text{width}^2)$ [85]. Mice were monitored and euthanized at humane endpoints or at the latest with a tumor width or length reaching 15 mm. Survival times with respect to the first injection of treatment were plotted as a Kaplan-Meier survival curve, and median survival times were calculated.

**Melanoma Kinetics**

Six-week-old female C57BL/6J mice were shaved and then injected with $2.4\times10^5$ B16-OVA cells subcutaneously in the right and left flank. One week after tumor implantation (approximate tumor size 20 – 50 $mm^3$), the treatment was initiated. Treatment schedules for the experiments are provided with the results. Mice were euthanized at day 2, 5 and 8 after the first treatment. Tumors, blood and spleens were harvested. Tumors were cut in half, when possible. The first tumor half was fixed in 4% paraformaldehyde for 24 h, then another 24 h in 80% ethanol, before it was embedded in paraffin for immunohistochemistry and hematoxylin/eosin staining for analysis of necrosis. The second half was mashed through a 40 µm filter after 30 min incubation in 20µg/ml Liberase TM (Roche) and a single cell suspension was used for staining of infiltrating antigen-specific T cells for analysis by flow cytometry.

Blood was collected in EDTA-coated microvettes by heart puncture from mice euthanized on day 2, 5 and 8 after first treatment to analyze kinetics of the immune response. Samples were centrifuged for 10 min at 1,000 x g. Plasma was removed and stored at -80°C for later analysis. For the cytokine array, samples were thawed completely and centrifuged to remove particulates. After sample preparation, the assay was performed according to the manufacturer's protocol.

Harvested spleens were mashed through a 40 µm filter and incubated with red blood cell lysis buffer for 2 min. After washing with mTCM and a second filtering step, the single cell suspension of splenocytes was frozen in FCS + 10% DMSO at -80°C and thawed for the peptide activation assay.

**Peptide Stimulation Assay**

Splenocytes were isolated from animals treated according to the experimental schedule of the melanoma kinetics experiment. Frozen splenocytes isolated from mice on days 2, 5 and 8 after treatment were thawed in mTCM and incubated for 5 h at 37°C before $2\times10^6$ are added to a 96-well plate prepared with peptide solution at a final concentration of 1µg/ml OVA or TRP2 peptide. After 1 h incubation at 37°C, Brefeldin A was added to each well in order to prevent secretion of cytokines produced in response to peptide stimulation. After 15 h incubation at 37°C cells were transferred to a V-bottom 96-well plate and stained for extracellular CD4 and CD8, as well as intracellular IFN$\gamma$, TNF-$\alpha$ and granzyme B, after fixation and washing using BD Cytofix and Perm/Wash.

**HCC Survival**

In the transgenic Alb-SV40-TAg (AST) mouse model, the viral oncogene Simian Vacuolating Virus 40 large T antigen (S40-LTAg) is expressed under the control of the liver-specific albumin promoter, when a Cre recombinase–encoding adenovirus (Ad.Cre) with high tropism for the liver deletes a LoxP-flanked stop cassette [86]. This induces malignant transformation resulting in orthotopic HCC (Fig. 11). Its structural motif encodes a high-affinity pRb-binding domain inhibiting the retinoblastoma (pRb) and p53 tumor suppressor proteins. TAg binds to several other cellular factors, including the transcriptional co-activators p300 and CBP, which may also contribute to its transformation function [87]. Adenovirus vector encoding the cre recombinase (kindly provided by Martina Anton, Institute of Molecular Immunology, Klinikum rechts der Isar, Munich) was injected via the tail vein at a dose of $1\times10^8$ pfu (plaque forming units) in male mice of 6-8 weeks of age. Starting approximately 5-weeks post-injection, the mice were screened for HCC development in weekly anatomical T2-weighted magnetic resonance imaging (MRI) scans.

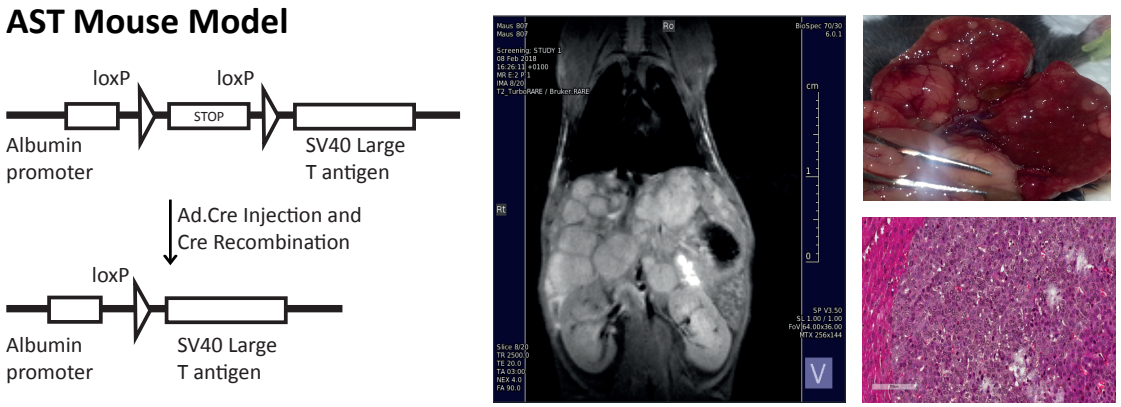


Figure 11: Hepatocellular carcinoma induction in AST mice via injection of adenovirus encoding the Cre Recombinase (Ad.Cre). Anatomical scans after 5-7 weeks by magnetic resonance imaging reveal multifocal lesions, that are localized within the liver due to the albumin promoter limiting oncogene expression. The lesions were also analyzed microscopically.

Treatment was started after the first detection of nodules with a minimum of 2 mm diameter, mice were randomized for treatment by tail vein injection with rVSV-NDV at a dose of $1\times10^7$ TCID50, or PBS in a 100 µl volume. Virus/PBS treatments were administered 3 times one week apart. On day 3 after the first treatment, TCR-transduced T cells were administered by tail vein injection at a dose of $1\times10^7$ cells/100 µl. Mice were monitored daily and euthanized at humane endpoints. Survival times with respect to the first injection of treatment were plotted as a Kaplan-Meier survival curve.

**Magnetic Resonance Imaging**

Abdominal images were acquired with a Mediso nanoScan 3T Positron Emission Tomography / Magnetic Resonance Imaging (PET/MRI) system (Mediso, Budapest, Hungary) using a 35 mm mouse body coil. A localizer scan was performed followed by a fast spin echo sequence in an axial orientation (TR/TE = 3000/55.5 ms, averages = 8, echoes per excitation = 8, slice thickness = 1 mm, matrix size = 192x128, field of view = 39x26 $mm^2$, respiratory triggering = on).

**Histology and Immunohistochemistry**

Tissue sections were fixed overnight in 4% paraformaldehyde, subsequently dehydrated and embedded in paraffin. 3 µm-thin slices were stained with hematoxylin-eosin or subjected to immunohistochemical staining using a rabbit monoclonal antibody against CD3, CD8, VSV-M (Cell Signaling Technology, Danvers, MA) on a Bond RX automated staining instrument (Leica). Analysis of pathological changes and confirmation of positive immunohistochemical reaction was performed by a certified pathologist to whom the respective treatment group of the specimen was not disclosed.

## 2.3 Statistical Analysis

Data were plotted and analyzed using GraphPad Prism 7.0 (GraphPad Software, San Diego, CA). Means and standard error of the mean (SEM) were plotted, when applicable. Data was analyzed for normal distribution by Shapiro-Wilk test and statistical significance was determined by Welch's ANOVA and Dunnett's T3 multiple comparisons test, when applicable. In some cases, observable differences statistical significance was determined by an unpaired t-test. Survival data was plotted in Kaplan-Meier curves and statistical significance calculated by log-rank test. Concerning significance, p-values of less than 0.05 were considered to be statistically significant (* $p < 0.05$, ** $p < 0.01$,*** $p < 0.001$, **** $p < 0.0001$) and for clarity only significant results were indicated in the graphs, if not stated otherwise.

# 3 Results

## 3.1 Advancing the VSV-NDV Platform

Development of an oncolytic platform such as VSV-NDV includes genetic engineering to advance the cytotoxic potential or immunotherapeutic effect, for example, by integrating therapeutic transgenes into the vector construct. Characterization of the virus platform is based on confirmation of transgene expression, as well as the analysis of effective replication and cytotoxicity in different cell lines. To simplify characterization *in vitro* and *in vivo*, viral vectors can be equipped with reporter transgenes that enable visualization by fluorescence microscopy or non-invasive imaging techniques.

### 3.1.1 Viral Cloning and Rescue

Based on the rVSV-NDV platform introduced by Abdullahi *et al.* [40], different transgene constructs were engineered (Fig. 12). For this purpose, a multiple cloning site was inserted between the HN and L genes to simplify the insertion of transgenes. The same cloning site was introduced into the wildtype VSV backbone to generate control constructs based on the VSV platform. The general cloning strategy is detailed in the methods section.

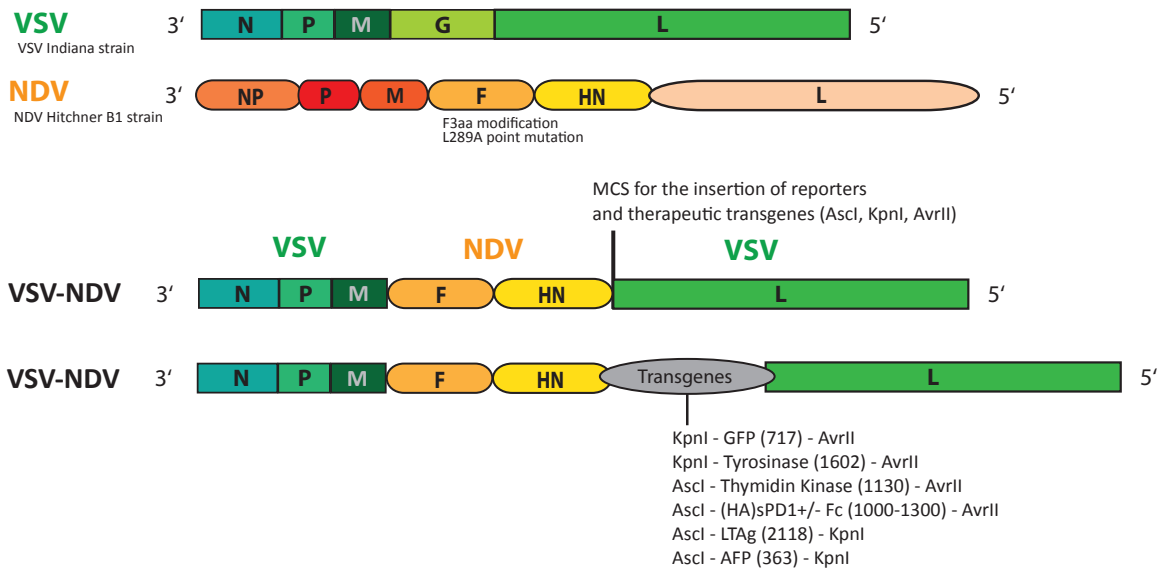


Figure 12: Genomic illustration of the hybrid VSV-NDV platform and its parental viruses VSV and NDV with modifications in the fusion protein prior to design of VSV-NDV. The multiple cloning site (MCS) as well as the mechanism of insertion of various transgenes is illustrated.

**VSV-NDV engineered to express GFP**

Using the multiple cloning site, a VSV-NDV vector encoding the gene for green fluorescent protein (GFP) was generated as a reporter virus to enable visualization of fusogenic infection. Successful cloning of GFP into the VSV-NDV construct was confirmed by sequencing (Eurofins, Munich). After virus rescue and purification, GFP expression by infected cells was confirmed via fluorescence microscopy (Fig. 13). Huh7 cells were infected with the different constructs VSV±GFP and VSV-NDV±GFP at MOI 0.01. The fusogenic effect and GFP expression were monitored over the course of the infection. As the representative images indicate, GFP signal correlates with syncytia formation in rVSV-NDV-GFP infected tumor cells.

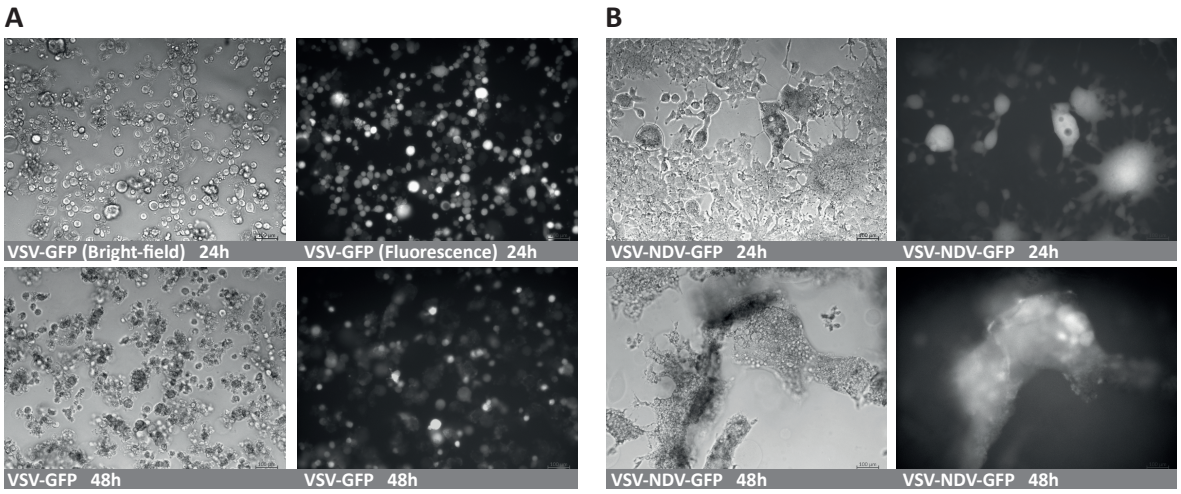


Figure 13: Confirmation of GFP expression. Huh7 cells infected with VSV±GFP (A) and VSV-NDV(VN)±GFP (B) were monitored over time. Representative images (10x) were captured 24 and 48 h after infection to illustrate GFP expression of infected cells with a fluorescence microscope (200x magnification).

**VSV-NDV engineered to express tyrosinase**

Another rVSV-NDV vector was designed to encode the tyrosinase gene conferring reporter as well as therapeutic functions. Tyrosinase (Tyr) is a copper-containing enzyme that controls the production of melanin in melanocytes by catalyzing multiple steps in melanogenesis from tyrosine. Stritzker *et al.* established targeted melanin overproduction in tumor cells through a recombinant vaccinia vector expressing tyrosinase as a reporter for optoacoustic imaging and MRI in live animals. Virus-mediated melanin production was used as a theranostic mediator combining diagnosis and therapy in a single agent. The therapeutic effect stems from the suitability of melanin as a target for laser-induced thermotherapy, which enhanced oncolytic virotherapy [88].

In a similar approach, rVSV-NDV-Tyr was constructed to enable the monitoring of virus replication and spread throughout the tumor *in vivo* using non-invasive imaging. Testing the imaging capabilities and additional therapeutic benefits of VSV-NDV-Tyr were beyond the experimental scope of this thesis, but are part of an ongoing project. Successful cloning of the *TYR* gene into the VSV-NDV construct was confirmed by sequencing (Eurofins, Munich). After virus rescue and purification, tyrosinase expression by infected cells was demonstrated using microscopy (Fig. 14).

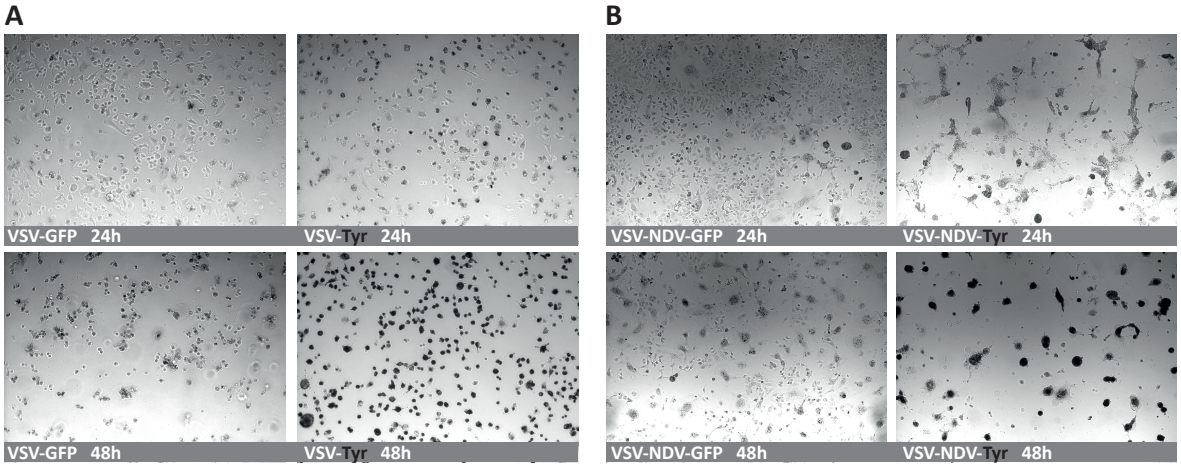


Figure 14: Confirmation of tyrosinase expression. Huh7 cells infected with VSV±Tyr (A) and VSV-NDV (VN)±Tyr (B) were monitored over time. Representative images (100x magnification) were captured 24 h and 48 h after infection to illustrate melanin accumulation as a result of tyrosinase overexpression.

Huh7 cells were infected with the different constructs VSV±Tyr and VSV-NDV±Tyr at MOI 0.01. The cytopathic effect and production of melanin were monitored over the course of the infection. As the representative images indicate, melanin formation could be visualized via microscopy only in cells infected with the tyrosinase-expressing viruses. An increase in melanin over time suggests accumulation of the protein in dying cells.

**VSV-NDV engineered to express HSV-TK**

A rVSV-NDV vector was also designed to encode a mutant HSV-1 thymidine kinase (HSV-TK) gene conferring reporter as well as therapeutic functions. Thymidine kinase is an enzyme that catalyzes phosphorylation. When viral HSV-TK is present in cells, a wide range of substrates is phosphorylated, including radioactive tracers introduced for non-invasive positron emission tomography (PET) [89].

Additionally, HSV-TK can function as a "suicide gene" in that TK expressing cells are susceptible to ganciclovir treatment as shown in a phase I clinical trial in advanced HCC [90]. An HSV-TK mutant, HSV1-sr39TK, created by random sequence mutagenesis, showed increased accumulation (net uptake) of radioactively labeled substrates and increased imaging sensitivity [91]. The rVSV-NDV construct expressing sr39TK was based on the VSV-sr39TK vector designed by Munoz-Alvarez *et al.* in 2015 [92]. Here, the vector was used to enable PET imaging in a preclinical HCC rat model. Testing the imaging capabilities and additional therapeutic benefits of rVSV-NDV-sr39TK were beyond the experimental scope of this thesis, but are part of an ongoing project.

Western Blot analysis of cell lysates was performed to confirm expression of TK from VSV-NDV-TK-infected cells (Fig. 15).

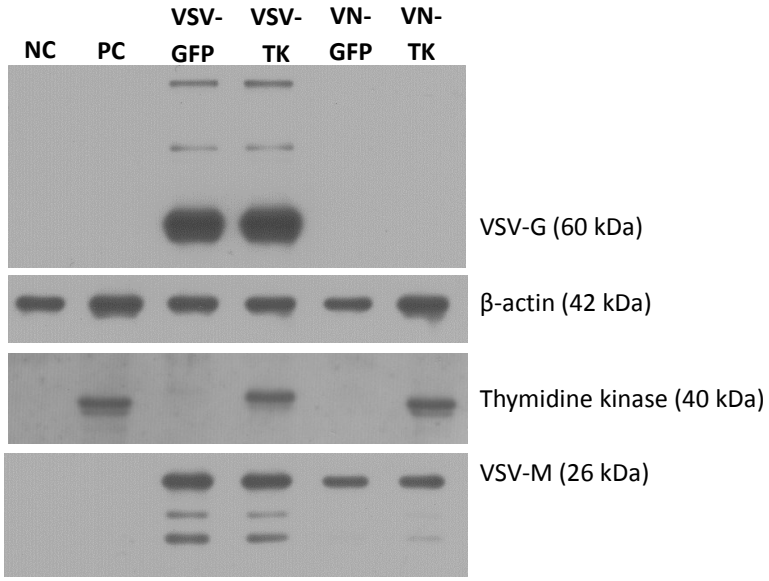


Figure 15: Confirmation of viral protein and TK expression by western blotting. Huh7 cells were infected with VSV±TK and VSV-NDV (VN)±TK at MOI 0.01 for 24 h. For a positive control (PC), Huh7 cells were transfected with a TK expression plasmid for 24 h. Untreated cells were used as negative control (NC). The cells were harvested, lysed and 50µg of protein used for western blot analysis.

Huh7 cells were infected with the different constructs VSV±TK and VSV-NDV±TK at MOI 0.01. Cells were harvested 24 h after infection, lysed and loaded onto a gel for SDS-PAGE. Untreated cells were used as a negative control (NC) for loading, while cells transfected with an HSV-TK expression plasmid served as a positive control (PC). The cytoskeletal protein β-actin was stained to ensure the equal loading of protein.

As expected, HSV-TK expression could only be detected in the positive control or cells infected with either VSV-TK or VSV-NDV-TK. To confirm VSV-G deletion of the rVSV-NDV constructs, viral proteins were also analyzed by western blotting. As expected, only VSV infection induced glycoprotein expression (VSV-G), while both VSV and VSV-NDV infection led to expression of the matrix protein (VSV-M).

**VSV-NDV engineered to express soluble PD-1 variants**

As introduced previously, immune checkpoint inhibition has become an important pillar of cancer immunotherapy. Checkpoint inhibitors are replacing standard therapeutic options for an increasing number of tumor types. In general, inhibitors approved for the clinic are monoclonal antibodies targeting CTLA-4, PD-1 or PD-L1. Administered systemically, they can have undesirable side effects, including the more common dermatological and gastrointestinal events, as well as less common toxicities associated with endocrine, hepatic, and neurological events. A meta-analysis revealed the incidence of immune-related adverse events could be as high as 65% [93].

It has been shown that localized expression of PD-1 in the tumor after infection with an engineered myxoma virus conveyed checkpoint inhibitor functions while minimizing off-target effects [94]. The mechanism of this approach is illustrated in Figure 16.

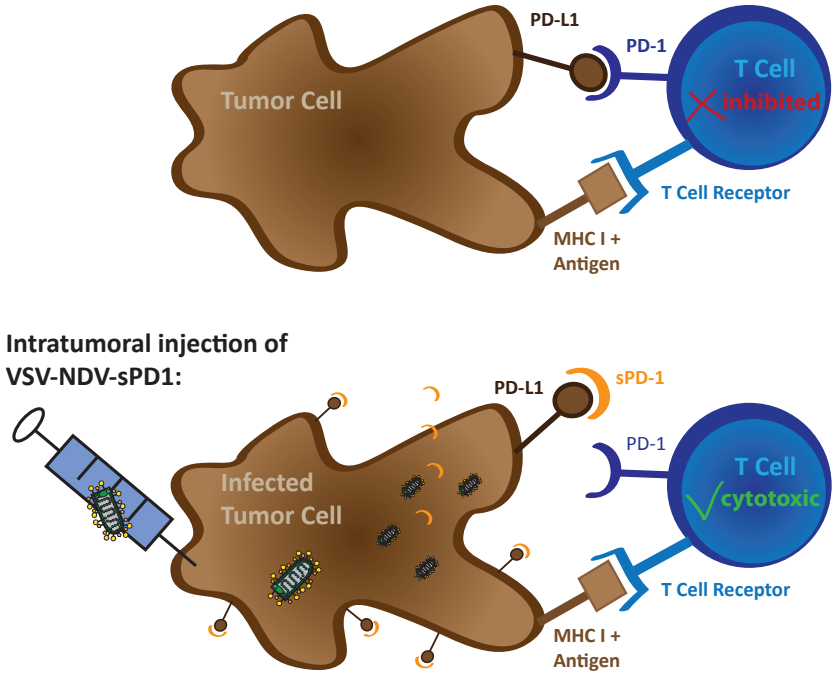


Figure 16: Mechanism of localized expression and release of soluble PD-1 (sPD1) infected tumor cells as opposed to active checkpoint inhibition. By saturating PD-L1 binding sites on the tumor cell surface with soluble PD1, activated T cells expressing PD-1 are no longer inhibited by PD-1/PD-L1 interaction, unleashing the anti-tumor immune response.

In a similar approach, the extracellular part of the human PD1 gene (bases 1-170) was inserted into the VSV-NDV backbone in order to enable the localized expression and secretion of PD-1 from infected tumor cells. Secreted PD1 can block PD-L1 expressed on tumor cells and inhibit the PD1/PD-L1 interaction of T cells and tumor cells, thereby alleviating T cell suppression. To stabilize the soluble protein, an Fc-fusion protein was created by combining sPD1 with the human IgG1-Fc1 (pFUSE-hIgG1-Fc1 by InvivoGen). The Fc region comprises the CH2 and CH3 domains of the IgG heavy chain and the hinge region. The hinge serves as a flexible spacer between the two parts of the Fc-fusion protein. Human IgG1 displays high antibody-dependent cellular cytotoxicity (ADCC) and complement-dependent cytotoxicity (CDC), and was designed for stabilization and potential benefit in human patients.

To improve sPD1 binding, the high affinity mutant with an A132L mutation described in detail by Lázár-Molnár *et al.* was also integrated into VSV-NDV backbone. In comparison to the wildtype, the high affinity mutation enhanced PD1 binding to human PD-L1 45-fold. The high affinity mutant also led to a 23-fold increase of PD1 binding to murine PD-L1 [95].

The four virus constructs, rVSV-NDV-sPD1±Fc and rVSV-NDV-HAsPD1±Fc, were rescued, produced and purified for a first characterization. Comparing the rVSV-NDV-sPD1 variants and testing their therapeutic benefit were beyond the experimental scope of this thesis, but are part of an ongoing project partly performed by and included in the thesis of Janina Marek.

Western Blot analysis of cell lysate was performed to confirm expression of the sPD1 variants. The secretion of soluble PD1 was verified using concentrated cell culture supernatant from infected cells for Western Blot (Fig. 17).

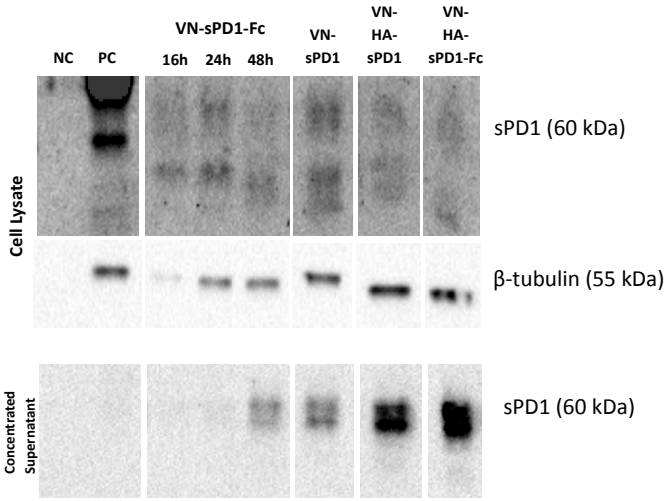


Figure 17: Confirmation of sPD1 expression and secretion by infected cells via western blotting. Huh7 cells were infected with the indicated viruses (MOI 0.01) for up to 72 h. Representative kinetic of sPD1 expression is shown for VSV-NDV (VN)-sPD1-Fc (16, 24 and 48 h). For a positive control (PC), Huh7 cells were transfected with an PD1 expression plasmid for 48 h. Untreated cells were used as negative control (NC). The cells were harvested and lysed, while supernatant was concentrated using Amplicon Ultra filters. 50µg of protein was used for western blot analysis.

Huh7 cells were infected with the variants VSV-NDV-sPD1±Fc and VSV-NDV-HAsPD1±Fc at MOI 0.01. Cells and supernatant were harvested at the indicated times after infection. Cells were lysed, supernatant concentrated, and then both were loaded onto a gel for SDS-PAGE and subsequent blotting onto a membrane to allow antibody staining (for details see the Materials and Methods section). Untreated cells were used as a negative control (NC) for loading, while cells transfected with a PD-1 expression plasmid served as a positive control (PC). The cytoskeletal protein β-tubulin was stained to ensure the equal loading of protein.

PD1 protein was detected in the cell lysate over the course of the infection, while secreted protein could only be detected during the late stages of infection. For VSV-NDV-(HA)sPD1 and VSV-NDV-HAsPD1-Fc secretion was confirmed at 48 h and 72 h, respectively. Differences of secretion could indicate a delayed replication.

In summary, VSV-NDV is a versatile platform that can be engineered to express various transgenes. Reporter transgenes enable visualization by fluorescence microscopy or non-invasive imaging techniques. Since transgene expression could interfere with virus replication or alter the cytotoxic effect, these parameters are examined in more detail in the following section.

### 3.1.2 Viral Oncolysis of Human Cancer Cell Lines by VSV-NDV

**Virus replication was affected by transgene expression**

After successful cloning of the constructs, rescue of the viruses and confirmation of transgene expression, virus replication and cytotoxic efficacy were characterized. Viral growth curve analysis was performed via infection of the Huh7 cell line and compared to the original rVSV-NDV. Cells were infected for 1 h and then incubated to take supernatant samples for TCID50 and LDH assay.

Virus titer was determined by TCID50 analysis (Fig. 18 A). In comparison to the original VSV-NDV, VSV-NDV-GFP showed no appreciable difference in replication kinetics, while replication of VSV-NDV-Tyr and VSV-NDV-HAsPD1-Fc seems delayed, but eventually reach similar titers.

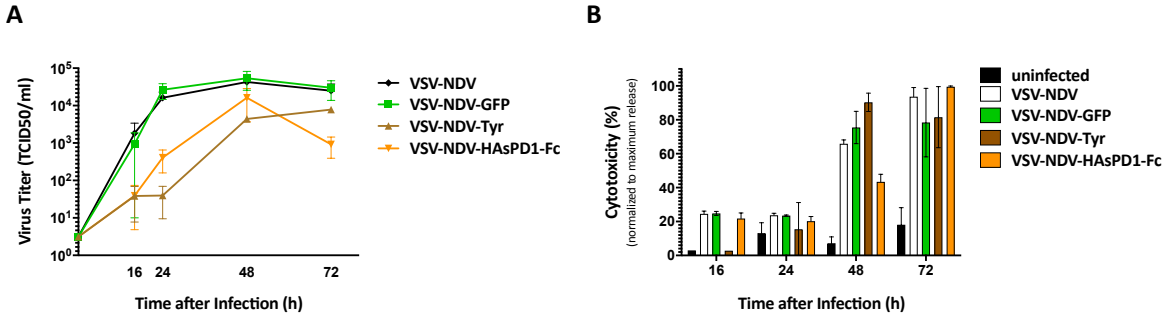


Figure 18: Growth curves of VSV-NDV variants and their cytotoxic potential in Huh7 cells. (A) Huh7 cells were infected with VSV-NVD variants and virus titer in the supernatant was determined 0, 16, 24, 48 and 72 h after infection via TCID50. (B) Cytotoxicity is analyzed via LDH measurements in the supernatant at 16, 24, 48 and 72 h post infection. Results were normalized to a maximum release control and cytotoxicity was plotted as mean±SEM.

Virus-mediated cytotoxicity was determined by LDH assay (Fig. 18 B). While VSV-NDV-Tyr showed delayed replication, no difference in terms of cytotoxicity was detected. The acceleration of cell death may be explained the cytotoxicity and antiproliferative activity of tyrosinase induced by quinone generation [96]. This effect has been leveraged to use tyrosinase as a prodrug catalyst in the treatment of melanoma [97]. In comparison with the original rVSV-NDV, only VSV-NDV-HAsPD1-Fc seemed to induce delayed replication together with a delayed cytotoxic effect. Since the insert was not expected to confer an additional cytotoxic effect in this experimental set-up, the delay in cytotoxicity could be attributed to slower replication kinetics.

**VSV-NDV-GFP induced cytotoxicity in a wide range of tumor cell lines**

An advantage of oncolytic viruses is their broad tumor tropism, potentially enabling the treatment of various tumor types. In order to investigate the susceptibility of different tumor types to VSV-NDV infection, the xCelligence RTCA DP system was used to monitor VSV-NDV-GFP-induced cytotoxicity, as a function of impedance, continuously over 72 h. Six different human tumor cell lines representing HCC (Huh7, HepG2) and pancreatic cancer (PSN-1, PatuT, MiaPaCa, BxPC3) were screened for VSV-NDV susceptibility. Cells were seeded one day prior to infection into a 16-well E-plate (part of the 6-month research grant kindly awarded by ACEA Biosciences), virus was then added at MOI 0.1 at the indicated time, and the plate incubated to detect changes in morphology and attachment of the cells indicated by the cell index (Fig. 19).

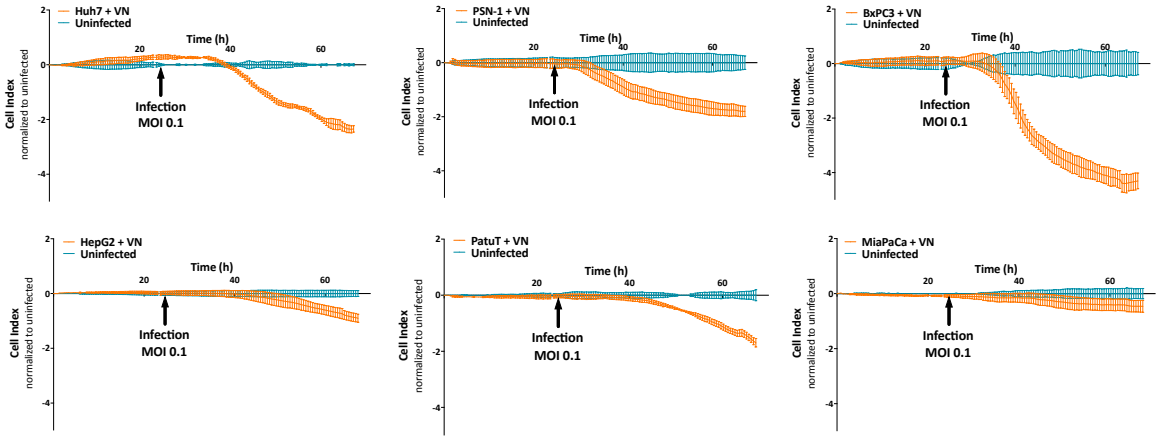


Figure 19: Continuous monitoring of VSV-NDV-GFP (VN) infection at MOI 0.1 in different cell lines via impedance monitoring. Changes in morphology and attachment of the six indicated tumor cell lines are represented by the cell index, a representative value of resistance measured on the bottom of each well. Results were normalized to an uninfected control and performed in duplicate.

All cell lines responded to VSV-NDV-GFP infection, although to varying degrees. The Huh7 cell line had been closely investigated in the context of VSV-NDV infection (Fig. 18) and was used as a positive control. PSN-1 showed a similar cell index kinetic, while infection of BxPC3 resulted in higher cell index values, which might indicate a greater detachment ratio of the infected population. PatuT and HepG2 seemed to show a delayed and decreased effect of VSV-NDV infection, despite visible syncytia formation, indicating that resistance monitoring is not sensitive enough to detect the morphologic changes involved in syncytia formation without considerable detachment in the early stages. Only the MiaPaCa cell line did not seem to respond to VSV-NDV infection, as confirmed by microscopic analysis (data not shown).

The mechanism behind the cell line-dependent susceptibility to VSV-NDV infection, replication and cytotoxicity are not entirely understood and need to be studied in more detail to enable a prediction of the cytotoxic effect of VSV-NDV in a specific tumor type. First experiments indicate that several mechanisms, including receptor expression and type I IFN, as well as apoptotic signaling, might be involved.

In summary, VSV-NDV variants expressing different transgenes typically maintained their replicative and cytotoxic potential. Only for the VSV-NDV construct encoding HAsPD1-Fc a delay was observed. In general, its broad tropism allowed infection of numerous tumor cell lines. rVSV-NDV-GFP was used in most experiments throughout this thesis, because of its reporter advantages that did not interfere with replication and cytotoxic potential. The reasons for cell-line dependent differences in replication and cytotoxicity need to be further investigated.

## 3.2 Combination Approach: Melanoma Model

The main focus of this doctoral thesis is the evaluation of a combination approach of the VSV-NDV platform with adoptive T cell transfer. The first examination of the combinatorial effects was performed in the well-established melanoma model that is based on the murine B16 melanoma cell line. The cell line can be subcutaneously implanted in syngeneic C57BL/6J mice and has been characterized in depth *in vitro* and *in vivo* [98]. B16 cells were transduced to stably express ovalbumin, a protein found in chicken eggs. Ovalbumin consists of 385 amino acids and gives rise to peptides, such as the immune dominant SIINFEKL ($OVA_{275–264}$), that can be targeted by cytotoxic T cells.

The OTI mouse has been genetically engineered to produce only SIINFEKL-specific TCR T cells, that can be isolated from the spleen and used in adoptive cell transfer experiments. This convenient set-up was used to evaluate combination therapy in a first proof-of-concept study to ensure feasibility and efficiency of the approach before moving into a more complex, but clinically more relevant animal model.

In the following section, viral infection, replication and cytotoxicity of B16 tumor cells will be examined. Additionally, the cytotoxic effect of OTI T cells on B16 tumor cells will be confirmed *in vitro* in preparation for combination experiments in co-culture. Furthermore, the experimental set-up for *in vivo* survival and kinetics experiments will be introduced, and data will be presented to characterize the therapeutic outcome of the combination approach.

### 3.2.1 Viral Oncolysis of Murine Melanoma Cells

In a first step, tumor cell lysis induced by VSV-NDV and effector T cells was analyzed separately, in order to allow assessment of the combinatorial mechanism of action later. VSV-NDV infection, replication and cytotoxicity was characterized in B16-OVA and B16-F10 tumor cells in comparison with the parental viruses, VSV and NDV. Isolated and cultured OTI splenocytes served as effector T cells. Their cytotoxic effect is well established and was confirmed in a simple co-culture experiment.

#### B16 cells were susceptible to VSV-NDV infection

Virus replication and cytotoxic efficacy in the B16 cell lines were characterized by performing growth curve analysis. The cells were seeded one day prior to infection, then infected at different MOIs for 1 h at 37°C and incubated to take samples for TCID50 and LDH assay. To visualize differences in VSV-NDV, VSV and NDV infections, representative images of B16-OVA cells were captured 16 h after infection (Fig. 20).

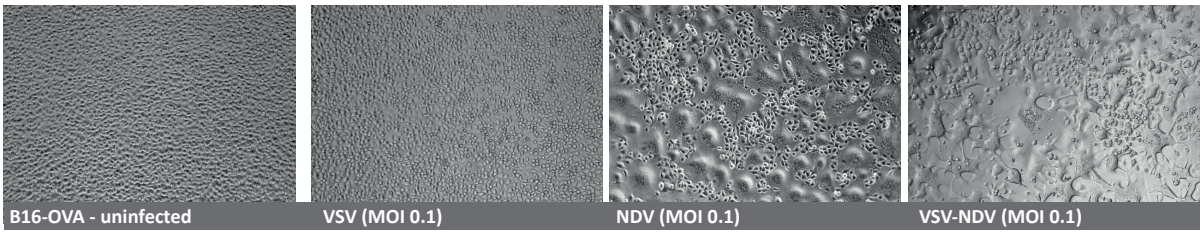


Figure 20: Morphological differences of the cytotoxic effect induced by VSV as opposed to the fusogenic viruses NDV and VSV-NDV in B16-OVA cells. Representative images (100x magnification) were captured 16 h after infection with the indicated viruses (MOI 0.1).

As expected, the syncytia formation caused by the expression of the fusion protein from cells infected with NDV and VSV-NDV can be clearly distinguished from the cytopathic effect induced by VSV that is typically characterized by rounding of infected cells. The visible differences in syncytia formation between VSV-NDV and NDV infected cells might indicate variations in the replication cycle, since VSV-NDV replication depends on the VSV part of the hybrid genome. To analyze replication kinetics, virus titer was determined for growth curve analysis.

Virus titers in supernatants of infected B16-OVA cells were determined by TCID50 analysis (Fig. 21 A). VSV, NDV and VSV-NDV reached their peak in virus titers by 24 h after infection. VSV replication was the most effective, reaching and maintaining the highest titers. Interestingly, the VSV-NDV growth kinetics were not substantially affected by the MOI used for infection, in that no dose-responsive differences in titers were observed. The slight decline in virus titers over time was indicative of rapid cell death, which was confirmed by the cytotoxicity results, as determined by LDH assay (Fig. 21 B). VSV-NDV's cytotoxic effect in B16 cells was dose-dependent on the MOI upon infection. In B16-OVA cells VSV-NDV induced cell death was detected already 16 h after infection for MOIs 1 and 0.1 and VSV-NDV at MOI 0.01, while VSV and NDV follow 24 h and 48 h after infection, respectively.

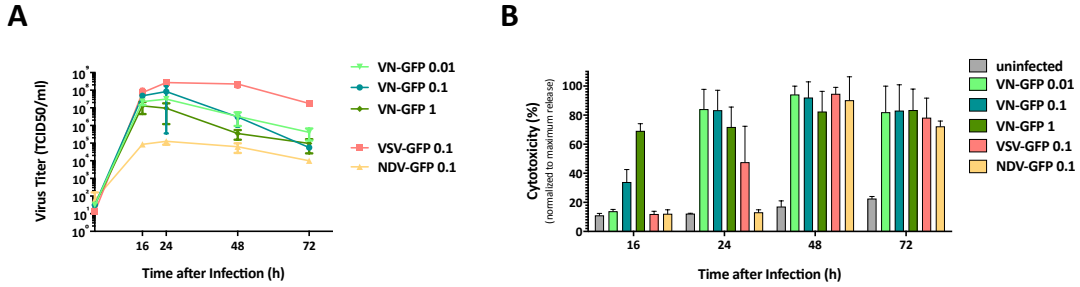


Figure 21: Comparison of VSV-NDV, VSV and NDV infection in the murine melanoma cell line, B16-OVA. (A) Growth curves demonstrate replication in B16 cells by viral titer analysis in supernatants at 0, 16, 24, 48 and 72 h post infection determined via TCID50. (B) Cytotoxicity was measured via LDH concentration in supernatants of infected cells 16, 24, 48 and 72 h after infection. Results were normalized to a maximum release control and cytotoxicity was plotted as mean±SEM of triplicate experiments.

The B16-F10 cell line was also analyzed for susceptibility to VSV-NDV infection. Due to its lack of OVA expression, it was used as a control cell line in later co-culture experiments.

In B16-F10 cells VSV, NDV and VSV-NDV reached their peak virus titer 24 h after infection, although the titers were approximately 10-fold lower for all viruses compared to B16-OVA infection (Fig. 22 A). The cytotoxic effect on B16-F10 cells also seemed to be delayed compared to B16-OVA cells, as determined by LDH assay (Fig. 22 B). The data indicates differences in susceptibility, possibly due to cell cycle variation or changes affecting viral replication due to the OVA transduction.

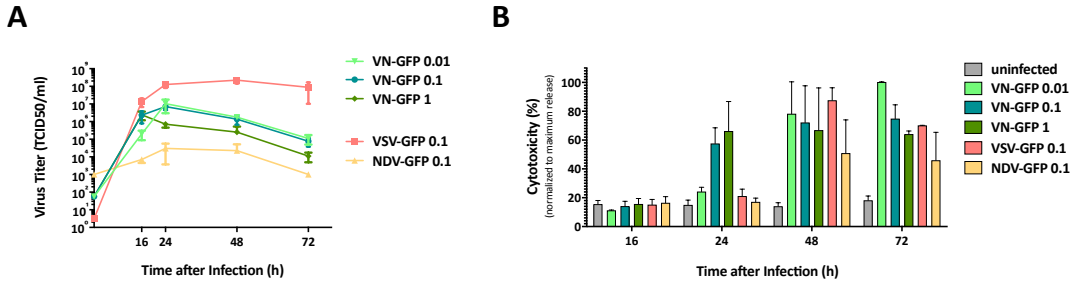


Figure 22: Comparison of VSV-NDV, VSV and NDV infection in the murine melanoma cell line, B16-F10. (A) Growth curves demonstrate replication in B16 cells by viral titer analysis at 0, 16, 24, 48 and 72 h post infection determined via TCID50. (B) Cytotoxicity is measured via LDH concentration in supernatants of infected cells 16, 24, 48 and 72 h after infection. Results were normalized to a maximum release control and cytotoxicity was plotted as mean±SEM.

In summary, the B16 cell lines are susceptible to virus infection, support VSV-NDV replication, and VSV-NDV induces rapid and potent tumor cell killing effects. Overall, the B16-OVA cell line seems to be slightly more susceptible to VSV-NDV infection than the B16-F10 cells. In the next section, the potency of antigen-specific T cells targeting an OVA peptide will be examined.

### 3.2.2 T cell-dependent Oncolysis of Murine Melanoma Cells

In order to assess combinatorial effects, viral and T cell effects were first characterized separately. The homozygous OTI mice produce mostly T cells expressing transgenic Tcra-V2 and Tcrb-V5 T cell receptor chains in order to recognize the SIINFEKL peptide (ovalbumin residues 257-264) in the context of the H-2K$^d$ MHC class I alloantigen. OTI T cells were isolated from splenocytes derived from OTI mice, aliquoted and frozen in 10% DMSO in FCS for later use. OTI T cells were expanded for one week prior to the experiments. Here, the effect of OTI T cells on B16-OVA tumor cells was analyzed.

**OTI T cells induced a dose-dependent cytotoxic effect in target cells**

OTI functionality was determined in co-culture experiments with antigen-expressing B16-OVA tumor cells. Tumor cells were seeded and incubated 24 h before OTI T cells were added to the co-culture at different effector-to-target ratios. LDH assay was performed to measure their cytotoxic effect after 24 h (Fig. 23). Unspecific T cells isolated from C57BL/6J mice were used as a negative control. As expected, unspecific T cells were unable to inhibit tumor cell proliferation, while OTI T cells specifically recognized and rapidly eliminated B16-OVA tumor cells in a dose-dependent manner.

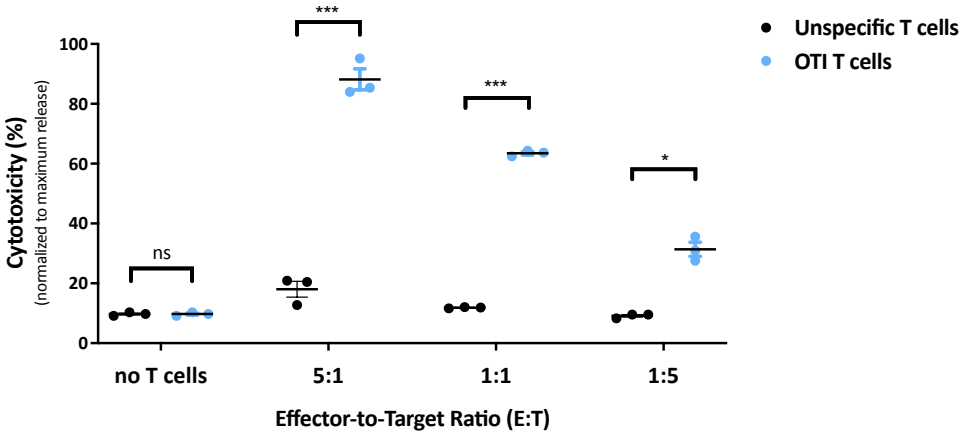


Figure 23: Cytotoxicity of OTI T cells co-cultured with B16-OVA tumor cells at different effector-to-target ratios. Tumor cells were seeded and incubated for 24 h before OTI T cells were added to the co-culture. 24 h later LDH was measured to determine the cytotoxic effect. Unspecific splenocytes were used as a negative control. Results were normalized to a maximum release control and cytotoxicity was plotted as individual values of triplicate experiments. Normal distribution was confirmed by Shapiro-Wilk test and statistical significance was determined by Welch's ANOVA and Dunnett's T3 multiple comparisons test (ns: not significant, * $p < 0.05$, *** $p < 0.001$).

In summary, the B16 melanoma cell lines were very susceptible to cell death induced by both VSV-NDV and OTI T cells. After assessing viral and T cell oncolysis separately, the next section focuses on their combination in order to evaluate additive, or possibly synergistic, effects on cytotoxicity of tumor cells *in vitro*.

### 3.2.3 Combination Co-Culture with Murine Melanoma Cells

B16 tumor cells were susceptible to both VSV-NDV and OTI T cell treatment alone, leaving a small window for therapeutic improvement *in vitro*. As tumor clearance is a lot more difficult to achieve *in vivo*, *in vitro* combination effects may not reflect the full potential of this approach. In preparation of the animal experiments, tumor cells were pre-infected with VSV-NDV to induce immunogenic cell death in order to complement OTI T cell effects by accelerating recruitment and activation.

**OTI co-culture with tumor cells benefited from oncolytic virus activity**

To examine combination effects, cytotoxicity was measured via LDH assay from co-culture supernatant in various conditions (Fig. 24). B16 cells were seeded one day prior to infection, then infected with VSV-NDV-GFP at MOI 0.1, and OTI T cells were added in a 1:1 effector-to-target ratio at the indicated times. Combination and monotherapy were first examined in co-culture with B16-OVA cells (Fig. 24 A). Here, the combination showed a slight increase in cytotoxicity, that is not statistically significant compared to the monotherapies, as they also induced rapid cell elimination of B16-OVA cells and after 16 h no differences in cytotoxicity was detected (data not shown).

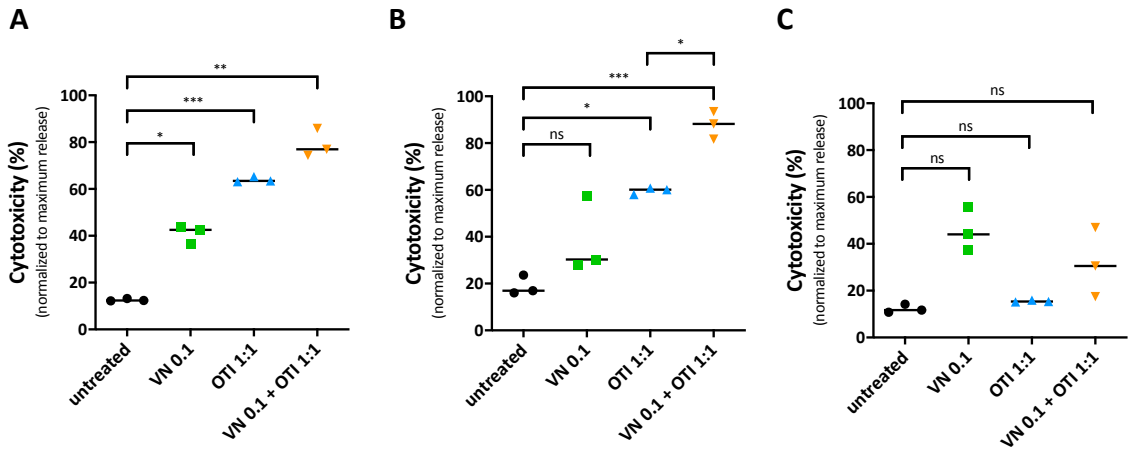


Figure 24: Cytotoxicity of OTI T cells in co-culture with VSV-NDV-infected B16 tumor cells. (A) B16-OVA cells were infected at MOI 0.1 with VSV-NDV-GFP (VN) and incubated for 16 h, before OTI T cells were added at an effector-to-target ratio of 1:1. After 8 h cytotoxicity was determined by LDH assay. (B) In a similar experimental set-up, a mixed tumor cell population of B16-OVA and B16-F10 cells (1:1) was used. Cytotoxicity was determined 16 h after OTI addition. (C) B16-F10 cells were used as a negative control. Cytotoxicity was measured 24 h after OTI addition. All results were normalized to a maximum release control and data plotted as means (n=3). Normal distribution was confirmed by Shapiro-Wilk test and statistical significance was determined by a Welch's ANOVA and Dunnett's T3 multiple comparisons test (ns: not significant; * $p < 0.05$, ** $p < 0.01$,*** $p < 0.001$).

In the artificial cell culture environment, B16-OVA tumor cells were used that express ovalbumin and are thus recognized and eliminated by OTI T cells in co-culture. To account for the presence of tumor cells not expressing the correct antigen, a situation to be expected *in vivo*, B16-OVA and B16-F10 cells were mixed at a 1:1 ratio before seeding (Fig. 24 B). In this set-up, the combination had the ability to improve cytotoxicity further even at later timepoints (16 h after OTI addition), since OTI T cells were only able to recognize half the tumor cells. As documented in Fig. 22, B16-F10 cells show a slight reduction in susceptibility compared to VSV-NDV infection of B16-OVA. To account for these differences, infection times were adapted to the specific cell line/cell line mix, in order to ensure similar progress of infection before addition of T cells. Still, a reduction in cytotoxicity induced by VSV-NDV monotherapy can be observed.

As a negative control, B16-F10 cells alone were used in these co-culture experiments (Fig. 24 C). To account for the difference in virus susceptibility, in this case, the co-culture was incubated for 24 h after OTI addition before samples were taken for LDH assay. As expected, OTI T cells alone had no effect, while VSV-NDV induced cytotoxicity. Although not significant, cytotoxicity in combination seems to be slightly decreased compared to virus treatment alone, possibly indicating a basal cytokine release from OTI T cells even without antigen-recognition that slightly inhibits virus replication and spread. This will be investigated further in the next section by taking a closer look at OTI T cell-induced IFN$\gamma$ release and production of other cytokines.

**OTI T cell recognition of B16-OVA cells resulted in activation and cytokine release that was not affected by pre-infection with VSV-NDV**

An important aspect of combination therapy is to understand implications the treatment approach could have on the immune system and its activation and/or suppression. For co-culture experiments, tumor cells were seeded one day prior to infection. Cells were infected at MOI 0.01 for 16 h, before OTI T cells were added. Supernatant was harvested 24 h after T cell addition in order to characterize cytokine secretion via a 13-plex bead array (BioLegend). B16-F10 cells served as a negative control for cytokine release in response to co-culture with OTI T cells, while VSV-NDV-induced cytokine release or induced change in activation should be independent of the cell line.

T cell activation in response to antigen recognition typically induce IFN$\gamma$ production. This was confirmed by the detection of IFN-$\gamma$ release after OTI T cell co-cultured with target B16-OVA, but not B16-F10 cells (Fig. 25). Similarly, although to varying degrees, the inflammatory cytokines TNF-$\alpha$, MCP-1, GM-CSF and IL-6 were released only upon T cell recognition of target cells.

IFN-β was the only cytokine induced by VSV-NDV infection, since it was induced in B16-OVA as well as the B16-F10 control cell line not recognized by OTI T cells. As part of the type I IFN family, IFNβ is well-established in the innate immune pathway of intracellular virus sensing and as a first responder during infection, explaining its release in response to VSV-NDV. No differences were detected for the remaining cytokines, i.e. IL-1α, IL-1β, IL-10, IL-12p70, IL-23, IL-27 (data not shown). VSV-NDV pre-infection did not alter cytokine release in co-culture experiments.

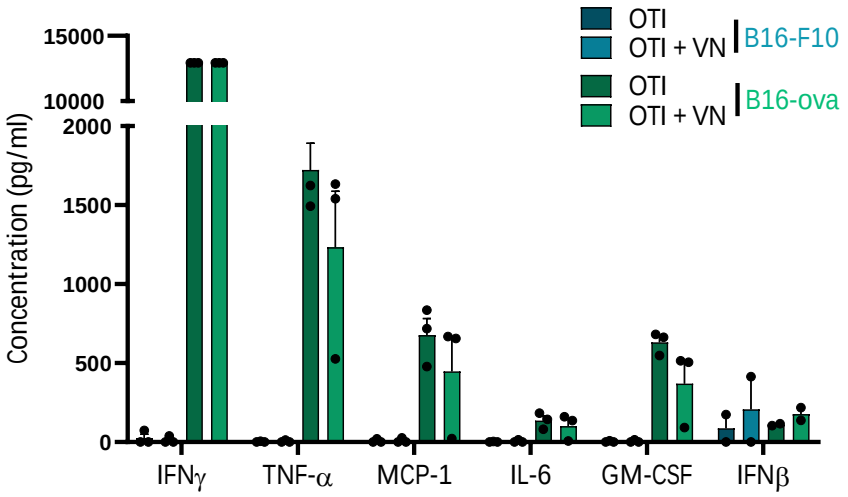


Figure 25: Cytokine secretion in response to combination co-culture. Tumor cells were seeded, infected at MOI 0.01 with VSV-NDV-GFP (VN) and incubated for 16 h before OTI T cells were added to the co-culture at an effector-to-target ratio of 1:1. 24 h later, supernatants were collected and analyzed in a multiplex bead array for inflammation-related cytokines (BioLegend). Concentration was plotted as mean±SD of triplicate experiments.

Apart from cytokine release, VSV-NDV might also change activation patterns in T cells through intracellular inflammatory signaling. Activation of T cells is reflected in the time-dependent upregulation of several surface proteins, e.g. CD25, CD69 or PD1. To assess changes in activation patterns of OTI T cells in the presence of VSV-NDV, co-culture experiments were set-up as detailed above, and OTI T cells were harvested 24 h after addition in order to characterize activation markers by flow cytometry (Fig. 26). This experiment demonstrated that OTI T cells upregulated surface expression of CD25, CD69 and PD1 in response to recognition of their target antigen-presenting tumor cells, and this induction was not altered by pre-infection with VSV-NDV. In this case, B16-F10 cells, that are not recognized, were used as a negative control and resulted in a limited increase of activation markers on OTI T cells.

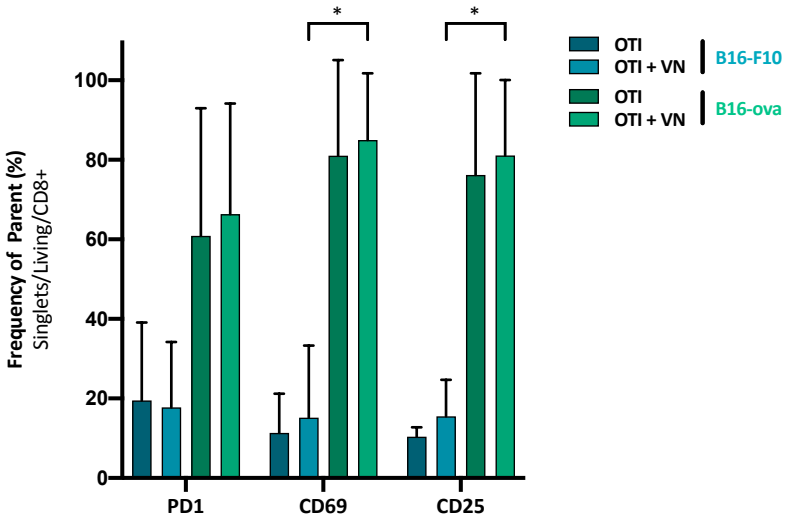


Figure 26: T cell activation markers PD1, CD25 and CD69 analyzed by flow cytometry after co-culture. B16-OVA or B16-F10 tumor cells were seeded, infected with VSV-NDV (MOI 0.01) and incubated for 16 h before T cells were added to the co-culture at an effector-to-target ratio of 1:1. 24 h later, T cells were harvested, stained for the indicated T cell activation markers and analyzed by flow cytometry. Experiments were performed in triplicate and results plotted as mean±SEM. Normal distribution was confirmed by Shapiro-Wilk test and statistical significance was determined by a Welch's ANOVA and Dunnett's T3 multiple comparisons test (* $p < 0.05$).

In summary, these findings demonstrate that OTI T cell activation and cytokine production are mainly induced by the recognition of antigen-presenting tumor cells, while an effect of VSV-NDV pre-infection could not be detected in these experiments. The presence of VSV-NDV does not seem to hamper with T cell activation, which is supported by the fact that VSV-NDV does not seem to replicate in these cells (data not shown). In the next section, the influence of VSV-NDV on infected tumor cells will be examined in more detail.

### Combination treatment accelerated increase in MHC-I expression, while limiting PD-L1 expression

Virus infection also effects intracellular processes of infected cells. Phenotypic changes in the tumor cells in response to combination or monotherapy could affect treatment outcome. Increased PD-L1 expression, for example, would indicate a more suppressive tumor microenvironment. Co-culture experiments were set up in triplicate as detailed above, and tumor cells were harvested 6 and 24 h after addition of T cells in order to characterize MHC-I and PD-L1 expression kinetics on the tumor cell surface via flow cytometry (Fig. 27).

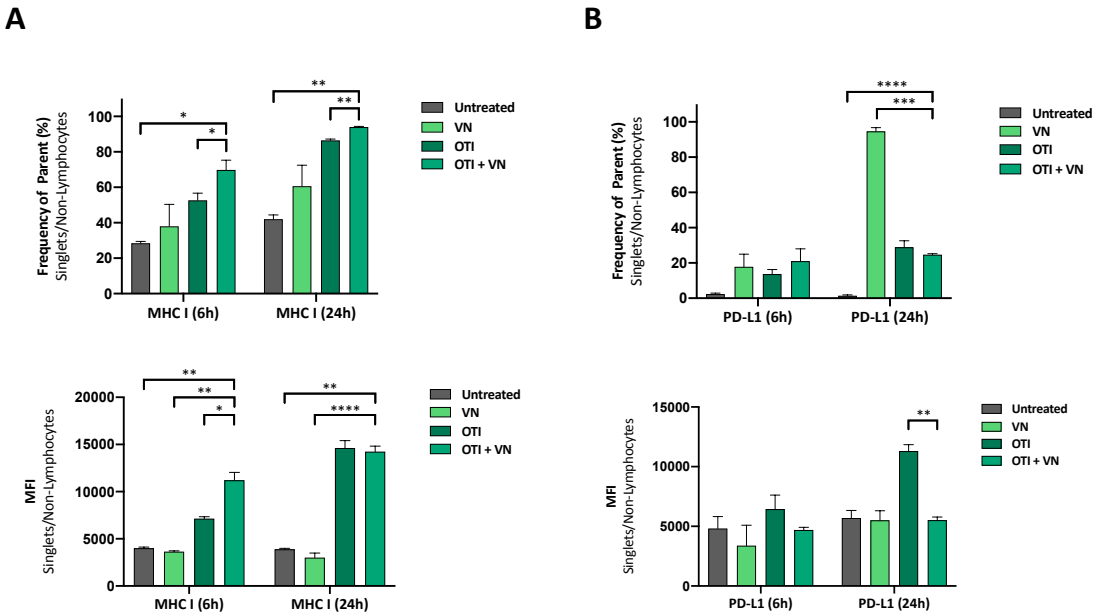


Figure 27: Changes of MHC-I and PD-L1 expression on tumor cells in response to combination co-culture. Tumor cells were seeded and cultured with or without VSV-NDV for 16 h, before OTI T cell addition. Tumor cells were harvested after 6 and 24 h in co-culture, stained for MHC-I (A) and PD-L1 (B) on the cell surface and analyzed by flow cytometry. In the lower panel, intensity of expression on a single cell basis was evaluated by mean fluorescence intensity (MFI) and plotted as mean±SEM of three separate experiments. Normal distribution was confirmed by Shapiro-Wilk test and statistical significance was determined by a Welch's ANOVA and Dunnett's T3 multiple comparisons test to combination group (* $p < 0.05$, ** $p < 0.01$,*** $p < 0.001$, **** $p < 0.0001$).

The percentage of tumor cells expressing MHC-I, as well as the expression level on individual cells (indicated by MFI), increased already 6 h after combination therapy and up to almost 100% after 24 h (Fig. 27 A). While OTI T cells alone showed a delayed MHC induction, VSV-NDV on its own was not able to significantly induce MHC-I expression. VSV-NDV alone did, on the other hand, result in a significant increase of PD-L1 expressing tumor cells after 24 h (Fig. 27 B), indicating a suppressive tumor microenvironment. This effect was abrogated in combination with ACT suggesting a positive effect on immunosuppression.

No change in cytokine release or surface expression of T cell activation markers was detected in response to VSV-NDV pre-infection of tumor cells in co-culture. Infection did, however, influence MHC-I and PD-L1 expression by tumor cells. Although both MHC-I and PD-L1 expression have been shown to be induced by IFN$\gamma$ signaling, it seems different pathways are involved, since they are independently regulated in response to different treatments.

**OTI T cells accumulated around VSV-NDV-induced syncytia**

During the co-culture experiments, an accumulation of OTI T cells was observed around virus-mediated syncytia. To better visualize this observation, co-culture experiments were set up as described above, but OTI T cells were stained with CellTrace™ Far Red Cell Proliferation Kit (ThermoFisher) according to the manufacturer's protocol before addition to the co-culture. Labeled OTI T cells were added to the co-culture at an E:T-ratio of 1:1, and co-culture was monitored over the course of one day. As illustrated in the representative images (Fig. 28), co-localization of labeled OTI T cells (red) could be detected around sites of VSV-NDV-induced syncytia formation (green) by 5 h after initiation of co-culture.

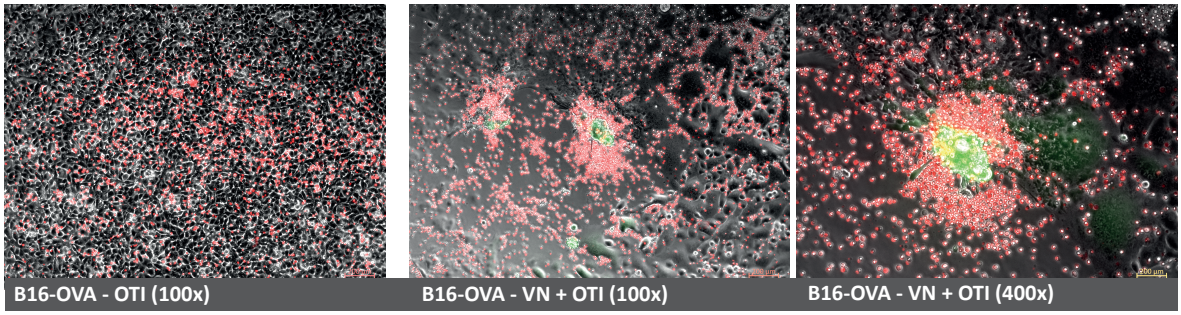


Figure 28: T cell accumulation at sites of VSV-NDV infection. Labeled OTI T cells (red) were added to the B16-OVA tumor cells pre-infected with VSV-NDV-GFP (VN) (green) at MOI 0.1 for 16 h or uninfected control cells at an effector-to-target ratio (E:T) of 1:1. Representative images were captured 5 h after T cell addition with a fluorescence microscope to visualize T cell recruitment around syncytia compared to their distribution on an uninfected monolayer.

This accumulation might indicate targeted recruitment of T cells to sites of VSV-NDV infection. A multiplex ELISA used to screen for chemokine expression after infection yielded no differences in chemokine concentrations of supernatants of infected B16 cells compared to uninfected controls (data not shown), suggesting the presence of a different recruiting signal released by infected cells. Possibly, the immunogenic cell death induced by VSV-NDV, with dying syncytia releasing, among others, the immunogenic factors HMGB1, HSP70 and HSP90 could play a role [40]. Further experiments to elucidate this beneficial aspect are warranted.

In summary, B16-OVA cells exposed to both VSV-NDV infection and OTI T cells show accelerated cytotoxicity and an early increase in MHC-I surface expression, while PD-L1 expression remains low. Tumor-specific T cell activation, as evidenced by the markers, CD25, CD69 and PD-1, as well as cytokine release, seem to be unaffected by the presence of VSV-NDV, and T cells are attracted to sites of syncytia formation. These results point towards a potential synergy of the two therapeutic agents and encouraged the continuation of the project in an *in vivo* setting.

### 3.2.4 Combination Treatment of Implanted Melanoma in Mice

Immunotherapeutic approaches are inherently difficult to test in cell culture, since the *in vitro* set-up cannot replicate the complex signaling cascades and features of the tumor microenvironment involved in an *in vivo* immune response. Because the treatment effects depend on an existing immune system, a proof-of-concept experiment was performed in immunocompetent, female C57BL/6J mice bearing syngeneic subcutaneously implanted B16-OVA tumors to analyze survival as well as the kinetics of treatment effects. Subcutaneous tumors are accessible for intratumoral injections and monitoring of tumor growth, thereby simplifying the proof-of-concept study, while taking into account immune-related effects. The experimental overview is illustrated in Figure 29 indicating times of tumor cell implantation and treatment injections. Mice were implanted with tumors on the right and left flank and intratumoral injections were only administered into the right tumor (injected tumor) in order to allow the observation of abscopal effects in the left tumor (uninjected tumor).

For the survival experiment, mice were implanted with $2.4\times10^5$ (right flank, injected tumor) and $1.2\times10^5$ (left flank, uninjected tumor) B16-OVA cells seven days prior to the first treatment. Fewer tumor cells were implanted for the uninjected tumor to account for debulking effects that are caused by intratumoral injections but unrelated to treatment. One week later, tumors had reached a size of approximately 0.3-0.5 $mm^2$ and mice were randomly distributed into treatment groups. Accordingly, they were injected intratumorally with VSV-NDV ($10^7$ TCID50) or PBS on day 0, followed by an intravenous OTI T cell injection ($5.5\times10^5$) on day 1 for combination treatment or OTI monotherapy. To compare time-dependent effects in combination therapy, additional treatment groups received OTI T cells on day 3 or day 5 after first virus treatment. For the survival experiment, intratumoral virus or PBS injections were repeated at the same dose on day 7 and 14.

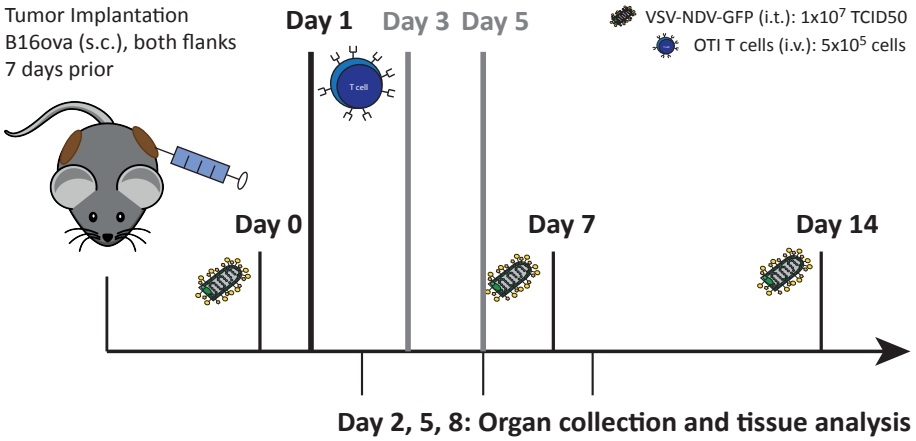


Figure 29: Experimental set-up of melanoma treatment *in vivo*. One week after tumor cell implantation, mice were randomly distributed to treatment groups (n=5-6), receiving PBS, VSV-NDV-GFP or OTI T cells as monotherapy or virus and OTI T cells in combination. VSV-NDV-GFP and PBS were administered intratumorally (i.t.) at indicated times (day 0, 7 and 14). To evaluate optimal ACT timing in combination, OTI T cells were administered intravenously (i.v.) on day 1, 3 or 5 after first virus treatment, and survival was monitored. For kinetics experiments based on tissue analysis, organs were collected on day 2, 5 and 8.

The kinetics experiment focused on the treatment groups VSV-NDV and OTI (Day 1) in monotherapy as well as in combination, with PBS as a control. For this experiment mice were implanted with $2.4\times10^5$ B16-OVA cells on both flanks seven days prior to the first treatment. To analyze treatment effects directly in the tumor and other organs, mice were euthanized at day 2, 5 and 8 after the first treatment and tumors, blood and spleen were harvested. The effect of the subsequent virus treatments as well as treatment effects after day 8 were not investigated in the scope of this work.

**VSV-NDV combined with ACT prolonged survival of tumor-bearing mice**

For survival analysis, mice were randomly distributed to treatment groups (n=5-6) one week after implantation and monitored until one tumor grew to a size of 15 mm in diameter or another humane endpoint was reached. Survival was plotted in a Kaplan-Meier curve and statistical significance was calculated by log-rank test. (Fig. 30).

Survival analysis of the tumor-bearing mice according to treatment group revealed a benefit of the combination approach compared to VSV-NDV and OTI monotherapy when T cells were injected on day 1 and 3 after virus administration (Fig. 30 A). Injecting the T cells on day 5 after virus treatment did not provide the same survival benefit as earlier OTI injections, indicating the importance of the timing in combination therapy. Possibly, at this time the virus may have been cleared already by the innate immune response, leaving behind no beneficial signaling for ACT.

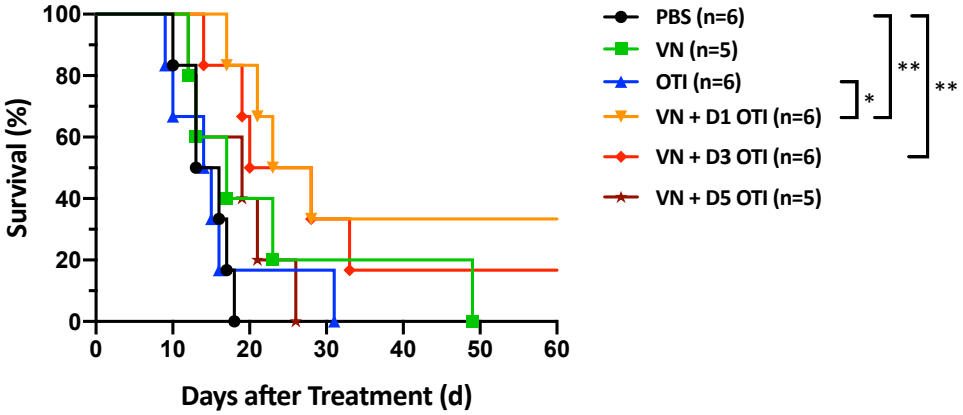


Figure 30: Treatment effect on survival of tumor-bearing mice. One week after implantation of B16-OVA tumor cells, mice were randomly distributed to the indicated treatment groups (n=5-6) and monitored until they reached a tumor diameter of 15 mm or another humane endpoint. Survival was plotted in a Kaplan-Meier curve. Statistical significance was determined by log-rank test (* $p < 0.05$, ** $p < 0.01$).

The best outcome was observed for mice treated with VSV-NDV together with OTI T cells on day 1 (Fig. 30 B). Two of five mice receiving this combination showed complete tumor regression and long-term survival (followed for 150 days). The median survival time also significantly increased compared to treatment with PBS (Phosphate-buffered saline) or OTI T cell alone (PBS/OTI: 14.5 d vs. VSV-NDV + OTI 25.5 d), while the difference to virotherapy alone (VSV-NDV: 17 d) was not significant. However, no complete tumor regression was achieved in this treatment group. The following data on tumor growth and kinetics is based on OTI T cells administered on day 1 after virus or control treatment.

### Combination therapy slows growth of injected and distant tumor lesions

Differences in survival times suggest a therapeutic effect on tumor progression in response to combination treatment. This was evaluated by monitoring tumor growth as part of the survival experiment described earlier. Tumor width and length were measured regularly with a caliper and the volume was calculated according to the modified ellipsoid volume: $1/2 \times (\text{length} \times \text{width}^2)$ [85]. Mean tumor growth up to day 14 was then plotted to facilitate the comparison between treatment groups as well as the effects in injected and uninjected tumors (Fig. 31).

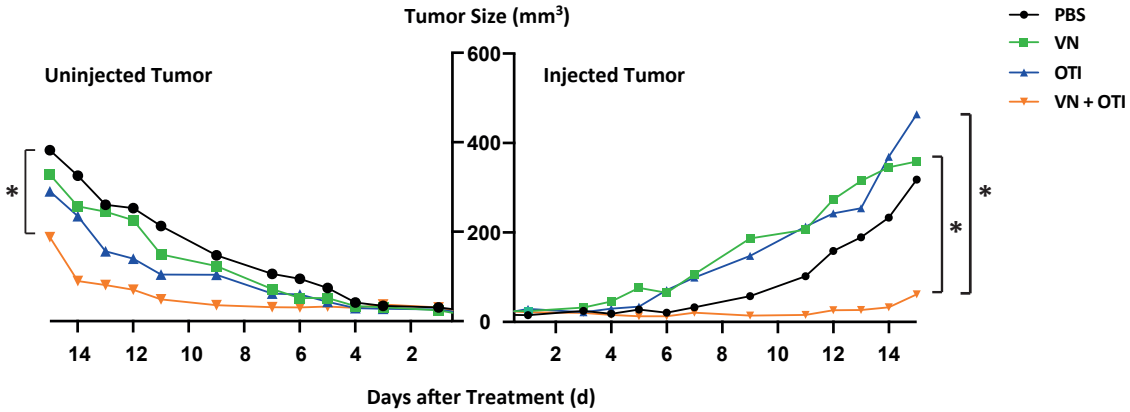


Figure 31: Effect of treatment approaches on tumor growth in the injected and uninjected tumor. One week after implantation, mice were randomly distributed to treatment groups and tumor growth was monitored by caliper measurements. Tumor volume was calculated using the modified ellipsoid formula, plotted as mean values up to day 14. Normal distribution was confirmed by Shapiro-Wilk test and statistical significance was determined by a Welch's ANOVA and Dunnett's T3 multiple comparisons test to combination group (* $p < 0.05$).

Combination treatment was able to significantly delay tumor growth in the injected, but also the uninjected tumor, suggesting abscopal effects. Under these experimental conditions, and up to day 14, monotherapies on average had little effect on tumor growth. The overall delay in tumor progression induced by combination treatment is emphasized in the visualization of individual tumor growth over time (Fig. 32). Injected (orange) and uninjected (black) tumors are differentiated by color.

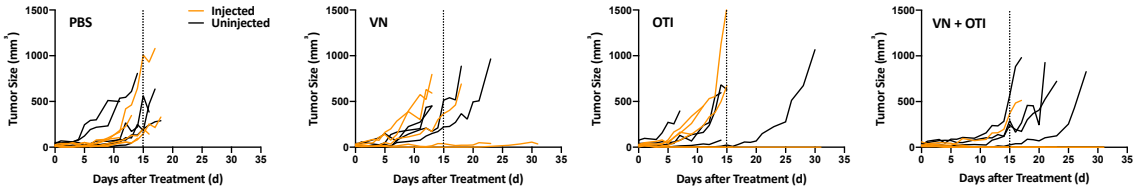


Figure 32: Tumor growth delay over time in response to combination or monotherapy. The experiment was performed as previously described (Fig. 29). Tumor volume was calculated using the modified ellipsoid formula and plotted over time for each individual tumor according to treatment group until endpoint criteria were reached. Injected (orange) and uninjected (black) tumors are differentiated as indicated.

VSV-NDV monotherapy effected especially tumor growth of the injected tumor, while OTI monotherapy individually slowed down tumor growth in an uninjected tumor. These results indicate that ACT is well complemented by oncolytic virotherapy.

Results would suggest that it is possible to use combination treatments at concentrations where monotherapy is inefficient, thereby reducing the likelihood of unwanted side effects and nevertheless leading to enhanced therapeutic effects.

To examine the mechanisms behind the delay in tumor growth and survival benefit observed for combination treatment, kinetics of tumor-infiltrating and antigen-specific lymphocytes as well as the cytokine profile were analyzed in subsequent experiments.

**Combination therapy boosted tumor infiltration of CD8$^+$ lymphocytes**

Kinetics experiments were performed as introduced in Figure 29 with one intratumoral VSV-NDV injection on day 0 and one intravenous OTI T cell injection on day 1. Tumors from both flanks (injected and uninjected) were isolated from mice euthanized at days 2, 5 and 8 after the first treatment (Fig. 29). Tumors were cut in half and processed for flow cytometry or prepared for immunohistochemical staining by fixation in paraformaldehyde (PFA) to investigate lymphocyte infiltration and tumor necrosis. A change in the number of tumor-infiltrating CD8$^+$ lymphocytes, as measured here by flow cytometry, could point to treatment-induced differences in the immunological phenotype of the tumor (Fig. 33).

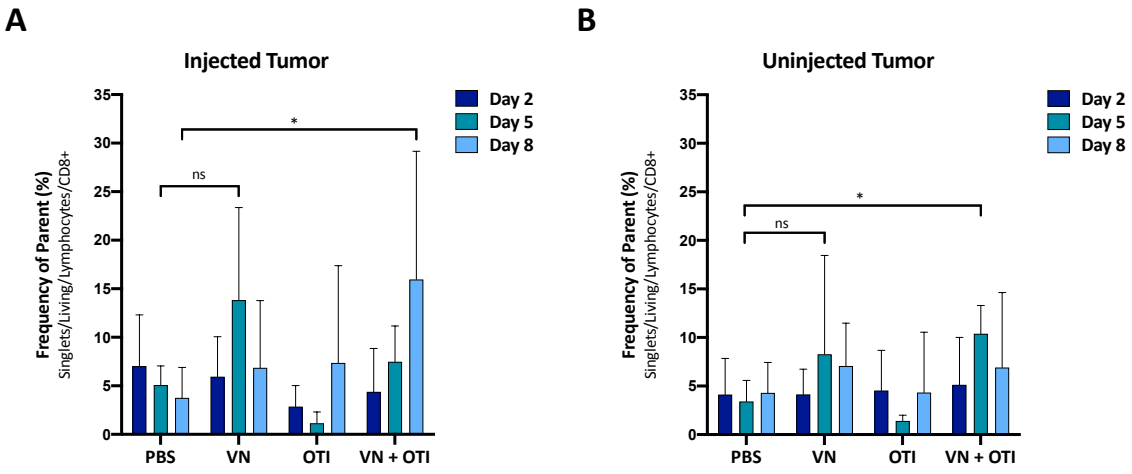


Figure 33: Tumor infiltration of CD8$^+$ T cells in response to treatment. A single cell suspension was generated from tumors (n = 3-6) harvested on day 2, 5 or 8 from mice treated with the indicated therapeutic approach. Cells were stained for CD8$^+$ surface expression and analyzed by flow cytometry. The data represent the percentage of living CD8$^+$ lymphocytes in tumor tissue, comparing the injected (A) and uninjected (B) tumor. Statistical significance was determined by unpaired t-test (* $p < 0.05$).

Results from Fig. 33 on the infiltration of $CD8^+$ lymphocytes important for further discussion are summarized in the following list according to treatment group (Tab. 9).

Table 9: Summary of results on $CD8^+$ infiltration.

| **Treatment Group** | **Treatment Effect** |
|---|---|
| **PBS** | Control group |
| **VN** | VSV-NDV tends to increase infiltration on day 5 in the injected and uninjected tumor. |
| **OTI** | Similar to control group, with a slight increase on day 8 in the PBS injected tumor |
| **VN + OTI** | Significant infiltration of $CD8^+$ lymphocytes on day 8 in the injected and day 5 in the uninjected tumor. |

On day 8, a significant increase of $CD8^+$ T cells was detected in the injected tumor after combination treatment, while in the uninjected tumor a slight increase was already observed on day 5. $CD8^+$ levels in the VSV-NDV treated tumors were not significantly elevated compared to PBS, but a high standard deviation might indicate an infiltration response in several, mostly injected, but also uninjected tumors on day 5. Surprisingly, for OTI treated mice, no increase of infiltrating $CD8^+$ cells could be shown compared to PBS. This correlates with the observation that OTI monotherapy had no beneficial effect on survival. Taken together, these results could indicate a poor OTI T cell engraftment or homing to the tumor in the absence of a pre-existing oncolytic virus infection.

Flow cytometric results on $CD8^+$ infiltration on day 8 were confirmed by immunohistochemical staining of CD8 T cells on 2 µm slices of the tumor pieces isolated and fixed in 4% paraformaldehyde. $CD8^+$ T cells were stained on a Bond RX automated staining instrument. (Fig. 34).

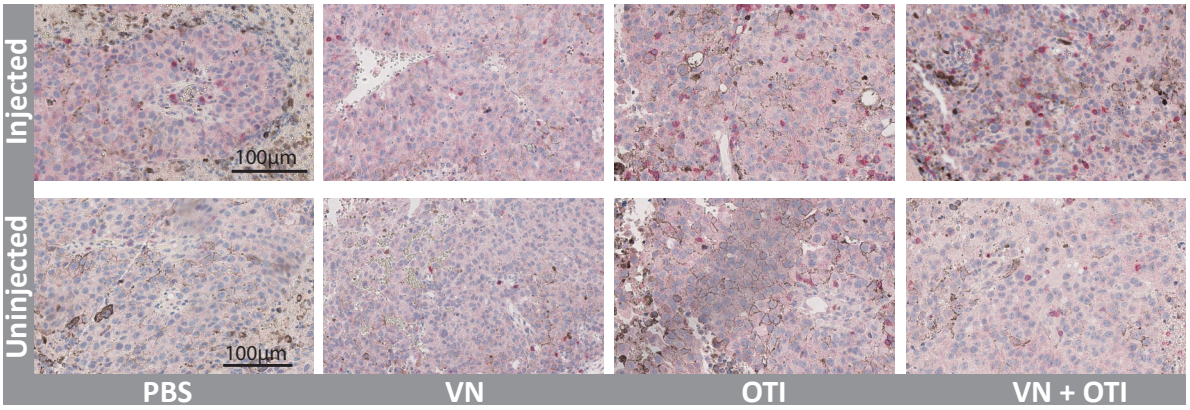


Figure 34: Tumor infiltration of CD8$^+$ T cells in response to treatment by IHC. Tumors were harvested on day 2, 5 or 8 from mice treated with the indicated therapeutic approach. Tumor pieces were fixed in 4% paraformaldehyde, dehydrated and embedded in paraffin. 2 µm slices were cut and sections stained for CD8$^+$ lymphocytes. Representative images show CD8$^+$ lymphocytes (red) in tumor tissue, comparing the injected and uninjected tumor.

To further characterize the infiltrating lymphocyte population, the next section focuses on the antigen specificity of these cells.

**VSV-NDV treatment led to infiltration of antigen-specific CD8$^+$ T cells**

Due to the presence of VSV-NDV, tumor infiltrating lymphocytes could indicate an anti-tumor response or an anti-viral response. Flow cytometric analysis via MHC-tetramer staining allows the differentiation of antigen-specific T cells by binding of specific TCRs to tetramer molecules that mimic MHC-peptide complexes and are coupled to a fluorophore. Tumors were isolated from treated animals on day 2, 5 or 8 after first treatment. To define the anti-tumor T cell response, the level of OVA-specific infiltrating lymphocytes was measured via MHC-tetramer staining of the SIINFEKL-TCR complex and flow cytometry (Fig. 35).

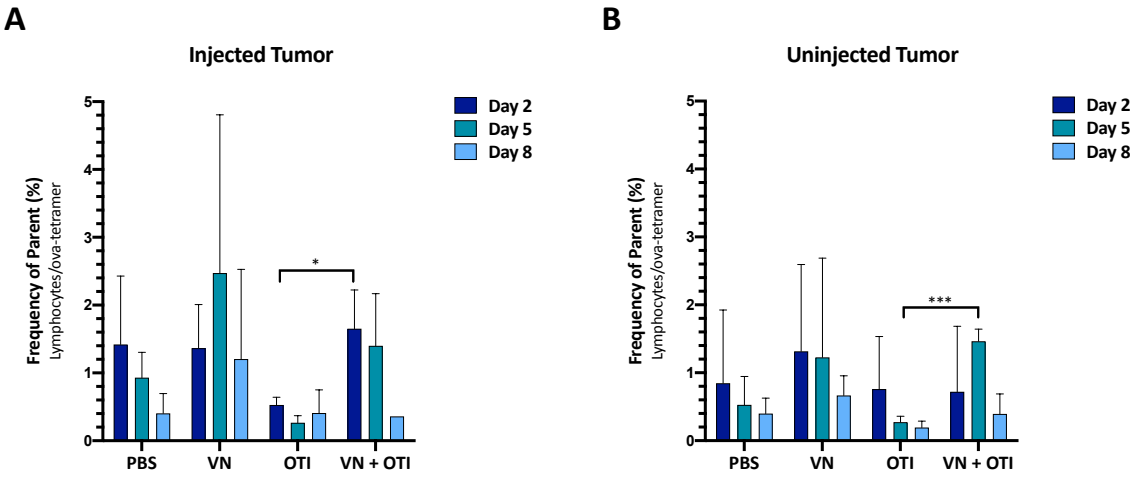


Figure 35: Tumor infiltration of OVA-specific T cells directed against the SIINFEKL peptide. A single cell suspension was generated from tumors (n = 3-6) harvested on day 2, 5 or 8 from mice treated with the indicated therapeutic approach. Cells were stained for an OVA-specific-TCR complex using an MHC-tetramer (MBL) and analyzed by flow cytometry. The data represent the percentage of OVA-specific lymphocytes in tumor tissue, comparing infiltration of the injected (A) and uninjected (B) tumor. Statistical significance was determined by unpaired t-test (* $p < 0.05$,*** $p < 0.001$).

Results on the infiltration of OVA-specific T cells important for further discussion are summarized in the following list according to treatment group (Tab. 10).

Table 10: Summary of results on OVA-specific lymphocyte infiltration.

| **Treatment Group** | **Treatment Effect** |
|---|---|
| **PBS** | Control group |
| **VN** | Increase of OVA-specific T cells in the injected tumor on day 5, that is reduced by day 8; similar trend in the uninjected tumor. |
| **OTI** | Similar to control group |
| **VN + OTI** | Significant increase of OVA-specific T cells on day 2 in the injected tumor, that drops again on day 8. Increase in the uninjected tumor by day 5. |

VSV-NDV monotherapy seems to result in an infiltration of OVA-specific T cells, although the effect is subject to inter-individual differences. Combination therapy also induced OVA-specific infiltration, however, due to tumor shrinkage only one injected tumor was available for analysis from the combination group on day 8.

**Combination therapy reduced infiltration of virus-specific CD8$^+$ T cells**

Virus replication is a strong inducer of innate immune responses and priming of a virus-specific T cell response a common byproduct of oncolytic virotherapy [99]. Tumors from the above experiment were analyzed for infiltration of virus-specific T cells into injected and uninjected tumor, as measured by MHC-tetramer staining of a VSV-N peptide (RGYVYQGL)-TCR complex and flow cytometry (Fig. 36). This marker for VSV-specific T cells is similarly specific for VSV-NDV-specific T cells as the VSV-N protein is part of viral backbone of VSV-NDV.

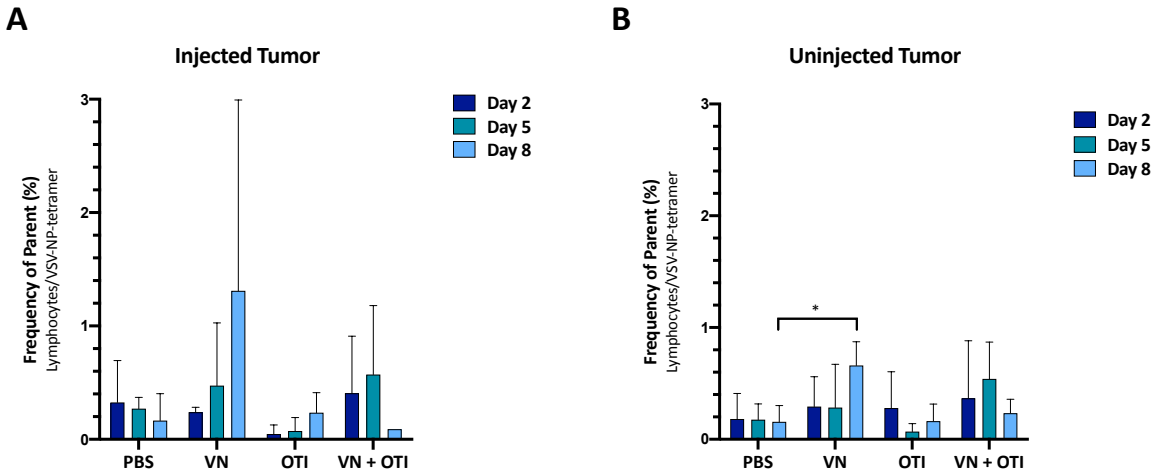


Figure 36: Tumor infiltration of VSV-specific T cells directed against the RGYVYQGL peptide. A single cell suspension was generated from tumors (n = 3-6) harvested on day 2, 5 or 8 from mice treated with the indicated therapeutic approach. Cells were stained for a VSV-specific-TCR complex using an MHC-tetramer (MBL) and analyzed by flow cytometry. The data represent the percentage of VSV-specific lymphocytes in tumor tissue, comparing infiltration of the injected (A) and uninjected (B) tumor. Statistical significance was determined by unpaired t-test (* $p < 0.05$).

Although the isolation of infectious particles was not successful, the tumor infiltration with VSV-specific T cells suggests the presence of virus in the injected tumor and to a lesser degree also the uninjected tumor. This may indicate a systemic transfer of the virus from the injected to the uninjected tumor or infiltration of circulating virus-specific T cells. The increase in VSV-specific T cells over time was not observed in the combination group, although again only one injected tumor was available for analysis, suggesting that the lymphocyte response may lean more toward a broad tumor-specific response that is not only directed against the OVA peptide.

Results on the infiltration of VSV-specific T cells important for further discussion are summarized in the following table according to treatment group (Tab. 11).

Table 11: Summary of results on VSV-specific lymphocyte infiltration

| Treatment Group | Treatment Effect |
|---|---|
| **PBS** | Control group |
| **VN** | Increase of VSV-specific T cells peaks on day 8 and is more distinct in the tumor directly injected with VSV-NDV, but also detectable in the uninjected tumor |
| **OTI** | Levels of VSV-specific T cells are similar to control group values, since no virus was injected. |
| **VN + OTI** | Minimal increase of VSV-specific T cells (peak on day 5) in both injected and uninjected tumor. |

### Cytokine profile of therapeutic approaches

A cytokine array was used to examine the systemic effects of the treatment approaches.

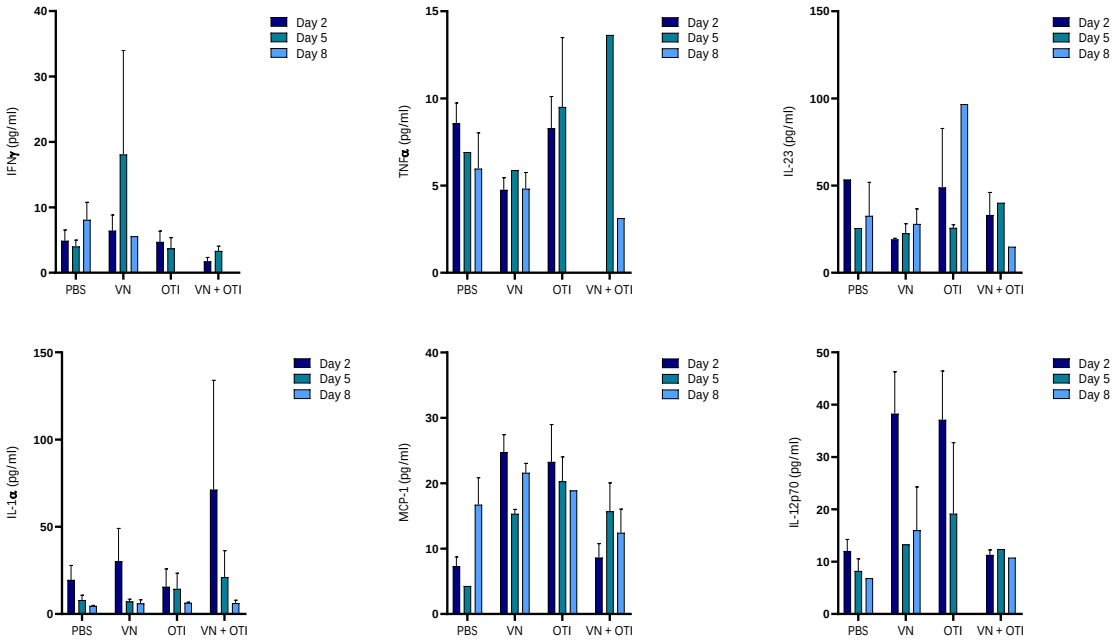


Figure 37: Analysis of systemic cytokines in the blood of treated animals. Blood was collected at day 2, 5 and 8 from tumor-bearing mice treated with PBS, VSV-NDV (VN), OTI T cells (OTI) or VN+OTI in combination (n=3). Plasma was generated and used in a multiplex bead array detecting inflammation-related cytokines (BioLegend). Results were plotted as mean±SD. Not all values were available, due to high inter-individual variability.

Plasma was isolated from blood taken on day 2, 5 and 8 after first treatment to analyze kinetics of the systemic cytokine effects. To detect different cytokines simultaneously, a bead-based array was used (LegendPlex Murine Inflammation Panel, BioLegend) and analyzed by flow cytometry (Fig. 37). Cytokine responses, in general, seem to be influenced strongly by inter-individual differences, resulting in a high standard deviation or missing values when the cytokine was not detectable and the need for larger groups to examine these effects and confirm trends.

*In vivo* cytokine data differ from results obtained in co-culture supernatants *in vitro*. This may be due to differences in systemic and local cytokine distribution, but also emphasizes the different signaling capacity *in vitro*. Systemically, only combination treatment tends to transiently induce IL-1$\alpha$ on day 2. This inflammatory cytokine has been implicated in the activation of tumorigenic pathways. A trend towards increased IFNy signaling was detected in response to VSV-NDV monotherapy, possibly indicating a more pronounced inflammatory response.

Due to a high inter-individual variability, group size needs to be increased in order to confirm suggested trends. The antigen-specificity of splenocytes was analyzed to further characterize systemic treatment effects.

**Combination treatment induced systemic OVA-specific CD4$^+$ T cells**

The goal of immunotherapeutic interventions is the induction of a broad anti-tumor immune response enabling tumor clearance and protection against tumor recurrence. A broad anti-tumor response is characterized by multiple tumor antigens being targeted by the induced anti-tumor immune response, in order to impede tumor escape variants.

To further analyze the systemic antigen-specific T cell population and potential antigen-spreading in response to therapy, splenocytes were isolated from the euthanized mice and used in a peptide activation assay. Splenocytes from each treatment group (n = 2-3) were cultured for 14 h in the presence of OVA. Addition of Brefeldin A inhibits secretion of cytokines produced in response to T cell stimulation. Extracellular staining of CD4 and CD8 was combined with intracellular staining of IFN$\gamma$, TNF-$\alpha$ and Granzyme B and analyzed by flow cytometry. CD8$^+$ and CD4$^+$ T cell populations were examined separately (Fig. 38).

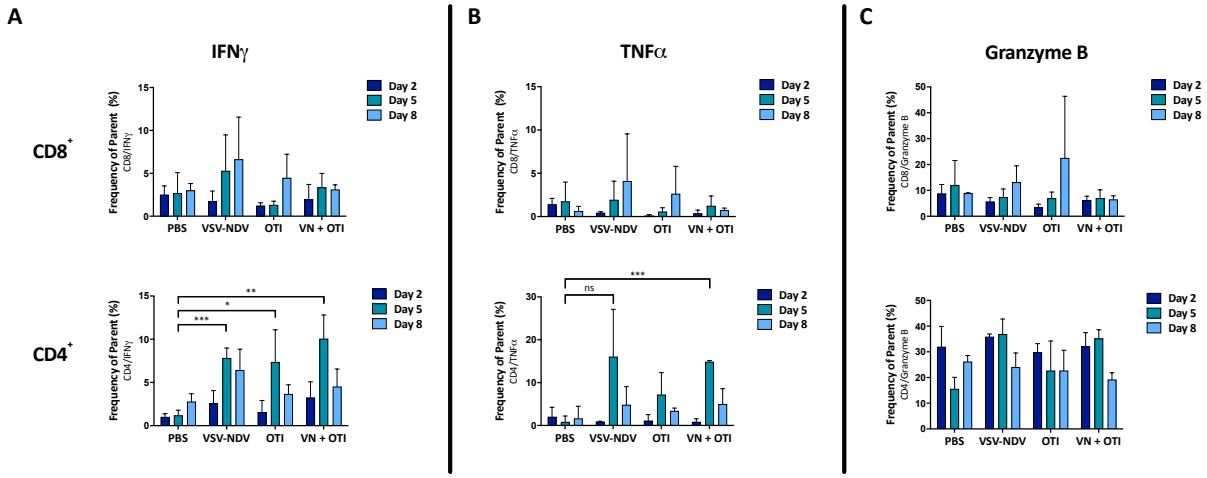


Figure 38: Activation of $CD8^+$ and $CD4^+$ lymphocytes in response to an OVA peptide. Splenocytes isolated from animals at day 2, 5 and 8 after first treatment (n=3) were used in a peptide activation assay with the OVA peptide SIINFEKL. Activation was determined by measuring intracellular IFN$\gamma$ (A), TNF-$\alpha$ (B) and granzyme B (C) via flow cytometry. Percentage of parent was plotted as mean±SD. Statistical significance was determined by unpaired t-test (* $p < 0.05$, ** $p < 0.01$,*** $p < 0.001$).

OVA-specific T cells detected among the tumor infiltrating lymphocytes indicated that VSV-NDV monotherapy slowly increased OVA-specific $CD8^+$ and $CD4^+$ T cells. While combination therapy seems to preferentially induce $CD4^+$ T cells responsive to the OVA peptide. These differences have not been investigated further, but hint at different immune mechanisms activated by the therapies.

Results on the infiltration of OVA-specific T cells important for further discussion are summarized in the following table according to treatment group (Tab. 12).

Table 12: Summary of results on OVA peptide activated $CD8^+$ T cells

| **Treatment Group** | **Treatment Effect** |
|---|---|
| **PBS** | Control group |
| **VN** | Increase in number of $CD8^+$ T cells on day 5 and 8 expressing IFN$\gamma$ and TNF-$\alpha$ in response to OVA peptide |
| **OTI** | Increase in number $CD8^+$ T cells on day 8 expressing Granzyme B |
| **VN + OTI** | Slight increase in MFI for IFN$\gamma$ and TNF-$\alpha$ on day 5 |

**Combination therapy induced epitope spreading**

Epitope spreading is defined as the expansion of the immune response to secondary epitopes which could help overcome antigen escape and generate sustained immunity against cancer relapse and metastasis. This concept is especially important for the establishment of a broad anti-tumor immune response to benefit overall survival [100].

In 1997, Tyrosinase-related protein 2 (TRP2) has been identified as a tumor rejection antigen [101]. It is expressed by melanoma cells and was chosen as a relevant B16-antigen apart from the immunogenic OVA peptide, SIINFEKL, to identify epitope spreading.

To analyze antigen-spreading in response to therapy, splenocytes were isolated from the euthanized mice and used in a peptide activation assay (as previously described) with a TRP2 peptide. Intracellular staining of IFN$\gamma$, TNF$\alpha$ and Granzyme B was performed and analyzed by flow cytometry (Fig. 39).

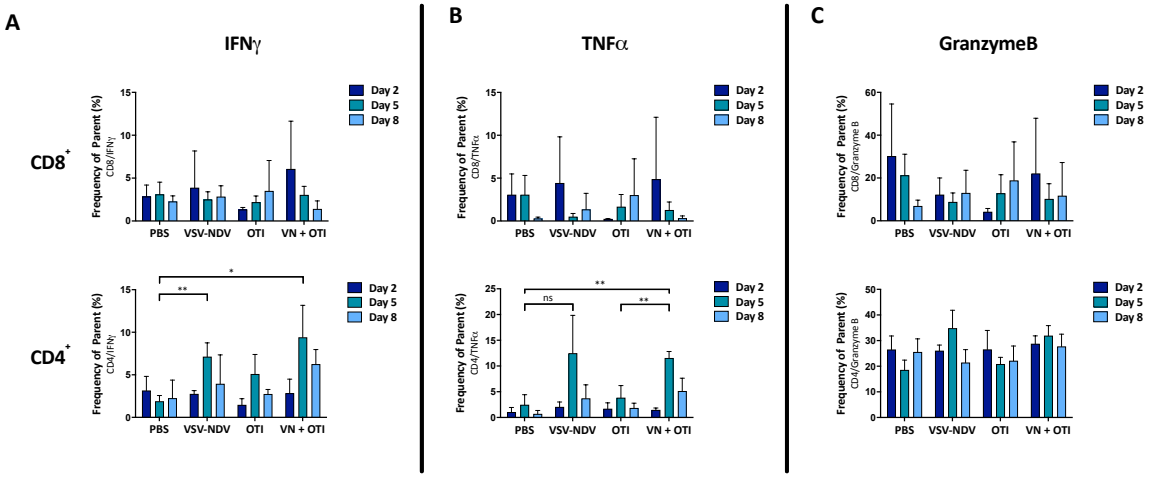


Figure 39: Activation of $CD8^+$ and $CD4^+$ lymphocytes in response to a TRP2 peptide. Splenocytes isolated from animals at day 2, 5 and 8 after first treatment (n=3) were used in a peptide activation assay with the TRP2 peptide SVYDFFVWL. Activation was determined by measuring intracellular IFN$\gamma$ (A), TNF$\alpha$ (B) and granzyme B (C) via flow cytometry. Percentage of parent was plotted as mean$\pm$SD. Statistical significance was determined by unpaired t-test (* $p < 0.05$, ** $p < 0.01$,*** $p < 0.001$).

Results on the infiltration of VSV-specific T cells important for further discussion are summarized in the following table according to treatment group (Tab. 13).

Table 13: Summary of results on TRP2 peptide activated T cells

| **Treatment Group** | **Treatment Effect** |
|---|---|
| **PBS** | Control group |
| **VN** | Increase of $CD4^+$ T cells on day 5 expressing IFN$\gamma$ and TNF$\alpha$ in response to TRP2 peptide |
| **OTI** | Similar to control group |
| **VN + OTI** | Increase of IFN$\gamma$ and TNF$\alpha$ expression in response to TRP2 peptide in $CD8^+$ Tcells on day 2 and $CD4^+$ T cells on day 5 |

Activated T cells detected after TRP2 stimulation suggest a stronger effect of combination therapy on both $CD8^+$ and $CD4^+$ T cells, while VSV-NDV monotherapy showed a slight trend that was more pronounced in $CD4^+$ T cells. Again, these differences have not been investigated further, but could indicate the activation of different immune mechanisms by the therapeutic approaches.

In summary, the effects of combination therapy on tumor growth can be associated with an increase of tumor infiltrating lymphocytes and their specificity towards an OVA-peptide. Also systemically, combination therapy affected the antigen-specific repertoire, especially $CD4^+$ T cells responded to a TRP2 peptide, suggesting epitope spreading. These differences might contribute to the mechanism that allowed combination therapy to be more successful in tumor clearance than VSV-NDV monotherapy.

**VSV-NDV-treated animals are resistant to tumor re-challenge**

Data collected during this doctoral thesis demonstrates a survival benefit for mice bearing subcutaneous melanoma lesions treated with combination therapy. Results from tumor-bearing mice treated with VSV-NDV followed by OTI administration on day 1, 3 and 5 after the first treatment (Fig. 30) already indicated that T cell timing is essential for combination efficacy. Along those lines, investigations were initiated to examine how virus dosing would affect therapeutic outcomes by administering VSV-NDV (i.t.) on day 0, 3 and 6, as opposed to day 0, 7 and 14 (Fig. 29). Intravenous OTI T cell administration on day 1 was kept the same for comparison (Fig. 40).

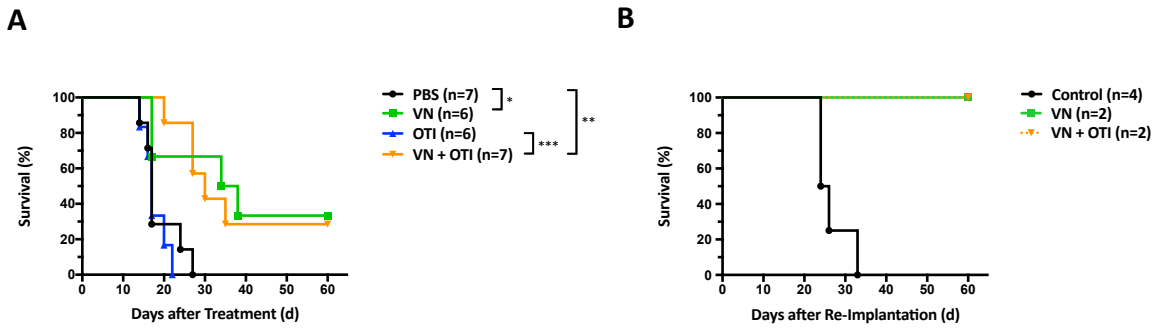


Figure 40: Treatment effect with adapted dosing scheme on survival and long-term protection. (A) One week after implantation mice were randomly distributed to indicated treatment groups (n=6-7) and monitored until they reached a tumor diameter of 15 mm or another humane endpoint. Survival was plotted in a Kaplan-Meier curve. Statistical significance was determined by log-rank test (* $p < 0.05$, ** $p < 0.01$, *** $p < 0.001$). (B) Surviving mice (n=2) were re-implanted with B16-OVA cells two months after the first treatment together with sex- and age-matched, previously untreated control mice (n=4) and survival was monitored.

The monotherapeutic outcome is improved by more frequent virus injections early on, while combination therapy is only slightly improved by a prolongation in median survival time (Fig. 40 A). This difference indicates mechanistic differences of both therapeutic approaches. These observations call for a more detailed investigation of the immunotherapeutic effects.

In a first follow-up experiment, mice that had undergone complete tumor clearance after treatment (n=2) with VSV-NDV or combination therapy were re-implanted with B16-OVA cells to examine the existence of a long-term memory response (Fig. 40 B). Naïve, age-matched, female C57BL/6J mice were similarly subcutaneously implanted with B16-OVA tumors as a control.

The long-term surviving mice that were subjected to tumor re-challenge showed no sign of tumor growth and survived long after the duration of the experiment indicating the existence of a long-term memory response. However, since there were only 2 long-term surviving mice in each treatment group that could be subjected to the re-implantation, this experiment should be repeated to confirm the results.

**Expression of soluble PD1 enhanced anti-tumor effect in the injected tumor**

To further improve the therapeutic outcome of the combination, a three-pronged approach was examined. First experiments using OTI T cells in combination with VSV-NDV-HAsPD1 delivering checkpoint inhibitor functions were performed in the experimental set-up introduced above. Preliminary data indicate that HAsPD1 release (Fig. 17) after intratumoral injection can provide prolonged tumor growth stabilization in combination therapy compared to VSV-NDV in combination (Fig. 41).


Figure 41: Effect of soluble PD1 on individual tumor growth after combination treatment. Tumor volume was calculated using the modified ellipsoid formula and plotted for each individual tumor according to the treatment groups (n=6-7), i.e. VSV-NDV ± HAsPD1 in combination with OTI T cells, differentiating injected (orange) and uninjected (black) tumors.

Effects could not be replicated in the distant (uninjected) tumor resulting in a similar median survival time and overall survival for both groups. Investigations on these effects are part of an ongoing project. The promising results in the melanoma model encouraged the continuation of the project in a more clinically relevant, inducible model of multifocal hepatocellular carcinoma in mice.

## 3.3 Combination Approach: Hepatocellular Carcinoma Model

Approximately 854,000 new cases of liver cancer, 85%-90% of which are hepatocellular carcinoma (HCC), are diagnosed annually, making it the sixth most common cancer worldwide [102]. Treatment options are still limited and even the standard of care in patients who are not candidates for curative treatment (i.e. liver transplantation) or tumor resection, the multikinase inhibitor Sorafenib, can only prolongs survival time for a few months [103]. In comparison, melanoma patients have a variety of treatment options and therapeutic efficiency is at almost 90%. Finding improved treatment options for HCC is, therefore, of immediate clinical relevance. Our combination therapy approach showed promising results in the treatment of the B16 melanoma model, however it has been shown that the immune context of implanted tumor growth and its characteristics can be very different from spontaneously occurring tumors as would be the case for human cancers [104]. To bridge the gap and move towards clinical translation, an inducible tumor model was used, where tumors grow orthotopically in the liver due to localized oncogene expression.

**Single cell clone isolation and characterization**

In order to establish the methods and examine the effects of VSV-NDV and antigen-specific T cells based on an HCC model, cell clones expressing the model tumor-antigen had to be generated. Multifocal orthotopic hepatocellular carcinoma lesions were induced in the AST mouse model harboring a LoxP-flanked SV40-LTAg oncogene under the control of an albumin promoter (see Materials and Methods for details). After MRI confirmed presence of lesions within the liver, tumors were harvested. Tumor cells were isolated, in the scope of a previous doctoral work, from diced tumor tissue after digestion in Liberase TM and filtration over a 100 μm filter. Cells were plated and cultured for several cycles of proliferation, before trypsinization and re-plating at low cell density to allow the outgrowth and isolation of single cell colonies. Multiple clones were characterized within the scope of a Master thesis completed by Sonja Glauss. Based on promising data indicating that the HCC clone 27-14 (HCCc27-14) expressed HCC markers as well as the SV40-LTAg protein and was susceptible to virus replication, this clone was chosen for all following co-culture experiments.

### 3.3.1 Viral Oncolysis of Isolated HCC Cell Clone

**HCCc27-14 cells supported VSV-NDV replication and showed cytotoxic effect in response to infection**

In a first step, susceptibility of the isolated tumor cell clone to VSV-NDV infection was confirmed by growth curve analysis. For measurements of virus replication and cytotoxic efficacy, HCCc27-14 cells were seeded one day prior to infection, then infected at different MOIs for 1 h at 37°C in PBS. After a washing step to remove free virus particles, medium was replenished and infected cells were incubated and aliquots of supernatant were collected at 16, 24, 48 and 72h after infection for TCID50 and LDH analysis. To visualize virus growth kinetics, virus titers were determined by TCID50 analysis (Fig. 42 A). VSV-GFP rapidly replicates to high titers and reaches peak titers as early as 16 h after infection. NDV-GFP and VSV-NDV-GFP showed similar replication kinetics and infectious virus production with peak virus titers starting at 24 h.

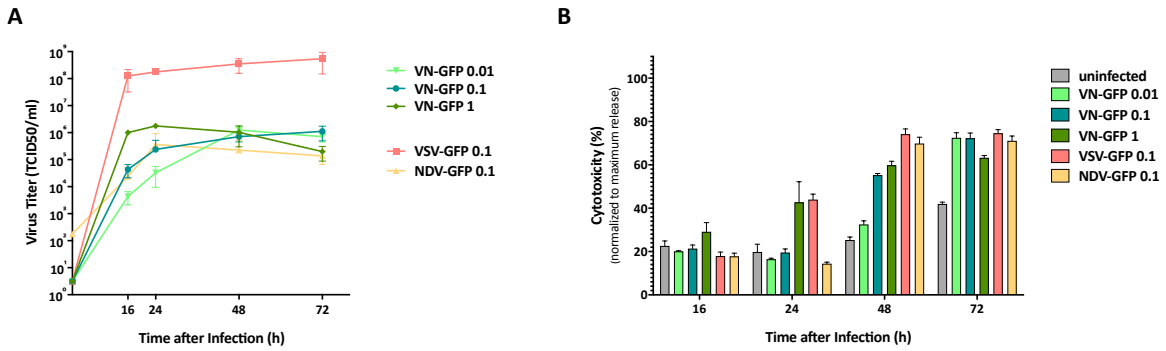


Figure 42: Comparison of VSV-NDV, VSV and NDV infection in the HCC cell clone 27-14. (A) Growth curves demonstrate replication by viral titer analysis at 0, 16, 24, 48 and 72 h post infection measured via TCID50. (B) Cytotoxicity is measured via LDH concentration in supernatants of infected cells 16, 24, 48 and 72 h after infection. Results were normalized to a maximum release control and cytotoxicity was plotted as mean±SEM.

Cells infected with VSV-NDV-GFP showed a dose-dependent delay in virus release. Virus replication plateaued after infection of all susceptible cells and remained stable until 72 h post infection. The slight decrease can be explained by dying cells no longer producing infectious virus particles. Cytotoxicity was determined by LDH assay (Fig. 42 B). The cytotoxic effect mediated by VSV-NDV-GFP infection at MOI 1 in HCC cells resembled the infection kinetics of the parental virus VSV at MOI 0.1 and was dose-dependent on the MOI upon infection. In these HCC cells, VSV-NDV-induced cell death was detected 24 h after infection for VSV-NDV-GFP at MOI 1 and VSV-GFP at MOI 0.1, while VSV-NDV-GFP and NDV-GFP at MOI 0.1 followed 24 h later.

The HCC clone 27-14 was susceptible to virus infection and VSV-NDV induced potent cytotoxic effects in tumor cells. In comparison with the B16 tumor cell lines, however, individual cell clusters usually remained and resistant tumor cells grew back over time. Based on these observations, HCCc27-14 is an optimal candidate for testing combination therapy *in vitro*, since VSV-NDV infection at lower MOIs was not sufficient to clear all tumor cells. For combination therapy, antigen-specific T cells recognizing the HCC clone had to be generated and their potency examined in the tumor cell clone.

### 3.3.2 T cell-dependent Oncolysis of Isolated HCC Cell Clone

**T cell transduction with the SV40-LTAg-specific TCR**

The T cell transduction method, protocol and retroviral producer cell line (PlatE) were generously provided by Matthias Leisegang (Max-Delbrück-Center for Molecular Medicine, Berlin). For a detailed description of the established protocol see the Material and Methods section. In short, spleens were harvested from C57BL/6N male mice and prepared as a single-cell suspension with prior lysis of red blood cells. Splenocytes were cultured for 24 h in mTCM supplemented with anti-CD3, anti-CD28 antibodies, and 40 U/ml IL-2 for general TCR activation and co-stimulation. Then T cells were transduced with a retroviral construct containing the T cell receptor sequence specific for MHC class I protein, H-2D$^b$, in complex with the SV40-LTAg peptide SAINNYAQKL (Fig. 8) [80]. Transduction rate was measured after a three-day expansion phase at 37°C via flow cytometry (Fig. 43).

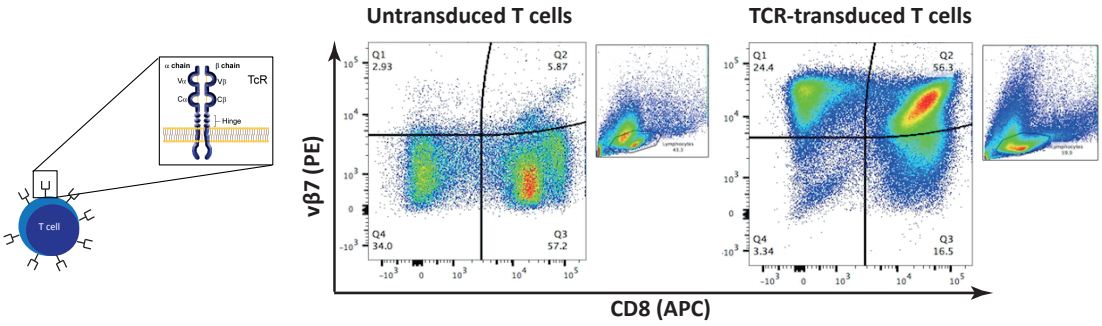


Figure 43: Analysis of retroviral transduction rate of murine splenocytes. Transduced and expanded CD8$^+$ T cells were stained for variable β-chain 7 on the cell surface as an indicator for successful transduction and analyzed by flow cytometry. Representative graphs were chosen to illustrate expression patterns of untransduced and TCR-transduced T cells.

For the calculation of the transduction rate, the number of endogenous T cells expressing the variable β-chain 7 (vβ7) measured in the untransduced control cells was subtracted from the number of vβ7 expressing cells measured in the transduced T cells. Although transduction efficiency in individual experiments varied, on average, approximately 50% transduction of $CD8^+$ T cells was achieved.

**TCR-transduced T cells showed a dose-dependent cytotoxic effect in target cells and were complemented by virotherapy**

Functionality of TCR-transduced T cells was analyzed in co-culture with HCCc27-14 cells in different effector-to-target ratios by measuring cytotoxicity via LDH assay (Fig. 44).

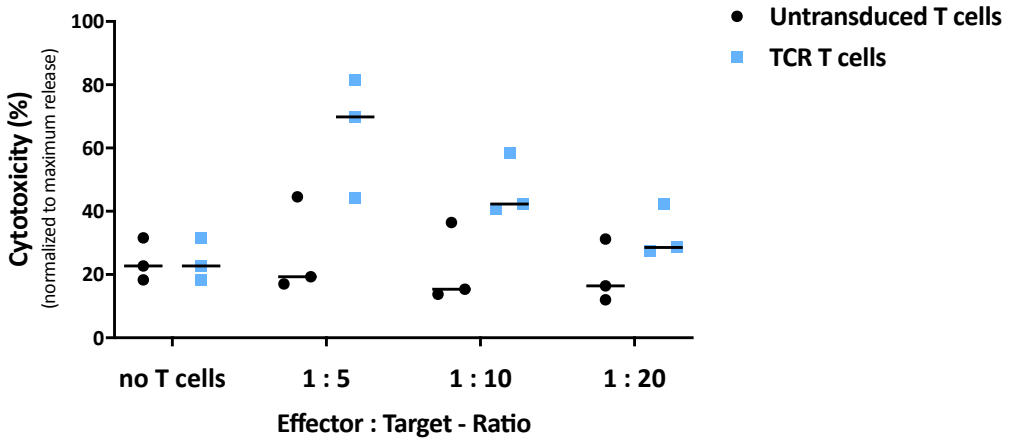


Figure 44: Cytotoxicity of TCR-transduced T cells co-cultured with HCCc27-14 tumor cells at different effector-to-target ratios. Tumor cells were seeded and incubated for 24 h, before T cells were added to the co-culture. 24 h later, LDH was measured to determine the cytotoxic effect. Mock-transduced splenocytes were used as a negative control. Results were normalized to a maximum release control and cytotoxicity was plotted as individual means of triplicate experiments. Normal distribution was confirmed by Shapiro-Wilk test and statistical significance was determined by a Welch's ANOVA and Dunnett's T3 multiple comparisons test (not significant).

Results indicated that TCR T cells specifically recognize and eliminate HCCc27-14 tumor cells expressing SV40-LTAg in a dose-dependent manner, although effects were not significant. Mock-transduced T cells were used as a negative control and show a minimal background cell killing effect. After demonstrating the efficacy of VSV-NDV and TCR-transduced T cells induced tumor cell death separately, in the next step, TCR T cells were used in co-culture experiments with pre-infected HCCc27-14 cells to evaluate combination effects.

### 3.3.3 Combination Co-Culture with Isolated HCC Cell Clone

**Combination co-culture resulted in enhanced cytotoxic effects**

For combination co-culture experiments, tumor cells were infected 24 h before T cell addition and then incubated another 24 h together with the T cells before cell killing was observed and confirmed by measuring LDH in supernatant samples (Fig. 45).

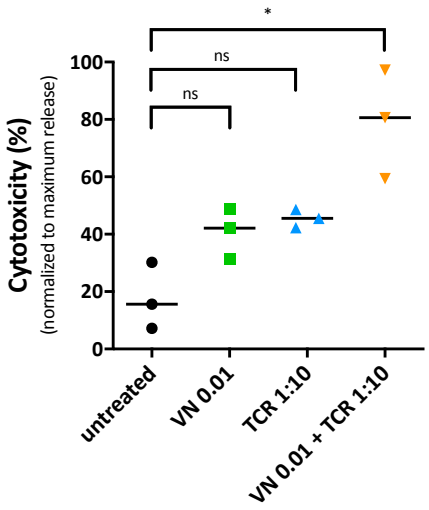


Figure 45: Cytotoxicity of TCR-transduced T cells co-cultured with pre-infected HCCc27-14 tumor cells at different effector-to-target ratios. Tumor cells were seeded and infected with VSV-NDV (MOI 0.01) and incubated for 24 h before T cells were added to the co-culture at an effector-to-target ratio of 1:10. 24 h later, LDH assay was performed to measure cytotoxicity. Normal distribution was confirmed by Shapiro-Wilk test and statistical significance was determined by a Welch's ANOVA and Dunnett's T3 multiple comparisons test to untreated control (ns: not significant; * $p < 0.05$).

Pre-infection of HCC cells in combination with TCR T cells led to a statistically significant enhancement of the cytotoxic effect. VSV-NDV and TCR-transduced T cells each induced around 40% cytotoxicity after 48 h and 24 h, respectively. In combination, an additive cytotoxic effect of around 80% was observed, indicating an acceleration of tumor cell killing and a benefit of combination treatment in this experimental set-up.

**TCR T cell recognition of HCC cells induced activation that was not affected by pre-infection with VSV-NDV**

Activation patterns of TCR T cells in co-culture were analyzed to investigate changes induced by VSV-NDV pre-infection of tumor cells. Co-culture experiments were set-up as detailed above and TCR T cells were harvested 24 h after addition in order to characterize the activation markers PD1, CD25 and CD69 by flow cytometry (Fig. 46).

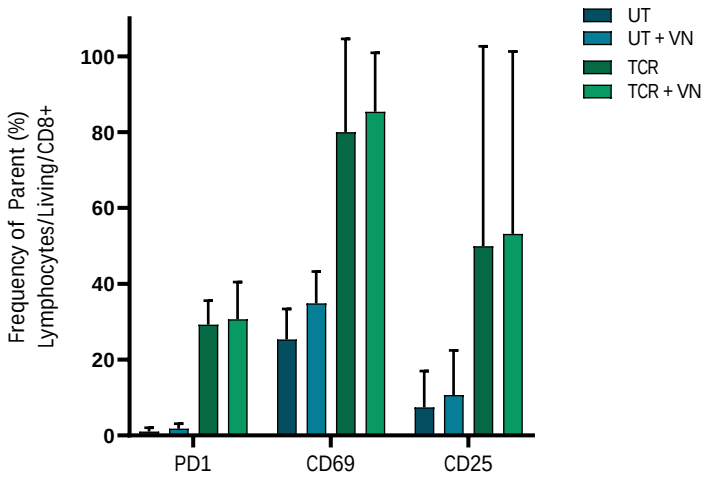


Figure 46: T cell activation markers PD1, CD25 and CD69 analyzed by flow cytometry after co-culture with HCC target cells. HCC tumor cells were seeded, infected with VSV-NDV (MOI 0.01) and incubated for 24 h before T cells were added to the co-culture at an effector-to-target ratio of 1:1. 24 h later, T cells were harvested, stained for the indicated activation markers and analyzed by flow cytometry. Experiments were performed in triplicate and results plotted as mean±SEM. Normal distribution was confirmed by Shapiro-Wilk test and statistical significance was determined by a Welch's ANOVA and Dunnett's T3 multiple comparisons test (not significant).

As was the case for B16-OVA co-culture, pre-infection with VSV-NDV did not change the activation pattern of TCR-transduced T cells induced by recognition of antigen-presenting tumor cells. In this case, untransduced T cells were used as a negative control showing a strongly reduced activation in response to tumor cells.

**Combination treatment induced MHC-I, while limiting PD-L1 expression**

Another important aspect was the examination of changes in the tumor cells in response to combination or monotherapy that could affect treatment outcome. Co-culture experiments were set-up as detailed above, and tumor cells were harvested 6 or 24 h after addition of T cells in order to characterize MHC-I and PD-L1 expression on the tumor cell surface via flow cytometry (Fig. 47 A+B).

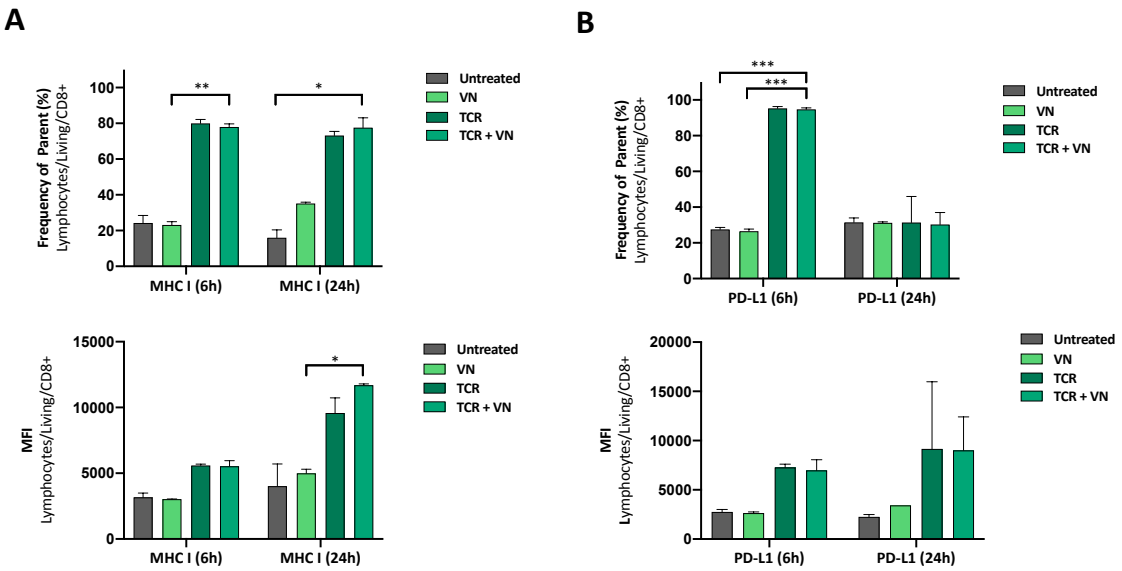


Figure 47: Changes of MHC-I and PD-L1 expression on tumor cells in response to combination co-culture. Tumor cells were seeded and cultured with or without VSV-NDV for 24 h before TCR T cells were added to the co-culture. Tumor cells were harvested after 6 or 24 h in co-culture, stained for MHC-I (A) and PD-L1 (B) on the cell surface and analyzed by flow cytometry. In the lower panel, intensity of expression on a single cell basis was evaluated by mean fluorescence intensity (MFI) and plotted as mean±SEM of three separate experiments. Normal distribution was confirmed by Shapiro-Wilk test and statistical significance was determined by a Welch's ANOVA and Dunnett's T3 multiple comparisons test to combination group (* $p < 0.05$, ** $p < 0.01$, *** $p < 0.001$).

The percentage of tumor cells expressing MHC-I was increased by 6 h after treatment with TCR T cells alone or in combination with VSV-NDV, similarly to the increase in expression levels on individual cells (indicated by MFI). This is in contrast to findings in B16-OVA cells that showed an accelerated effect on MHC-I expression after combination. This difference could possibly be due to the reduced susceptibility of HCCc27-14 cells to VSV-NDV infection. VSV-NDV alone was not able to significantly induce MHC-I expression, nor did it affect PD-L1 expression of these HCC tumor cells. TCR T cells alone and in combination with VSV-NDV, on the other hand, led to a quick increase in the number of PD-L1 expressing cells that dropped to background levels after 24 h.

Since pre-infection of HCC cells with VSV-NDV did not hinder TCR T cell activation, induced MHC-I presentation and improved cytotoxicity in co-culture (similar to B16 *in vitro* results), this data encouraged the transfer to an *in vivo* system detailed in the next section.

### 3.3.4 Combination Treatment of Induced Multifocal HCC in Mice

For the survival experiment, multifocal orthotopic hepatocellular carcinoma lesions were induced in the AST mouse model harboring a LoxP-flanked SV40-LTAg oncogene under the control of an albumin promoter by injection of adenovirus expressing cre recombinase (see Materials and Methods for details). After six weeks, animals were subjected to MR imaging to monitor tumor growth. As soon as tumor lesions began to appear (visible at around 2 mm), mice were categorized according to tumor progression and randomly distributed to treatment groups. Accordingly, they were injected intravenously with VSV-NDV ($1\times10^7$ TCID50) or PBS on day 0, followed by an intravenous OTI T cell injection ($1\times10^7$) on day 1 for combination treatment or OTI monotherapy. Intravenous virus or PBS injections were repeated weekly on day 7 and 14 (Fig. 48).

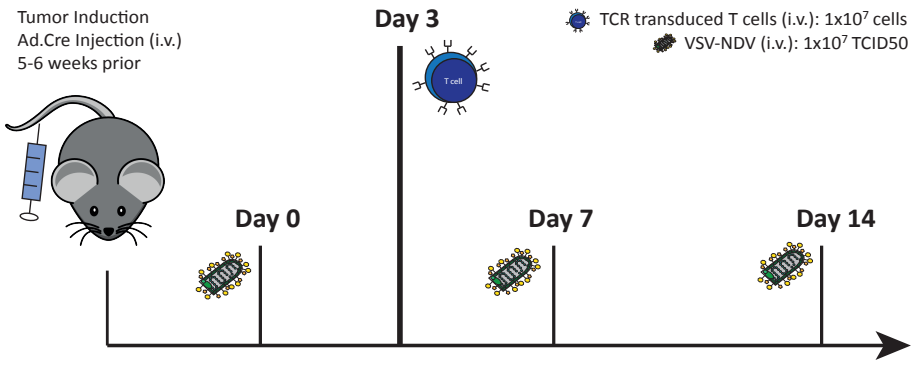


Figure 48: Experimental set-up of *in vivo* HCC treatment. Six weeks after tumor induction by adenovirus injection, mice were subjected to weekly MR imaging and randomly distributed to treatment groups upon tumor development. VSV-NDV was administered i.v. at indicated times (day 0, 7 and 14). TCR T cells were administered i.v. on day 3 after the first virus treatment. Animals were monitored and euthanized at humane endpoints.

Mice were monitored until their body weight increased more than 15% (due to expansion of the abdominal cavity caused by tumor growth and accumulation of ascites) or another humane endpoint was reached. Despite promising results in the treatment of murine melanoma, a treatment benefit could not be replicated in this experimental set-up (Fig. 49), possibly due to insufficient virus replication within the tumor lesions and a lack of T cell recruitment. Virus kinetics in the AST mouse model need to be investigated in more detail to elucidate this lack of treatment benefit.

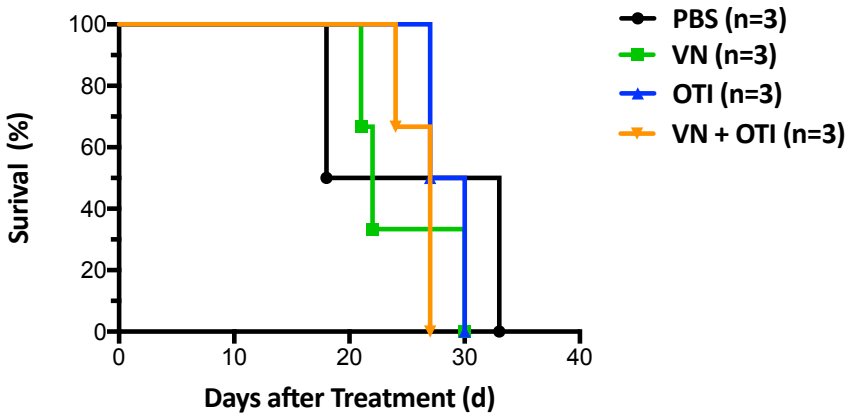


Figure 49: Treatment effects on survival of HCC-bearing mice. Five to six weeks after implantation, mice were screened for tumor formation and randomly distributed to the indicated treatment groups (n=3). Treatments were administered intravenously and survival was monitored and plotted in a Kaplan-Meier curve. Statistical significance was determined by log-rank test (ns: not significant).

In summary, VSV-NDV in combination with adoptive T cell transfer had beneficial effects on the tumor microenvironment, such as MHC-I upregulation and recruitment of T cells to areas of infection. Furthermore, combination therapy was able to prolong survival and even cure melanoma-bearing mice after intratumoral virus injection followed by OTI T cell administration, indicating the importance and potency of combination therapy as a curative treatment approach. *In vitro* susceptibility of an isolated HCC clone to VSV-NDV infection and efficient cytotoxic effect of TCR-transduced T cells targeting a model antigen expressed by these tumor cells could be confirmed. The additive treatment effect observed in combination co-culture, however, could not be transferred to an anti-tumor effect in the AST mouse model bearing orthotopic multifocal tumor lesion after systemic treatment administration. Improvements to be made and open questions to be answered, are discussed in the following section.

# 4 Discussion and Outlook

Adoptive cell transfer (ACT) and oncolytic virotherapy (OV) have evolved into promising immunotherapeutic agents as evidenced by the recent approval of CAR T cell therapies targeting CD19 for leukemia treatment [105], as well as the approval of an oncolytic herpes simplex virus expressing GM-CSF for the treatment of malignant melanoma [36]. Numerous agents are currently under preclinical investigation or clinical development and facing a multitude of challenges. One important challenge for ACT is the identification of potent tumor-associated antigens. Unknown variables concerning immunodominance of tumor antigens, intratumoral heterogeneity or the process of cancer immunoediting, lead to the selection of escape variants that can cause relapse [8]. Addressing this and other shortcomings of single agent approaches, immunotherapeutic combination strategies are emerging as a rational strategy targeting multiple mechanisms in order to induce synergistic tumor debulking, immune stimulation and potentially tumor clearance, as well as long-term protection against the tumor [62].

The aim of this doctoral thesis was to follow a two-pronged approach focusing on the development and characterization of the oncolytic VSV-NDV platform and adoptive T cell transfer in parallel in order to prepare the evaluation of the potential treatment benefits of their combination *in vitro* and *in vivo* (Fig. 7). Along these lines, Figure 50 presents a short overview of the findings that will be discussed in more detail.

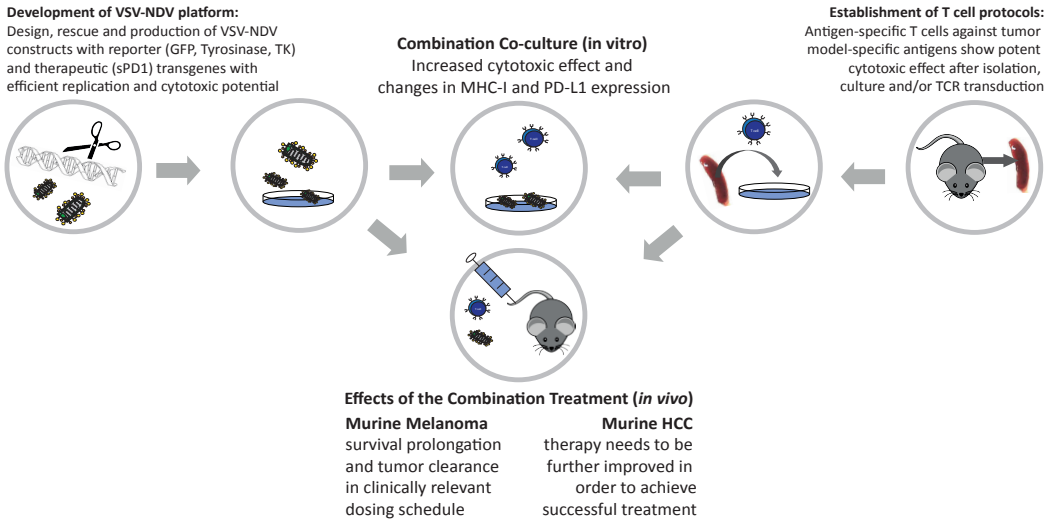


Figure 50: Illustrated overview of findings along the two-pronged experimental approach introduced in the aims of this thesis, including enhancement of the VSV-NDV platform by integrating reporter and therapeutic transgenes and the culturing and/or transduction of antigen-specifc T cells, as well as their combination *in vitro* and *in vivo*.

This doctoral thesis reports that the oncolytic VSV-NDV platform can be advanced by integration of reporter and therapeutic transgenes, including GFP, thymidine kinase, tyrosinase and soluble PD1 (Fig. 12). Replication kinetics and cytotoxicity can be affected by the insertion, as is the case for VSV-NDV-HAsPD1-Fc, that seems to have an attenuated effect compared to the parental VSV-NDV vector. Whether this attenuation is trangene-dependent or influenced by other possible genetic changes within the selected and purified virus clone should be further investigated. VSV-NDV is a versatile platform with a broad tumor tropism and its fusogenic mechanism of cell killing is effective in multiple tumor cell lines (Fig. 19).

This work demonstrates that VSV-NDV can complement adoptive T cell therapy by prolonging the median survival time as well as improving the overall survival in an immune competent melanoma mouse model. Combination therapy showed improved anti-tumor effects by at least three potential mechanisms.

- First, a rapid increase in MHC-I expression suggested by *in vitro* co-culture experiments and the maintenance of low PD-L1 expression levels (Fig. 27) indicate that the approach could lead to enhanced downstream immune-mediated anti-tumor effects. A lack of MHC-I and overexpression of PD-L1 are well-documented mechanisms that interfere with potential T cell responses [106, 107].

- Second, combination therapy results in an increased recruitment of $CD8^+$ T cells. *In vitro* observations using labeled T cells in co-culture (Fig. 28) were confirmed by flow cytometry analysis of tumor infiltrating lymphocytes from treated animals (Fig. 33). Infiltration of other immune cells, such as DCs, is essential to an effective anti-tumor immune response [108] and will be analyzed in future experiments.

- Third, data from a peptide activation assay using splenocytes from treated mice suggests an induction of epitope spreading after combination treatment (Fig. 39). In particular, the $CD4^+$ population responded to a TRP2 peptide with increased expression of IFN$\gamma$ and TNF-$\alpha$.

Additionally, VSV-NDV monotherapy led to an increase in OVA- and VSV-specific tumor infiltrating lymphocytes, while combination therapy seemed to limit the rise of a VSV-specific response. This difference will have to be further investigated, for example, by analyzing antibody responses against viral proteins in the animals at later time points. Furthermore, the impact of a reduced anti-viral immune response on subsequent virus injections has yet to be determined and could add an interesting piece of evidence to the ongoing discussion in the field, concerning the role of the anti-viral response in oncolytic virotherapy.

In summary, combination therapy improved survival in the B16 melanoma model even in a clinically relevant dosing scheme where monotherapies were ineffective. This trend could not be confirmed as clearly in the HCC model, due to various reasons, which will be discussed in more detail. In the next sections, important aspects concerning challenges of combination therapy, improvement possibilities for the continuation of the project will be discussed, leading up to an evaluation of the clinical potential of adoptive T cell transfer in combination with oncolytic VSV-NDV virotherapy.

## 4.1 Overcoming Challenges of Combination Therapy

Despite promising first results, the long-term survival rate of the combination therapy on overall survival was only 20% in the B16 experiments presented earlier, indicating that further improvements are needed. Different approaches have been suggested to improve combination therapy and a selection relevant to the experiments presented here will be discussed in the following paragraphs.

**Improving efficacy of transferred T cells**

Efficacy of transferred T cells can be improved by various strategies. The most basic strategies go back to the engineering of antigen-specific T cells. As mentioned earlier, leukemia patients have been successfully treated with CAR T cells and several reviews detail the combination advantages of CAR T cells and oncolytic viruses [109,110]. Comparison of the differences in efficacy of VSV-NDV combined with CAR T cells, as opposed to TCR T cells (shown here), could reveal interesting factors influencing combination therapy. Other engineering ideas have been proposed, such as the TCR and CD3 gene-modified T cells designed by Ahmadi *et al.*, that infiltrated tumors faster and in larger numbers, which resulted in more rapid tumor elimination compared with T cells modified by TCR only [111].

In general, lymphodepletion plays a key role in improving engraftment of transferred T cells. Treatment efficacy is enhanced by the elimination of regulatory T cells and competing elements of the immune system. As mentioned earlier, the benefits have been confirmed in a preclinical as well as a clinical setting. Moreover, research shows that lymphodepletion can further improve combination approaches. Cole *et al.* showed that anti-tumor effects of combination therapy were further improved in lymphopenic hosts [66]. Radical lymphodepletion may, however, cause severe side effects and toxicities related to radiation [112]. Only a small subset of patients would be suitable for such an aggressive protocol.

Furthermore, lymphodepletion removes not only the suppressive parts of the immune system, but also potentially important cells participating in the anti-tumor immune response. Research suggests, for example, the importance of endogenous T cells in preventing tumor immune escape [113]. Therefore, nonmyeloablative approaches accessible for a larger patient population would be preferable [112].

Based on the results presented here, complimentary virotherapy improves ACT when monotherapy is insufficient to control the tumor and the comparison between prior radiation, virotherapy or ACT monotherapy might provide more insight into its ability to replace lymphodepletion. Previous research indicates that cytokines play a key role in the benefits of lymphodepletion [114], suggesting that alternative therapies might be able to replace lymphodepletion by changing suppressive signaling pathways. Exogenous IL-2 or IL-15 therapy augmented the efficacy of adoptively transferred effector $CD8^+$ T cells more efficiently than enhanced lymphodepletion [115].

Combination therapy could even replace ACT monotherapy coupled with lymphodepletion as shown by Santos *et al.* using an adenovirus expressing TNF-$\alpha$ and IL-2 in combination with ACT [116]. These studies indicate the importance and advantages of adjuvant agents, such as cytokines, that can be engineered into viral vectors and improve immunotherapeutic approaches.

**Adjuvant agents complementing the combination**

In general, pharmacological or immunological agents that modify the effect of other therapeutic agents are termed adjuvants. They are most common in vaccination regimens, but can be similarly applied to improve immunotherapeutic approaches. Several strategies have been shown to serve as adjuvants for oncolytic virotherapy, ACT or both. The chemotherapeutic agent, Fludarabine, has been used as an adjuvant to enhance virotherapy [117] as well as in combination with cyclophosphamide to induce lymphodepletion and improve ACT [118].

Moving away from chemotherapeutic approaches due to their common adverse events, research is turning to alternative strategies. As Table 1 indicates, the majority of oncolytic vectors used in combination with ACT has been engineered to express therapeutic transgenes, such as cytokines, that work as T cell adjuvants improving therapeutic outcome. The advantages of cytokines have already been discussed as replacement strategies for lymphodepletion, and combination with cytokine-expressing vectors has, in general, been very successful in enhancing ACT effectivity in combination experiments [119–121].

Bispecific tumor-targeted T cell engager (BiTE) molecules, on the other hand, improve the targeting of heterogeneous tumor cells via the engagement of two distinct classes of receptors, i.e. CAR as well as native TCR. In combination experiments, this significantly improved tumor control and survival [122, 123]. Another type of adjuvant that has been successfully included into oncolytic virus vectors is checkpoint inhibitors.

**Checkpoint inhibition improving the combination**

Checkpoint inhibition experienced a success story like few other anti-tumor drug candidates. Over the last few years it has become the most successful immunotherapeutic agent approved for various tumor entities. Despite its success, non-responders or patients experiencing relapse remain common [25]. Additionally, checkpoint inhibitors cause undesirable side effects and adverse events in the majority of patients if administered systemically [93]. It has been shown that localized expression of PD-1 in the tumor after infection with an engineered myxoma virus can convey checkpoint inhibitor functions while minimizing off-target effects [94]. Since ACT is similarly sensitive to immune suppressive mechanisms as the endogenous immune response, it stands to reason that ACT will similarly benefit from checkpoint inhibition.

Upregulation of PD-L1 was observed in co-culture experiments of HCC in response to monotherapy (Fig. 27), as well as combination treatment (Fig. 47). Differences in MHC-I and PD-L1 responses to treatment suggest independent activation pathways. PD-L1 is regulated by IFN$\gamma$ and other cytokines/chemokines [124]. A PD-L1 increase in response to combination treatment would warrant the use of PD-1/L1 checkpoint blockers.

In this more complex scenario of a triple combination approach, adoptively transferred T cells are drawn to the tumor by oncolytic virus activity, their activation is further improved by a favorable tumor microenvironment and the response is prolonged by minimizing exhaustion effects. First results provided by an adenovirus expressing a PD-L1 mini-antibody in combination with CAR T cell therapy indicate a synergism of the treatment strategies resulting in an improved therapeutic outcome [125, 126].

First impressive results were revealed injecting VSV-NDV-HAsPD1-Fc intratumorally in a combination treatment set-up (Fig. 16). These effects will be further investigated in an ongoing project on a triple combination approach. The next section will provide an overview of the ongoing experiments focusing on the continued development of the VSV-NDV platform and a more detailed investigation of its combination with adoptive T cell transfer.

**Continued development of the VSV-NDV platform**

Investigations will be continued for VSV-NDV vectors expressing thymidine kinase, tyrosinase and soluble PD1. Moreover, the fusogenic VSV-NDV will be used as an immunotherapeutic platform expressing different cytokines and other therapeutic transgenes. The benefit of vectors equipped with cytokines has been discussed here previously.

Kinetics experiments evaluating the infection and replication of VSV-NDV in tumor tissue are needed to assess intratumoral spread and cell killing, innate immune signaling in response to the virus, generation of neutralizing antibodies and the amount of free virus particles that could be relevant for shedding or off-target effects. These vectors can then be included in the ongoing investigations of the combination approach.

Improvement strategies mentioned above might also enhance therapeutic efficacy in the HCC mouse model. However, HCC also presents a new set of challenges that will have to be specifically addressed in order to improve therapy.

## 4.2 Improving HCC Therapy

Research to develop improved treatment options for HCC is based on artificial implantable models or transgenic mouse models characterized by oncogene overexpression, e.g. AST mouse model (Fig.11), or tumor suppressor inhibition. This method of tumor induction does not resemble human tumor evolution depending on the sequential accumulation of individually different mutations. However, for this reason, these models often give rise to immunologically cold and genetically stable tumors that typically do not respond well to checkpoint inhibition, a finding also observed in human tumors [8].

Despite the fact that VSV-NDV monotherapy already showed promising therapeutic effects after systemic administration in the treatment of an inducible murine HCC model [40], this effect could not be replicated in combination experiments (Fig. 49). Data suggest that the complex immunosuppressive liver environment, together with reduced virus delivery to orthotopic tumor lesions after systemic administration and minimized T cell engraftment due to a lack of a prior myeloablative treatment (discussed previously) could not be overcome with the experimental set-up presented here.

The liver is associated with various mechanisms of immune tolerance [127]. Myeloid-derived suppressor cells, Kupffer cells, and liver dendritic cells predominantly promote a network of active immunosuppressive pathways, dampening the activation of $CD8^+$ and $CD4^+$ effector T cells.

Liver metastases were also associated with reduced marginal $CD8^+$ T-cell infiltration [128], leading to reduced responses and limited treatment effect of the PD-1 inhibitor, pembrolizumab. MDSCs and hepatic stellate cells constituting the architecture of the liver, together with cancer-associated fibroblasts, present an effective barrier for T cell migration and infiltration, resulting in minimized activation and tumor cell elimination. These mechanisms could potentially be overcome by efficient virus replication and active inflammatory signaling [129]. However, it seems that systemic delivery and efficient replication in this experimental set-up was not potent enough to break immune tolerance and recruit antigen-specific T cells to the tumor site. Systemic delivery is still an essential problem to be solved in order to provide access to the full potential of oncolytic virotherapy, also in combination approaches.

**Improving systemic virus delivery**

Combination therapy offers an option to bypass the limitations of systemic delivery by using adoptively transferred cells as carriers. A very limited amount of systemically injected oncolytic virus is able to reach the tumor and effectively infect tumor cells. This is due to sequestration of virus particles in the liver and spleen, neutralization by antiviral antibodies and complement proteins in the blood, as well as limited permeability of tumor vessels and interstitial pressure of certain tumor lesions inhibiting infiltration of virus particles [38].

These factors limit the number of intratumoral infectious centers that may lead to tumor destruction upon expansion. Approaches, such as virus particle shielding, have been developed to avoid neutralization in the blood [130]. Most of these barriers, however, could be overcome at the same time by using cell carriers to transport virus particles directly to the tumor lesions. In previous studies, virus hitchhiking on immune cells has led to viral replication in tumor cells and improved the therapeutic outcome in several tumor models [70–72, 74, 75]. This approach could limit viral sequestration in the liver and spleen to improve transport to tumor lesions disseminated throughout the body.

Successful transport of VSV particles using $CD8^+$ memory T cells as carrier cells has already been established previously [131]. However, pilot experiments to evaluate the potential of VSV-NDV to be transported by murine T cells would need to be performed, since preliminary data indicate that these cells do not support VSV-NDV replication (data not shown). Differences between murine and human T cells in terms of their abilities to serve as virus carrier would also need to be examined and taken into consideration to evaluate the feasibility of a potential clinical translation of the approach.

## 4.3 Clinical Translation

Experimental approaches using model antigens, such as SV40-LTAg or ovalbumin, are widely accepted for the preclinical investigation of therapeutic effects on tumor progression and immune responses. In most cases, however, immunogenicity is far less pronounced for physiological TAAs compared with model antigens. Moreover, human tumors are characterized by heterologous expression of antigens throughout the tumor. This contributes to the lack of reproducibility of impressive preclinical findings in a clinical setting. On the path towards clinical translation, these limitations will need be rigorously addressed by adapting the therapeutic approach to target real tumor antigens and by utilizing more predictive preclinical models to better reflect the clinical scenario.

Alpha-fetoprotein (AFP) is a TAA expressed by tumors induced in the AST mouse model, as well as in up to 80% of clinical HCC cases. It has been used as a biomarker for diagnosis and clinical outcome as well as a target in clinical immunotherapeutic applications [132, 133]. Adoptive T cell therapies targeting AFP have shown first promising results in HepG2 treatment in NSG mice [134]. Considering all this, the AFP antigen can be used as a target-antigen in studies combining ACT with oncolytic virotherapy. Experiments and evaluations leading up to clinical translation will be performed based on methods and experience established during this doctoral thesis.

Differences between murine and human immune systems as well as the limitations of murine tumor models mentioned above, impede valid predictions from preclinical data on the use of these therapeutic approaches in human patients. It has been estimated that only 10%–20% of cancer drug candidates show effectiveness in clinical trials [135]. This high rate of clinical failure also drives the cost of cancer therapy. Differences between mouse and human immunology, such as divergent immune signaling, T cell polarization and distinct co-stimulatory mechanisms [136], have a direct impact on the efficacy of immunotherapies, since they are closely intertwined with the complex immune signaling network. This may be one of the reasons why some immunotherapeutic agents, such as individual oncolytic viruses, demonstrated very promising preclinical data, that could not be confirmed in the clinic. Only one oncolytic virus has been approved for clinical use so far, despite the clinical development of numerous oncolytic agents.

Furthermore, dosing schemes with frequent virus injections that show significant tumor reduction in a preclinical setting are not suitable for clinical translation [39]. Our results comparing VSV-NDV in a frequent dosing scheme (3 times within one week; Fig 40) to a clinically more relevant dosing scheme (3 times one week apart; Fig 30) confirm the importance of virus dosing for therapeutic outcome.

Only combination therapy was similarly effective in both dosing schemes, suggesting a more stable response and easier transfer into the clinic.

**ACT and OV in combination trials**

Despite a significant increase in the number of combination trials in general, only very recently have the first clinical studies examining adoptive cell transfer in combination with oncolytic virotherapy been introduced. As of April 2020, two small phase I trials examining the combination of oncolytic virus with adoptive cell transfer have been registered with the NIH and started or will start recruiting in 2020 (*www.clinicaltrials.gov*).

- A First in Human Phase I Trial of Binary Oncolytic Adenovirus in Combination With HER2-Specific Autologous CAR T Cells in Patients With Advanced HER2 Positive Solid Tumors (VISTA) - NCT03740256
- A Phase 1, Open-Label, Dose-Escalation Clinical Trial of Tumor Necrosis Factor Alpha and Interleukin 2 Coding Oncolytic Adenovirus TILT-123 in Melanoma Patients Receiving Adoptive Cell Therapy With Tumor Infiltrating Lymphocytes (TUNINTIL) - NCT04217473

In both studies, T cell transfer is complemented with oncolytic adenovirus enhanced by the expression of a therapeutic transgene, providing additional stimulatory signals or checkpoint inhibitor functions, respectively. Preclinical data on their approaches was mentioned earlier and can be found in the introductory section on combination therapy (Tab. 1). These considerations emphasize the potential of combination therapy based on adoptive T cell transfer complemented by oncolytic virotherapy with VSV-NDV as a translational approach that can advance patient treatment in the future.

**The clinical translation of VSV-NDV**

The VSV-NDV platform has shown potential in preclinical studies and is under development for clinical application in the framework of a pre-seed start-up idea called Fusix Biotech. In order to provide patient therapy, the VSV-NDV vector has to undergo rigorous testing of efficacy and safety in different preclinical models. The project plan includes the completion of a preclinical data package and adaptation of the VSV-NDV manufacturing process to industry standards, including scalable production and purification methods according to CMC procedures and eventually GMP production. These will be the first steps on the way of transferring the fusogenic VSV-NDV into the clinic. Therefore, the development of effective combination therapy approaches based on this oncolytic virus platform, has the potential to one day achieve clinical application in patients.

# 5 Summary

With immunotherapeutic approaches gaining ground in the clinic, combination approaches are pursued to target multiple mechanisms of the complex anti-tumor immune response. Adoptive cell transfer (ACT) and oncolytic virotherapy (OV) have evolved into promising immunotherapeutic agents. While effective against leukemic cells, ACT has not been as successful in the treatment of solid tumors due immunosuppressive tumor microenvironments. OV therapy has shown great promise in preclinical models, but up to now only one oncolytic agent has been approved for clinical application. The doctoral thesis presented here investigates the rationale behind combining these powerful immunotherapeutic agents and presents experimental data concerning the potential of combining the hybrid oncolytic VSV-NDV platform with adoptively transferred antigen-specific T cells.

VSV-NDV is a versatile platform with a broad tumor tropism and a fusogenic mechanism of cell killing, that can be further advanced by integration of reporter and therapeutic transgenes, as confirmed here by the construction of VSV-NDV variants expressing GFP, thymidine kinase, tyrosinase and soluble PD1. Replication kinetics and cytotoxicity can be affected by the insertion.

This work demonstrates, that VSV-NDV can complement adoptive T cell therapy by prolonging the median survival time as well as improving the overall survival in an immune competent melanoma mouse model in a clinically relevant dosing scheme, where mono-therapies show no treatment effect. Combination treatment induces $CD8^+$ T cell infiltration and data on epitope spreading suggest the induction of a broad anti-tumor immune response. The mechanisms of the combination approach need to be characterized further and adapted accordingly in order to improve treatment of other tumor entities, since combination failed to show an anti-tumor response in an aggressive, orthotopic liver cancer model in mice.

Preliminary data suggests that further improvements could be based on a virus construct with a therapeutic transgene conferring checkpoint inhibitor functions upon expression in the infected cell. Moving towards multiple agents, combination approaches are becoming more complex and in order to identify a potentially curative treatment regimen, the therapeutic agents and their combination effects have to be well-characterized and examined in predictive animal models as a basis for clinical translation. This thesis offers a glimpse into the complex and fascinating field of combination immunotherapy using oncolytic virotherapy to complement adoptive T cell transfer.

# 6 List of Abbreviations

**Abbreviations**

| | |
|---|---|
| ACT | Adoptive cell therapy |
| ADCC | Antibody-dependent cellular cytotoxicity |
| AFP | Alpha-fetoprotein |
| APC | Antigen-presenting cell |
| BiTE | Bispecific tumor-targeted T cell engager |
| CAR | Chimeric antigen receptor |
| CDC | Complement-dependent cytotoxicity |
| CIK | Cytokine-induced killer cell |
| CTL | Cytotoxic T lymphocytes |
| CTLA-4 | Cytotoxic T lymphocyte-associated molecule-4 |
| DAMP | Damage-associated molecular pattern |
| DC | Dendritic cell |
| GFP | Green fluorescent protein |
| GM-CSF | Granulocyte-macrophage colony-stimulating factor |
| HCC | Hepatocellular carcinoma |
| HRP | Horseradish peroxidase |
| HSV | Herpes simplex virus |
| Huh7 | human hepatocellular carcinoma cell line |
| i.t. | intratumoral |
| i.v. | intravenous |
| IFN | Interferon |
| IL | Interleukin |
| MDSC | Myeloid-derived suppressor cell |
| MHC | Major histocompatibility complex |
| MOI | Multiplicity of infection |
| MRI | Magnetic resonance imaging |

| | |
|---|---|
| NDV | Newcastle Disease Virus |
| NK cell | Natural killer cell |
| NKT cell | Natural killer T cell |
| OV | Oncolytic virus |
| OVA | Ovalbumin |
| PAMP | Pathogen-associated molecular pattern |
| PBS | Phosphate-buffered saline |
| PD-1 | Programmed cell death receptor-1 |
| PD-L1 | Programmed cell death receptor ligand-1 |
| PET | Positron emission tomography |
| PFU | Plaque forming units |
| PPR | Pattern-recognition receptors |
| RT | Room temperature |
| SEM | Standard error of the mean |
| $T_{reg}$ | Regulatory T cells |
| TAA | Tumor-associated antigens |
| TAM | Tumor-associated macrophages |
| TCID50 | 50% tissue culture infective dose |
| TCR | T cell receptor |
| TK | Thymidine kinase |
| TME | Tumor microenvironment |
| TNF | Tumor necrosis factor |
| TRP2 | Tyrosinase-related protein 2 |
| TSA | Tumor-specific antigens |
| VSV | Vesicular Stomatitis Virus |

# 7 List of Figures and Tables

## List of Figures

# List of Tables

# 8 References

[1] D. Hanahan and R. A. Weinberg. The hallmarks of cancer. *Cell*, 100(1):57–70, 2000.

[2] D. Hanahan and R. A. Weinberg. Hallmarks of cancer: the next generation. *Cell*, 144(5):646–74, 2011.

[3] F. Cavallo, C. De Giovanni, P. Nanni, G. Forni, and P. L. Lollini. 2011: the immune hallmarks of cancer. *Cancer Immunol Immunother*, 60(3):319–26, 2011.

[4] D. S. Chen and I. Mellman. Oncology meets immunology: the cancer-immunity cycle. *Immunity*, 39(1):1–10, 2013.

[5] Nima Rezaei. *Cancer Immunology A Translational Medicine Context*. Springer, Cham, 2020.

[6] Charles Janeway. Immunobiology : the immune system in health and disease. 2001.

[7] S. D. Martin, S. D. Brown, D. A. Wick, J. S. Nielsen, D. R. Kroeger, K. Twumasi-Boateng, R. A. Holt, and B. H. Nelson. Low mutation burden in ovarian cancer may limit the utility of neoantigen-targeted vaccines. *PLoS One*, 11(5):e0155189, 2016.

[8] P. S. Hegde and D. S. Chen. Top 10 challenges in cancer immunotherapy. *Immunity*, 52(1):17–35, 2020.

[9] J. Galon and D. Bruni. Approaches to treat immune hot, altered and cold tumours with combination immunotherapies. *Nat Rev Drug Discov*, 18(3):197–218, 2019.

[10] D. M. Pardoll. The blockade of immune checkpoints in cancer immunotherapy. *Nat Rev Cancer*, 12(4):252–64, 2012.

[11] A. Chen, Y. Zhang, G. Meng, D. Jiang, H. Zhang, M. Zheng, M. Xia, A. Jiang, J. Wu, C. Beltinger, and J. Wei. Oncolytic measles virus enhances antitumour responses of adoptive cd8(+)nkg2d(+) cells in hepatocellular carcinoma treatment. *Sci Rep*, 7(1):5170, 2017.

[12] Nicolas van Baren and Benoît J. Van den Eynde. Tryptophan-degrading enzymes in tumoral immune resistance. *Frontiers in Immunology*, 6:34, 2016.

[13] R. M. Gibbons Johnson and H. Dong. Functional expression of programmed death-ligand 1 (b7-h1) by immune cells and tumor cells. *Front Immunol*, 8:961, 2017.

[14] A. Sugiura and J. C. Rathmell. Metabolic barriers to t cell function in tumors. *J Immunol*, 200(2):400–407, 2018.

[15] J. A. Marin-Acevedo, B. Dholaria, A. E. Soyano, K. L. Knutson, S. Chumsri, and Y. Lou. Next generation of immune checkpoint therapy in cancer: new developments and challenges. *J Hematol Oncol*, 11(1):39, 2018.

[16] J. Tang, A. Shalabi, and V. M. Hubbard-Lucey. Comprehensive analysis of the clinical immuno-oncology landscape. *Ann Oncol*, 29(1):84–91, 2018.

[17] M. Reck, D. Heigener, and N. Reinmuth. Immunotherapy for small-cell lung cancer: emerging evidence. *Future Oncol*, 12(7):931–43, 2016.

[18] O. Hamid, C. Robert, A. Ribas, F. S. Hodi, E. Walpole, A. Daud, A. S. Arance, E. Brown, C. Hoeller, L. Mortier, J. Schachter, J. Long, S. Ebbinghaus, N. Ibrahim, and M. Butler. Antitumour activity of pembrolizumab in advanced mucosal melanoma: a post-hoc analysis of keynote-001, 002, 006. *Br J Cancer*, 119(6):670–674, 2018.

[19] T. L. Walunas, D. J. Lenschow, C. Y. Bakker, P. S. Linsley, G. J. Freeman, J. M. Green, C. B. Thompson, and J. A. Bluestone. Ctla-4 can function as a negative regulator of t cell activation. *Immunity*, 1(5):405–13, 1994.

[20] D. R. Leach, M. F. Krummel, and J. P. Allison. Enhancement of antitumor immunity by ctla-4 blockade. *Science*, 271(5256):1734–6, 1996.

[21] A. Ribas and J. D. Wolchok. Cancer immunotherapy using checkpoint blockade. *Science*, 359(6382):1350–1355, 2018.

[22] Y. Ishida, Y. Agata, K. Shibahara, and T. Honjo. Induced expression of pd-1, a novel member of the immunoglobulin gene superfamily, upon programmed cell death. *Embo j*, 11(11):3887–95, 1992.

[23] H. Dong, S. E. Strome, D. R. Salomao, H. Tamura, F. Hirano, D. B. Flies, P. C. Roche, J. Lu, G. Zhu, K. Tamada, V. A. Lennon, E. Celis, and L. Chen. Tumor-associated b7-h1 promotes t-cell apoptosis: a potential mechanism of immune evasion. *Nat Med*, 8(8):793–800, 2002.

[24] R. Mandal, R. M. Samstein, K. W. Lee, J. J. Havel, H. Wang, C. Krishna, E. Y. Sabio, V. Makarov, F. Kuo, P. Blecua, A. T. Ramaswamy, J. N. Durham, B. Bartlett, X. Ma, R. Srivastava, S. Middha, A. Zehir, J. F. Hechtman, L. G. Morris, N. Weinhold, N. Riaz, D. T. Le, Jr. Diaz, L. A., and T. A. Chan. Genetic diversity of tumors with mismatch repair deficiency influences anti-pd-1 immunotherapy response. *Science*, 364(6439):485–491, 2019.

[25] R. W. Jenkins, D. A. Barbie, and K. T. Flaherty. Mechanisms of resistance to immune checkpoint inhibitors. *Br J Cancer*, 118(1):9–16, 2018.

[26] Anand Rotte. Combination of ctla-4 and pd-1 blockers for treatment of cancer. *Journal of Experimental & Clinical Cancer Research*, 38(1):255, 2019.

[27] S. A. Rosenberg, B. S. Packard, P. M. Aebersold, D. Solomon, S. L. Topalian, S. T. Toy, P. Simon, M. T. Lotze, J. C. Yang, C. A. Seipp, and et al. Use of tumor-infiltrating lymphocytes and interleukin-2 in the immunotherapy of patients with metastatic melanoma. a preliminary report. *N Engl J Med*, 319(25):1676–80, 1988.

[28] M. E. Dudley, J. R. Wunderlich, P. F. Robbins, J. C. Yang, P. Hwu, D. J. Schwartzentruber, S. L. Topalian, R. Sherry, N. P. Restifo, A. M. Hubicki, M. R. Robinson, M. Raffeld, P. Duray, C. A. Seipp, L. Rogers-Freezer, K. E. Morton, S. A. Mavroukakis, D. E. White, and S. A. Rosenberg. Cancer regression and autoimmunity in patients after clonal repopulation with antitumor lymphocytes. *Science*, 298(5594):850–4, 2002.

[29] C. June, S. A. Rosenberg, M. Sadelain, and J. S. Weber. T-cell therapy at the threshold. *Nat Biotechnol*, 30(7):611–4, 2012.

[30] M. H. Kershaw, J. A. Westwood, and P. K. Darcy. Gene-engineered t cells for cancer therapy. *Nat Rev Cancer*, 13(8):525–41, 2013.

[31] D. Seimetz, K. Heller, and J. Richter. Approval of first car-ts: Have we solved all hurdles for atmps? *Cell Med*, 11, 2019.

[32] S. A. Grupp, M. Kalos, D. Barrett, R. Aplenc, D. L. Porter, S. R. Rheingold, D. T. Teachey, A. Chew, B. Hauck, J. F. Wright, M. C. Milone, B. L. Levine, and C. H. June. Chimeric antigen receptor-modified t cells for acute lymphoid leukemia. *N Engl J Med*, 368(16):1509–1518, 2013.

[33] N. P. Restifo, F. M. Marincola, Y. Kawakami, J. Taubenberger, J. R. Yannelli, and S. A. Rosenberg. Loss of functional beta 2-microglobulin in metastatic melanomas from five patients receiving immunotherapy. *J Natl Cancer Inst*, 88(2):100–8, 1996.

[34] Eric Tran, Paul F. Robbins, Yong-Chen Lu, Todd D. Prickett, Jared J. Gartner, Li Jia, Anna Pasetto, Zhili Zheng, Satyajit Ray, Eric M. Groh, Isaac R. Kriley, and Steven A. Rosenberg. T-cell transfer therapy targeting mutant kras in cancer. *New England Journal of Medicine*, 375(23):2255–2262, 2016.

[35] B. D. Lichty, C. J. Breitbach, D. F. Stojdl, and J. C. Bell. Going viral with cancer immunotherapy. *Nat Rev Cancer*, 14(8):559–67, 2014.

[36] Robert M. Conry, Brian Westbrook, Svetlana McKee, and Timothy Graham Norwood. Talimogene laherparepvec: First in class oncolytic virotherapy. *Human vaccines & immunotherapeutics*, 14(4):839–846, 2018.

[37] E. Katsoulidis, S. Kaur, and L. C. Platanias. Deregulation of interferon signaling in malignant cells. *Pharmaceuticals (Basel)*, 3(2):406–418, 2010.

[38] S. J. Russell, K. W. Peng, and J. C. Bell. Oncolytic virotherapy. *Nat Biotechnol*, 30(7):658–70, 2012.

[39] M. Lalu, G. J. Leung, Y. Y. Dong, J. Montroy, C. Butler, R. C. Auer, and D. A. Fergusson. Mapping the preclinical to clinical evidence and development trajectory of the oncolytic virus talimogene laherparepvec (t-vec): a systematic review. *BMJ Open*, 9(12):e029475, 2019.

[40] S. Abdullahi, M. Jakel, S. J. Behrend, K. Steiger, G. Topping, T. Krabbe, A. Colombo, V. Sandig, T. S. Schiergens, W. E. Thasler, J. Werner, S. F. Lichtenthaler, R. M. Schmid, O. Ebert, and J. Altomonte. A novel chimeric oncolytic

virus vector for improved safety and efficacy as a platform for the treatment of hepatocellular carcinoma. *J Virol*, 92(23), 2018.

[41] P. Ge, J. Tsao, S. Schein, T. J. Green, M. Luo, and Z. H. Zhou. Cryo-em model of the bullet-shaped vesicular stomatitis virus. *Science*, 327(5966):689–93, 2010.

[42] D. F. Stojdl, B. Lichty, S. Knowles, R. Marius, H. Atkins, N. Sonenberg, and J. C. Bell. Exploiting tumor-specific defects in the interferon pathway with a previously unknown oncolytic virus. *Nat Med*, 6(7):821–5, 2000.

[43] K. X. Zhang, Y. Matsui, B. A. Hadaschik, C. Lee, W. Jia, J. C. Bell, L. Fazli, A. I. So, and P. S. Rennie. Down-regulation of type i interferon receptor sensitizes bladder cancer cells to vesicular stomatitis virus-induced cell death. *Int J Cancer*, 127(4):830–8, 2010.

[44] B. D. Lichty, A. T. Power, D. F. Stojdl, and J. C. Bell. Vesicular stomatitis virus: re-inventing the bullet. *Trends Mol Med*, 10(5):210–6, 2004.

[45] S. U. Emerson. Reconstitution studies detect a single polymerase entry site on the vesicular stomatitis virus genome. *Cell*, 31(3 Pt 2):635–42, 1982.

[46] S. Bishnoi, R. Tiwari, S. Gupta, S. N. Byrareddy, and D. Nayak. Oncotargeting by vesicular stomatitis virus (vsv): Advances in cancer therapy. *Viruses*, 10(2), 2018.

[47] J. Cronin, X. Y. Zhang, and J. Reiser. Altering the tropism of lentiviral vectors through pseudotyping. *Curr Gene Ther*, 5(4):387–98, 2005.

[48] K. Shinozaki, O. Ebert, A. Suriawinata, S. N. Thung, and S. L. Woo. Prophylactic alpha interferon treatment increases the therapeutic index of oncolytic vesicular stomatitis virus virotherapy for advanced hepatocellular carcinoma in immune-competent rats. *J Virol*, 79(21):13705–13, 2005.

[49] J. E. Johnson, F. Nasar, J. W. Coleman, R. E. Price, A. Javadian, K. Draper, M. Lee, P. A. Reilly, D. K. Clarke, R. M. Hendry, and S. A. Udem. Neurovirulence properties of recombinant vesicular stomatitis virus vectors in non-human primates. *Virology*, 360(1):36–49, 2007.

[50] Z. Gray, A. Tabarraei, A. Moradi, and M. R. Kalani. M51r and delta-m51 matrix protein of the vesicular stomatitis virus induce apoptosis in colorectal cancer cells. *Mol Biol Rep*, 46(3):3371–3379, 2019.

[51] L. Zhang, M. B. Steele, N. Jenks, J. Grell, L. Suksanpaisan, S. Naik, M. J. Federspiel, M. Q. Lacy, S. J. Russell, and K. W. Peng. Safety studies in tumor and non-tumor-bearing mice in support of clinical trials using oncolytic vsv-ifnbeta-nis. *Hum Gene Ther Clin Dev*, 27(3):111–22, 2016.

[52] G. Wollmann, E. Drokhlyansky, J. N. Davis, C. Cepko, and A. N. van den Pol. Lassa-vesicular stomatitis chimeric virus safely destroys brain tumors. *J Virol*, 89(13):6711–24, 2015.

[53] A. Muik, L. J. Stubbert, R. Z. Jahedi, Y. Geibeta, J. Kimpel, C. Dold, R. Tober, A. Volk, S. Klein, U. Dietrich, B. Yadollahi, T. Falls, H. Miletic, D. Stojdl, J. C. Bell, and D. von Laer. Re-engineering vesicular stomatitis virus to abrogate neurotoxicity, circumvent humoral immunity, and enhance oncolytic potency. *Cancer Res*, 74(13):3567–78, 2014.

[54] P. Fournier and V. Schirrmacher. Oncolytic newcastle disease virus as cutting edge between tumor and host. *Biology (Basel)*, 2(3):936–75, 2013.

[55] R. A. Lamb. Paramyxovirus fusion: a hypothesis for changes. *Virology*, 197(1):1–11, 1993.

[56] L. Sanchez-Felipe, E. Villar, and I. Munoz-Barroso. alpha2-3- and alpha2-6- n-linked sialic acids allow efficient interaction of newcastle disease virus with target cells. *Glycoconj J*, 29(7):539–49, 2012.

[57] A. L. Pecora, N. Rizvi, G. I. Cohen, N. J. Meropol, D. Sterman, J. L. Marshall, S. Goldberg, P. Gross, J. D. O'Neil, W. S. Groene, M. S. Roberts, H. Rabin, M. K. Bamat, and R. M. Lorence. Phase i trial of intravenous administration of pv701, an oncolytic virus, in patients with advanced solid cancers. *J Clin Oncol*, 20(9):2251–66, 2002.

[58] T. Krabbe and J. Altomonte. Fusogenic viruses in oncolytic immunotherapy. *Cancers (Basel)*, 10(7), 2018.

[59] C. Burton and E. Bartee. Syncytia formation in oncolytic virotherapy. *Mol Ther Oncolytics*, 15:131–139, 2019.

[60] A. Vigil, M. S. Park, O. Martinez, M. A. Chua, S. Xiao, J. F. Cros, L. Martinez-Sobrido, S. L. Woo, and A. Garcia-Sastre. Use of reverse genetics to enhance the oncolytic properties of newcastle disease virus. *Cancer Res*, 67(17):8285–92, 2007.

[61] J. Altomonte, S. Marozin, R. M. Schmid, and O. Ebert. Engineered newcastle disease virus as an improved oncolytic agent against hepatocellular carcinoma. *Mol Ther*, 18(2):275–84, 2010.

[62] C. Schmidt. The benefits of immunotherapy combinations. *Nature*, 552(7685):S67–s69, 2017.

[63] P. Sharma and J. P. Allison. Immune checkpoint targeting in cancer therapy: toward combination strategies with curative potential. *Cell*, 161(2):205–14, 2015.

[64] C. J. Breitbach, B. D. Lichty, and J. C. Bell. Oncolytic viruses: Therapeutics with an identity crisis. *EBioMedicine*, 9:31–36, 2016.

[65] N. Woller, E. Gurlevik, B. Fleischmann-Mundt, A. Schumacher, S. Knocke, A. M. Kloos, M. Saborowski, R. Geffers, M. P. Manns, T. C. Wirth, S. Kubicka, and F. Kuhnel. Viral infection of tumors overcomes resistance to pd-1-immunotherapy by broadening neoantigenome-directed t-cell responses. *Mol Ther*, 23(10):1630–40, 2015.

[66] C. Cole, J. Qiao, T. Kottke, R. M. Diaz, A. Ahmed, L. Sanchez-Perez, G. Brunn, J. Thompson, J. Chester, and R. G. Vile. Tumor-targeted, systemic delivery of therapeutic viral vectors using hitchhiking on antigen-specific t cells. *Nat Med*, 11(10):1073–81, 2005.

[67] J. Qiao, H. Wang, T. Kottke, R. M. Diaz, C. Willmon, A. Hudacek, J. Thompson, K. Parato, J. Bell, J. Naik, J. Chester, P. Selby, K. Harrington, A. Melcher, and R. G. Vile. Loading of oncolytic vesicular stomatitis virus onto antigen-specific t cells enhances the efficacy of adoptive t-cell therapy of tumors. *Gene Ther*, 15(8):604–16, 2008.

[68] P. Wongthida, R. M. Diaz, C. Pulido, D. Rommelfanger, F. Galivo, K. Kaluza, T. Kottke, J. Thompson, A. Melcher, and R. Vile. Activating systemic t-cell immunity against self tumor antigens to support oncolytic virotherapy with vesicular stomatitis virus. *Hum Gene Ther*, 22(11):1343–53, 2011.

[69] D. M. Rommelfanger, P. Wongthida, R. M. Diaz, K. M. Kaluza, J. M. Thompson, T. J. Kottke, and R. G. Vile. Systemic combination virotherapy for melanoma with tumor antigen-expressing vesicular stomatitis virus and adoptive t-cell transfer. *Cancer Res*, 72(18):4753–64, 2012.

[70] S. H. Thorne, R. S. Negrin, and C. H. Contag. Synergistic antitumor effects of immune cell-viral biotherapy. *Science*, 311(5768):1780–4, 2006.

[71] S. H. Thorne, W. Liang, P. Sampath, T. Schmidt, R. Sikorski, A. Beilhack, and C. H. Contag. Targeting localized immune suppression within the tumor through repeat cycles of immune cell-oncolytic virus combination therapy. *Mol Ther*, 18(9):1698–705, 2010.

[72] X. Zhao, W. Ouyang, C. Chester, S. Long, N. Wang, and Z. He. Cytokine-induced killer cell delivery enhances the antitumor activity of oncolytic reovirus. *PLoS One*, 12(9):e0184816, 2017.

[73] X. Fu, A. Rivera, L. Tao, and X. Zhang. An hsv-2 based oncolytic virus can function as an attractant to guide migration of adoptively transferred t cells to tumor sites. *Oncotarget*, 6(2):902–14, 2015.

[74] C. Pfirschke and V. Schirrmacher. Cross-infection of tumor cells by contact with t lymphocytes loaded with newcastle disease virus. *Int J Oncol*, 34(4):951–62, 2009.

[75] H. VanSeggelen, D. G. Tantalo, A. Afsahi, J. A. Hammill, and J. L. Bramson. Chimeric antigen receptor-engineered t cells as oncolytic virus carriers. *Mol Ther Oncolytics*, 2:15014, 2015.

[76] D. Zamarin, R. B. Holmgaard, S. K. Subudhi, J. S. Park, M. Mansour, P. Palese, T. Merghoub, J. D. Wolchok, and J. P. Allison. Localized oncolytic virotherapy overcomes systemic tumor resistance to immune checkpoint blockade immunotherapy. *Sci Transl Med*, 6(226):226ra32, 2014.

[77] S. Morita, T. Kojima, and T. Kitamura. Plat-e: an efficient and stable system for transient packaging of retroviruses. *Gene Ther*, 7(12):1063–6, 2000.

[78] I. Jordan, A. Vos, S. Beilfuss, A. Neubert, S. Breul, and V. Sandig. An avian cell line designed for production of highly attenuated viruses. *Vaccine*, 27(5):748–56, 2009.

[79] V. Lohr, O. Hadicke, Y. Genzel, I. Jordan, H. Buntemeyer, S. Klamt, and U. Reichl. The avian cell line age1.cr.pix characterized by metabolic flux analysis. *BMC Biotechnol*, 14:72, 2014.

[80] A. Textor, K. Schmidt, P. M. Kloetzel, B. Weissbrich, C. Perez, J. Charo, K. Anders, J. Sidney, A. Sette, T. N. Schumacher, C. Keller, D. H. Busch, U. Seifert, and T. Blankenstein. Preventing tumor escape by targeting a post-proteasomal trimming independent epitope. *J Exp Med*, 213(11):2333–2348, 2016.

[81] B. Engels, H. Cam, T. Schuler, S. Indraccolo, M. Gladow, C. Baum, T. Blankenstein, and W. Uckert. Retroviral vectors for high-level transgene expression in t lymphocytes. *Hum Gene Ther*, 14(12):1155–68, 2003.

[82] J. Altomonte, R. Braren, S. Schulz, S. Marozin, E. J. Rummeny, R. M. Schmid, and O. Ebert. Synergistic antitumor effects of transarterial viroembolization for multifocal hepatocellular carcinoma in rats. *Hepatology*, 48(6):1864–73, 2008.

[83] N. D. Lawson, E. A. Stillman, M. A. Whitt, and J. K. Rose. Recombinant vesicular stomatitis viruses from dna. *Proc Natl Acad Sci U S A*, 92(10):4477–81, 1995.

[84] T. R. Fuerst, E. G. Niles, F. W. Studier, and B. Moss. Eukaryotic transient-expression system based on recombinant vaccinia virus that synthesizes bacteriophage t7 rna polymerase. *Proc Natl Acad Sci U S A*, 83(21):8122–6, 1986.

[85] M. M. Jensen, J. T. Jorgensen, T. Binderup, and A. Kjaer. Tumor volume in subcutaneous mouse xenografts measured by microct is more accurate and reproducible than determined by 18f-fdg-micropet or external caliper. *BMC Med Imaging*, 8:16, 2008.

[86] S. Stahl, T. Sacher, A. Bechtold, U. Protzer, R. Ganss, G. J. Hammerling, B. Arnold, and N. Garbi. Tumor agonist peptides break tolerance and elicit effective ctl responses in an inducible mouse model of hepatocellular carcinoma. *Immunol Lett*, 123(1):31–7, 2009.

[87] S. H. Ali and J. A. DeCaprio. Cellular transformation by sv40 large t antigen: interaction with host proteins. *Semin Cancer Biol*, 11(1):15–23, 2001.

[88] J. Stritzker, L. Kirscher, M. Scadeng, N. C. Deliolanis, S. Morscher, P. Symvoulidis, K. Schaefer, Q. Zhang, L. Buckel, M. Hess, U. Donat, W. G. Bradley, V. Ntziachristos, and A. A. Szalay. Vaccinia virus-mediated melanin production allows mr and optoacoustic deep tissue imaging and laser-induced thermotherapy of cancer. *Proc Natl Acad Sci U S A*, 110(9):3316–20, 2013.

[89] J. G. Tjuvajev, M. Doubrovin, T. Akhurst, S. Cai, J. Balatoni, M. M. Alauddin, R. Finn, W. Bornmann, H. Thaler, P. S. Conti, and R. G. Blasberg. Comparison of radiolabeled nucleoside probes (fiau, fhbg, and fhpg) for pet imaging of hsv1-tk gene expression. *J Nucl Med*, 43(8):1072–83, 2002.

[90] B. Sangro, G. Mazzolini, M. Ruiz, J. Ruiz, J. Quiroga, I. Herrero, C. Qian, A. Benito, J. Larrache, C. Olague, J. Boan, I. Penuelas, B. Sadaba, and J. Prieto. A phase i clinical trial of thymidine kinase-based gene therapy in advanced hepatocellular carcinoma. *Cancer Gene Ther*, 17(12):837–43, 2010.

[91] S. S. Gambhir, E. Bauer, M. E. Black, Q. Liang, M. S. Kokoris, J. R. Barrio, M. Iyer, M. Namavari, M. E. Phelps, and H. R. Herschman. A mutant herpes simplex virus type 1 thymidine kinase reporter gene shows improved sensitivity for imaging reporter gene expression with positron emission tomography. *Proc Natl Acad Sci U S A*, 97(6):2785–90, 2000.

[92] K. A. Munoz-Alvarez, J. Altomonte, I. Laitinen, S. Ziegler, K. Steiger, I. Esposito, R. M. Schmid, and O. Ebert. Pet imaging of oncolytic vsv expressing the mutant hsv-1 thymidine kinase transgene in a preclinical hcc rat model. *Mol Ther*, 23(4):728–36, 2015.

[93] G. De Velasco, Y. Je, D. Bossé, M. M. Awad, P. A. Ott, R. B. Moreira, F. Schutz, J. Bellmunt, G. P. Sonpavde, F. S. Hodi, and T. K. Choueiri. Comprehensive meta-analysis of key immune-related adverse events from ctla-4 and pd-1/pd-l1 inhibitors in cancer patients. *Cancer Immunol Res*, 5(4):312–318, 2017.

[94] M. Y. Bartee, K. M. Dunlap, and E. Bartee. Tumor-localized secretion of soluble pd1 enhances oncolytic virotherapy. *Cancer Res*, 77(11):2952–2963, 2017.

[95] E. Lazar-Molnar, L. Scandiuzzi, I. Basu, T. Quinn, E. Sylvestre, E. Palmieri, U. A. Ramagopal, S. G. Nathenson, C. Guha, and S. C. Almo. Structure-guided development of a high-affinity human programmed cell death-1: Implications for tumor immunotherapy. *EBioMedicine*, 17:30–44, 2017.

[96] P. A. Riley, C. J. Cooksey, C. I. Johnson, E. J. Land, A. M. Latter, and C. A. Ramsden. Melanogenesis-targeted anti-melanoma pro-drug development: Effect of side-chain variations on the cytotoxicity of tyrosinase-generated ortho-quinones in a model screening system. *European Journal of Cancer*, 33(1):135–143, 1997.

[97] J. A. Prezioso, N. Wang, and W. D. Bloomer. Thymidylate synthase as a target enzyme for the melanoma-specific toxicity of 4-s-cysteaminylphenol and n-acetyl-4-s-cysteaminylphenol. *Cancer Chemother Pharmacol*, 30(5):394–400, 1992.

[98] W. W. Overwijk and N. P. Restifo. B16 as a mouse model for human melanoma. *Curr Protoc Immunol*, Chapter 20:Unit 20.1, 2001.

[99] S. Gujar, J. G. Pol, Y. Kim, P. W. Lee, and G. Kroemer. Antitumor benefits of antiviral immunity: An underappreciated aspect of oncolytic virotherapies. *Trends Immunol*, 39(3):209–221, 2018.

[100] J. L. Gulley, R. A. Madan, R. Pachynski, P. Mulders, N. A. Sheikh, J. Trager, and C. G. Drake. Role of antigen spread and distinctive characteristics of immunotherapy in cancer treatment. *J Natl Cancer Inst*, 109(4), 2017.

[101] M. B. Bloom, D. Perry-Lalley, P. F. Robbins, Y. Li, M. el Gamil, S. A. Rosenberg, and J. C. Yang. Identification of tyrosinase-related protein 2 as a tumor rejection antigen for the b16 melanoma. *J Exp Med*, 185(3):453–9, 1997.

[102] C. Fitzmaurice, C. Allen, R. M. Barber, L. Barregard, Z. A. Bhutta, H. Brenner, D. J. Dicker, O. Chimed-Orchir, R. Dandona, L. Dandona, T. Fleming, M. H. Forouzanfar, J. Hancock, R. J. Hay, R. Hunter-Merrill, C. Huynh, H. D. Hosgood, C. O. Johnson, J. B. Jonas, J. Khubchandani, G. A. Kumar, M. Kutz, Q. Lan, H. J. Larson, X. Liang, S. S. Lim, A. D. Lopez, M. F. MacIntyre, L. Marczak, N. Marquez, A. H. Mokdad, C. Pinho, F. Pourmalek, J. A. Salomon, J. R. Sanabria, L. Sandar, B. Sartorius, S. M. Schwartz, K. A. Shackelford, K. Shibuya, J. Stanaway, C. Steiner, J. Sun, K. Takahashi, S. E. Vollset, T. Vos, J. A. Wagner, H. Wang, R. Westerman, H. Zeeb, L. Zoeckler, F. Abd-Allah, M. B. Ahmed, S. Alabed, N. K. Alam, S. F. Aldhahri, G. Alem, M. A. Alemayohu, R. Ali, R. Al-Raddadi, A. Amare, Y. Amoako, A. Artaman, H. Asayesh, N. Atnafu, A. Awasthi, H. B. Saleem, A. Barac, N. Bedi, I. Bensenor, A. Berhane, E. Bernabé, B. Betsu, A. Binagwaho, D. Boneya, I. Campos-Nonato, C. Castañeda-Orjuela, F. Catalá-López, P. Chiang, C. Chibueze, A. Chitheer, J. Y. Choi, B. Cowie, S. Damtew, J. das Neves, S. Dey, S. Dharmaratne, P. Dhillon, E. Ding, T. Driscoll, D. Ekwueme, A. Y. Endries, M. Farvid, F. Farzadfar, J. Fernandes, F. Fischer, G. Hiwot TT, A. Gebru, S. Gopalani, A. Hailu, et al. Global, regional, and national cancer incidence, mortality, years of life lost, years lived with disability, and disability-adjusted life-years for 32 cancer groups, 1990 to 2015: A systematic analysis for the global burden of disease study. *JAMA Oncol*, 3(4):524–548, 2017.

[103] J. M. Llovet, S. Ricci, V. Mazzaferro, P. Hilgard, E. Gane, J. F. Blanc, A. C. de Oliveira, A. Santoro, J. L. Raoul, A. Forner, M. Schwartz, C. Porta, S. Zeuzem, L. Bolondi, T. F. Greten, P. R. Galle, J. F. Seitz, I. Borbath, D. Häussinger, T. Giannaris, M. Shan, M. Moscovici, D. Voliotis, and J. Bruix. Sorafenib in advanced hepatocellular carcinoma. *N Engl J Med*, 359(4):378–90, 2008.

[104] W. H. Fridman, F. Pagès, C. Sautès-Fridman, and J. Galon. The immune contexture in human tumours: impact on clinical outcome. *Nat Rev Cancer*, 12(4):298–306, 2012.

[105] M. Lamprecht and C. Dansereau. Car t-cell therapy: Update on the state of the science. *Clin J Oncol Nurs*, 23(2):6–12, 2019.

[106] F. Garrido, N. Aptsiauri, E. M. Doorduijn, A. M. Garcia Lora, and T. van Hall. The urgent need to recover mhc class i in cancers for effective immunotherapy. *Curr Opin Immunol*, 39:44–51, 2016.

[107] C. Blank, I. Brown, A. C. Peterson, M. Spiotto, Y. Iwai, T. Honjo, and T. F. Gajewski. Pd-l1/b7h-1 inhibits the effector phase of tumor rejection by t cell receptor (tcr) transgenic cd8+ t cells. *Cancer Res*, 64(3):1140–5, 2004.

[108] E. W. Roberts, M. L. Broz, M. Binnewies, M. B. Headley, A. E. Nelson, D. M. Wolf, T. Kaisho, D. Bogunovic, N. Bhardwaj, and M. F. Krummel. Critical role

for cd103(+)/cd141(+) dendritic cells bearing ccr7 for tumor antigen trafficking and priming of t cell immunity in melanoma. *Cancer Cell*, 30(2):324–336, 2016.

[109] A. Ajina and J. Maher. Prospects for combined use of oncolytic viruses and car t-cells. *J Immunother Cancer*, 5(1):90, 2017.

[110] S. Guedan and R. Alemany. Car-t cells and oncolytic viruses: Joining forces to overcome the solid tumor challenge. *Front Immunol*, 9:2460, 2018.

[111] M. Ahmadi, J. W. King, S. A. Xue, C. Voisine, A. Holler, G. P. Wright, J. Waxman, E. Morris, and H. J. Stauss. Cd3 limits the efficacy of tcr gene therapy in vivo. *Blood*, 118(13):3528–37, 2011.

[112] P. Muranski, A. Boni, C. Wrzesinski, D. E. Citrin, S. A. Rosenberg, R. Childs, and N. P. Restifo. Increased intensity lymphodepletion and adoptive immunotherapy–how far can we go? *Nat Clin Pract Oncol*, 3(12):668–81, 2006.

[113] S. R. Walsh, B. Simovic, L. Chen, D. Bastin, A. Nguyen, K. Stephenson, T. S. Mandur, J. L. Bramson, B. D. Lichty, and Y. Wan. Endogenous t cells prevent tumor immune escape following adoptive t cell therapy. *J Clin Invest*, 129(12):5400–5410, 2019.

[114] Adrian Bot, John M. Rossi, Yizhou Jiang, Lynn Navale, Yueh-wei Shen, Marika Sherman, Armen Mardiros, Sean C. Yoder, William Y. Go, Steven A. Rosenberg, Jeff Wiezorek, David D. Chang, James N. Kochenderfer, and Margo R. Roberts. Cyclophosphamide and fludarabine conditioning chemotherapy induces a key homeostatic cytokine profile in patients prior to car t cell therapy. *Blood*, 126(23):4426–4426, 2015.

[115] C. B. Johnson, B. R. May, B. P. Riesenberg, S. Suriano, S. Mehrotra, E. Garrett-Mayer, M. L. Salem, E. K. Jeng, H. C. Wong, C. M. Paulos, J. M. Wrangle, D. J. Cole, and M. P. Rubinstein. Enhanced lymphodepletion is insufficient to replace exogenous il2 or il15 therapy in augmenting the efficacy of adoptively transferred effector cd8(+) t cells. *Cancer Res*, 78(11):3067–3074, 2018.

[116] J. M. Santos, V. Cervera-Carrascon, R. Havunen, S. Zafar, M. Siurala, S. Sorsa, M. Anttila, A. Kanerva, and A. Hemminki. Adenovirus coding for interleukin-2 and tumor necrosis factor alpha replaces lymphodepleting chemotherapy in adoptive t cell therapy. *Mol Ther*, 26(9):2243–2254, 2018.

[117] G. Meng, Z. Fei, M. Fang, B. Li, A. Chen, C. Xu, M. Xia, D. Yu, and J. Wei. Fludarabine as an adjuvant improves newcastle disease virus-mediated antitumor immunity in hepatocellular carcinoma. *Mol Ther Oncolytics*, 13:22–34, 2019.

[118] Cameron J. Turtle, Laila-Aicha Hanafi, Carolina Berger, Daniel Sommermeyer, Barbara Pender, Emily M. Robinson, Katherine Melville, Tanya M. Budiarto, Natalia N. Steevens, Colette Chaney, Sindhu Cherian, Brent L. Wood, Lorinda Soma, Xueyan Chen, Shelly Heimfeld, Michael C. Jensen, Stanley R. Riddell, and David G. Maloney. Addition of fludarabine to cyclophosphamide lymphodepletion improves in vivo expansion of cd19 chimeric antigen receptor-modified t cells

and clinical outcome in adults with b cell acute lymphoblastic leukemia. *Blood*, 126(23):3773–3773, 2015.

[119] K. Watanabe, Y. Luo, T. Da, S. Guedan, M. Ruella, J. Scholler, B. Keith, R. M. Young, B. Engels, S. Sorsa, M. Siurala, R. Havunen, S. Tahtinen, A. Hemminki, and C. H. June. Pancreatic cancer therapy with combined mesothelin-redirected chimeric antigen receptor t cells and cytokine-armed oncolytic adenoviruses. *JCI Insight*, 3(7), 2018.

[120] E. K. Moon, L. S. Wang, K. Bekdache, R. C. Lynn, A. Lo, S. H. Thorne, and S. M. Albelda. Intra-tumoral delivery of cxcl11 via a vaccinia virus, but not by modified t cells, enhances the efficacy of adoptive t cell therapy and vaccines. *Oncoimmunology*, 7(3):e1395997, 2018.

[121] B. Tang, Z. S. Guo, D. L. Bartlett, D. Z. Yan, C. P. Schane, J. Liu, G. McFadden, D. L. Thomas, J. L. Shisler, and E. J. Roy. Synergistic combination of oncolytic virotherapy and immunotherapy for glioma. *Clin Cancer Res*, 2020.

[122] A. Wing, C. A. Fajardo, Jr. Posey, A. D., C. Shaw, T. Da, R. M. Young, R. Alemany, C. H. June, and S. Guedan. Improving cart-cell therapy of solid tumors with oncolytic virus-driven production of a bispecific t-cell engager. *Cancer Immunol Res*, 6(5):605–616, 2018.

[123] C. E. Porter, A. Rosewell Shaw, Y. Jung, T. Yip, P. D. Castro, V. C. Sandulache, A. Sikora, S. Gottschalk, M. M. Ittman, M. K. Brenner, and M. Suzuki. Oncolytic adenovirus armed with bite, cytokine, and checkpoint inhibitor enables car t cells to control the growth of heterogeneous tumors. *Mol Ther*, 2020.

[124] Shuming Chen, George A. Crabill, Theresa S. Pritchard, Tracee L. McMiller, Ping Wei, Drew M. Pardoll, Fan Pan, and Suzanne L. Topalian. Mechanisms regulating pd-l1 expression on tumor and immune cells. *Journal for ImmunoTherapy of Cancer*, 7(1):305, 2019.

[125] K. Tanoue, A. Rosewell Shaw, N. Watanabe, C. Porter, B. Rana, S. Gottschalk, M. Brenner, and M. Suzuki. Armed oncolytic adenovirus-expressing pd-l1 minibody enhances antitumor effects of chimeric antigen receptor t cells in solid tumors. *Cancer Res*, 77(8):2040–2051, 2017.

[126] A. Rosewell Shaw, C. E. Porter, N. Watanabe, K. Tanoue, A. Sikora, S. Gottschalk, M. K. Brenner, and M. Suzuki. Adenovirotherapy delivering cytokine and checkpoint inhibitor augments car t cells against metastatic head and neck cancer. *Mol Ther*, 25(11):2440–2451, 2017.

[127] Meijuan Zheng and Zhigang Tian. Liver-mediated adaptive immune tolerance. *Frontiers in Immunology*, 10:2525, 2019.

[128] P. C. Tumeh, M. D. Hellmann, O. Hamid, K. K. Tsai, K. L. Loo, M. A. Gubens, M. Rosenblum, C. L. Harview, J. M. Taube, N. Handley, N. Khurana, A. Nosrati, M. F. Krummel, A. Tucker, E. V. Sosa, P. J. Sanchez, N. Banayan, J. C. Osorio, D. L. Nguyen-Kim, J. Chang, I. P. Shintaku, P. D. Boasberg, E. J. Taylor, P. N.

Munster, A. P. Algazi, B. Chmielowski, R. Dummer, T. R. Grogan, D. Elashoff, J. Hwang, S. M. Goldinger, E. B. Garon, R. H. Pierce, and A. Daud. Liver metastasis and treatment outcome with anti-pd-1 monoclonal antibody in patients with melanoma and nsclc. *Cancer Immunol Res*, 5(5):417–424, 2017.

[129] Yong Luo, Chaolong Lin, Wenfeng Ren, Fei Ju, Zilong Xu, Huiling Liu, Zeng Yu, Jun Chen, Jun Zhang, Pingguo Liu, Chenghao Huang, and Ningshao Xia. Intravenous injections of a rationally selected oncolytic herpes virus as a potent virotherapy for hepatocellular carcinoma. *Molecular Therapy - Oncolytics*, 15:153–165, 2019.

[130] C. Hill and R. Carlisle. Achieving systemic delivery of oncolytic viruses. *Expert Opin Drug Deliv*, 16(6):607–620, 2019.

[131] M. K. Melzer, L. Zeitlinger, S. Mall, K. Steiger, R. M. Schmid, O. Ebert, A. Krackhardt, and J. Altomonte. Enhanced safety and efficacy of oncolytic vsv therapy by combination with t cell receptor transgenic t cells as carriers. *Mol Ther Oncolytics*, 12:26–40, 2019.

[132] S. R. Vora, H. Zheng, Z. K. Stadler, C. S. Fuchs, and A. X. Zhu. Serum alpha-fetoprotein response as a surrogate for clinical outcome in patients receiving systemic therapy for advanced hepatocellular carcinoma. *Oncologist*, 14(7):717–25, 2009.

[133] L. H. Butterfield, A. Ribas, W. S. Meng, V. B. Dissette, S. Amarnani, H. T. Vu, E. Seja, K. Todd, J. A. Glaspy, W. H. McBride, and J. S. Economou. T-cell responses to hla-a*0201 immunodominant peptides derived from alpha-fetoprotein in patients with hepatocellular cancer. *Clin Cancer Res*, 9(16 Pt 1):5902–8, 2003.

[134] W. Zhu, Y. Peng, L. Wang, Y. Hong, X. Jiang, Q. Li, H. Liu, L. Huang, J. Wu, E. Celis, T. Merchen, E. Kruse, and Y. He. Identification of alpha-fetoprotein-specific t-cell receptors for hepatocellular carcinoma immunotherapy. *Hepatology*, 68(2):574–589, 2018.

[135] J. Woodcock and R. Woosley. The fda critical path initiative and its influence on new drug development. *Annu Rev Med*, 59:1–12, 2008.

[136] J. Mestas and C. C. Hughes. Of mice and not men: differences between mouse and human immunology. *J Immunol*, 172(5):2731–8, 2004.

# 9 Acknowledgements

I would like to end this doctoral thesis with a heartfelt thank you to everyone who supported me and my PhD, I couldn't have done it without you.

First of all, I would like to thank Jennifer for giving me the opportunity to work with her and her fascinating oncolytic virus platform. We were starting out very small and I feel like we have come such a long way and grown to be a wonderful team over the years. Thank you for all the morning talks in your office, for always being there for the scientific discussions as well as the stupid questions. You are brilliant and very kind and I couldn't imagine a better PhD supervisor. I am very much looking forward to all that we can achieve in the future.

I also want to thank Angela Krackhardt and Florian Kreppel for fruitful discussions and all the scientific and statistical support advancing my thesis and research. Also a big thank you to the current and past lab members for your company and friendship. On a different note, I would also like to thank the Institute, TUM Graduate School and PhD program for providing (infra)structure and guidance and for organizing the kick-off seminar, where I was lucky enough to meet the love of my life, who made my PhD time the best time of my life. Thank you, dear husband, for sharing all the joys and worries. I just love every minute I get to spend with you.

Lastly, I would like to thank my family and friends. Dear Franzi and Marc, thank you for wonderful evenings filled with whiskey sour and great talks about science, business and the world in general. Dear Gina, thank you for always having an open ear and, although far away, always being a pillar of support and a great friend. And the biggest thank you, to my lovely parents. Without you none of this would have been possible and I will be forever grateful for the wonderful life that you have opened up for me. Thank you for always supporting me and thank you for always being my home.